

**LOW SALINITY INJECTION FLUIDS WITH
ADDITIVES FOR ENHANCED OIL RECOVERY
FROM CLASTIC RESERVOIRS: THE MACRO TO
PORE SCALE STUDIES**

A THESIS

Submitted by

NILESH KUMAR JHA

for the award of the degree

of

DOCTOR OF PHILOSOPHY

JOINTLY WITH



**PETROLEUM ENGINEERING PROGRAM
DEPARTMENT OF OCEAN ENGINEERING**

INDIAN INSTITUTE OF TECHNOLOGY MADRAS

CHENNAI-600036

MAY 2020

Dedicated to my parents

THESIS CERTIFICATE

This is to certify that the thesis entitled “**LOW SALINITY INJECTION FLUIDS WITH ADDITIVES FOR ENHANCED OIL RECOVERY FROM CLASTIC RESERVOIRS: THE MACRO TO PORE SCALE STUDIES**” submitted by **NILESH KUMAR JHA** to the Indian Institute of Technology, Madras and Curtin University, Australia for the award of the degree of **Doctor of Philosophy** is a bonafide record of research work carried out by him under our supervision. The contents of this thesis, in full or in parts, have not been submitted to any other Institute or University for the award of any degree or diploma.

Dr. Jitendra Sangwai
Professor,
Petroleum Engineering Program,
Department of Ocean Engineering
Indian Institute of Technology Madras
Chennai – 600036.

Dr. Mohammad Sarmadivaleh
Senior Lecturer,
Western Australian School of Mines (WASM):
Minerals, Energy and Chemical Engineering,
Curtin University, Australia.
Western Australia – 6151.

Place: Chennai/Kensington

Date: May 19, 2020

ACKNOWLEDGEMENTS

It gives me a sense of fulfillment to write a few words to acknowledge people. Firstly, I would like to express my sincere gratitude to my supervisors Dr. Jitendra Sangwai and Dr. Mohammad Sarmadivaleh, for the continuous support of my Ph.D. study and related research, for their patience, motivation, and immense knowledge. Their guidance helped me in all the time of research and writing of this thesis. I could not have imagined having better advisors and mentors for my Ph.D. study and enlightening me on the first glance of research.

Besides them, I would like to thank my doctoral committees from both the universities: Dr. K. Murali, Dr. P. Shanmugam, Dr. Abdus Samad, Dr. S. M. Shiva Nagendra, Dr. Mofazzal Hossain, Dr. Stefan Iglauer, Dr. Maxim Lebedev, Dr. Hamid Roshan, and Dr. Ahmed Barifcani for their insightful comments and encouragement, but also for the hard question which incited me to widen my research from various perspectives. My sincere thanks go to Dr. R. Nagarajan, Dr. Abhijit Mukherjee, Dr. A. K. Mishra, Dr. S. A. Sannasiraj, and Dr. Stefan Iglauer, who were instrumental to this collaborative work. I am grateful to administrative staffs, technical staffs, hostel staffs, hosts, and colleagues who directly or indirectly contributed during my Ph.D. work. I thank all my fellow labmates in both the universities for the stimulating discussions, for the sleepless nights we were working together before deadlines, and for all the fun we have had in the last four years. I thank my friends for making my life memorable at Chennai and Perth. All thanks are due to my mentor Dr. Jitendra Sangwai who believed in me and facilitated this part of my journey. Finally, I would like to thank my family members for supporting me mentally and physically throughout the research and my life in general.

ABSTRACT

Keywords: Low salinity; Enhanced oil recovery; Surfactants; Nanoparticles; Interfacial tension; Wettability; Micro-CT coreflooding

The core of the present work is the studies of the use of additives in low salinity water for their suitability for injection into oil-bearing sandstone reservoirs to improve the oil recovery performance in an enhanced oil recovery process by this method. This work carried out various investigations to find out the possibilities to mitigate the shortcomings of the existing process of low salinity water injection enhanced oil recovery.

A very low interfacial tension, γ , can be achieved between an oil phase and an aqueous solution containing anionic surfactant and salt at a very low concentration. This phenomenon can have potential applications in recovering residual oil from the reservoir through low salinity-low surfactant enhanced oil recovery flooding. Measurements of γ between n-heptane and the aqueous solution of anionic surfactants in the concentration range of 0.141 – 2.167 mM and salts in the concentration range of 9.010 – 119.780 mM at 313.15 ± 0.1 K have been carried out. The experimental results show that the value of γ falls to a lowest value at a temperature above the Krafft point when the concentration of anionic surfactants [sodium dodecyl sulfate (SDS), and dioctyl sulfosuccinate sodium salt (AOT)] is increased up to a maximum surface excess concentration in an aqueous solution in the presence of monovalent [sodium chloride, (NaCl)] and divalent [calcium chloride, (CaCl₂)] salts in the low concentration range. To understand and adequately capture the reduction of γ in such systems with n-heptane as an oil phase, a simplistic model is being proposed here. This model is an extension of the Petersen and Saykally model which was earlier developed to capture the Jones-Ray effect.

In this study, additives such as surfactant and nanoparticles in combination with low salinity water appeared to be promising formulations for rock wettability modification and surfactant adsorption control. The detailed interaction of these novel formulations and the rock surface is, however, not well understood. Thus, an experimental study was conducted here, and results show that anionic surfactant (AOT, 11.247 mM) augmented the effect of silica nanoparticles (1000-3000 mg/L concentration) at low salinity conditions as effective surfactant adsorption control agents when used at appropriate divalent cation to sulphate ion ratios. Low salinity surfactant nanofluids may thus be applied for wettability alteration of oil-bearing sandstone reservoirs for recovering residual oil. Here it demonstrates that the ratio of divalent cations to sulphate ions ($0 \leq M^{2+}/SO_4^{2-} \leq 4.427$) has a significant role in surfactant adsorption irrespective of the divalent to monovalent cations' ratio or presence of nanoparticles when sulphate ions are present in the solution. It is further shown by using USBM wettability measurements that initial water-wet Berea sandstone can be rendered more water-wet when 1000 mg/L of silica nanoparticles (SNP) is used in the low salinity formulation although further incremental nanoparticle concentration has no significant effect on the wettability. Wettability controls the capillary pressure and relative permeability behaviour and thus influences the rate of hydrocarbon displacement and ultimate recovery.

The experimental study was conducted in this study to investigate the interfacial tension and wettability of carbon dioxide and anionic surfactant (SDBS, 1.435 mM) at high pressure (20 MPa) and temperature (343.15 K) using pendant drop IFT cell. The results show that the anionic surfactant (SDBS, 1.435 mM) augmented the effect of zirconia (ZrO_2) nanoparticles (ZNP) (100–2000 mg/L concentration) at low-salinity conditions and proved to be an effective wettability and interfacial tension modifier when used at appropriate divalent cation/sulfate ion ratios. Low-salinity surfactant nanofluids may thus be applied for wettability alteration and interfacial tension reduction for recovering residual oil, carbon dioxide enhanced oil recovery

as well as carbon dioxide geosequestration. It has also been demonstrated in this study that the ratio of divalent cations to sulfate ions ($0 \leq M^{2+}/SO_4^{2-} \leq 4.427$) has a significant role in interfacial tension reduction and wettability modification. It is further shown using contact angle wettability measurements that initial weak water-wet quartz surfaces can turn to more water-wet when zirconia nanoparticles used in the low-salinity formulation are in the range of 100-1000 mg/L. Interestingly, further incremental nanoparticle concentration decreases the water wettability but further reduces the carbon dioxide/brine interfacial tension.

Low salinity surfactant nanofluids have shown promising characteristics in wettability alteration of the silicate-based rock representative substrate and interfacial tension reduction of oil/aqueous phase interface. Pore level understanding of the physical processes entailed in this new class of low salinity injection fluids in oil-phase saturated real rock porous media is required, which has not been conceived yet. Thus, we investigate the oil recovery performance and possible mechanisms of oil recovery by the injection of low salinity surfactant (SDBS, 1.435 mM) aqueous solutions (with 0%, 0.01% and 0.1% (by weight) ZrO_2 nanoparticles) into the oil phase saturated Doddington sandstone miniature core plugs. The designed experiment involves core flooding with X-ray transparent core-holder developed in-house and analysis/processing of the acquired image data. The injection of low salinity surfactant nanofluids with 0.01% ZrO_2 nanoparticles leads to maximum oil phase recovery. The results suggest that the dominating mechanisms for oil recovery are wettability alteration, inherent interfacial tension reduction, and the effect of the significant amount of microemulsions formation is rather trivial. Low salinity effect, even in combination with the surfactant, caused fines migrations (not reported earlier), is found to be significantly mitigated using nanoparticles. These new class of fluids may significantly enhance oil recovery.

TABLE OF CONTENTS

| | |
|---|-----------|
| ABSTRACT | ii |
| TABLE OF CONTENTS | v |
| LIST OF FIGURES | viii |
| LIST OF TABLES | xii |
| ORGANIZATION OF THE THESIS | xiii |
| Chapter 1 | 14 |
| INTRODUCTION | 14 |
| 1.1 INTRODUCTION | 14 |
| 1.1.1 Proposed mechanisms for LSWI effect on sandstone rocks | 15 |
| 1.2 OBJECTIVE OF THE WORK | 23 |
| 1.3 SCOPE OF THE THESIS | 23 |
| Chapter 2 | 24 |
| EFFECT OF SALT TYPE ON THE INTERFACIAL TENSION BETWEEN OIL AND AQUEOUS PHASE | 24 |
| 2.1 INTRODUCTION | 24 |
| 2.2 MATERIALS AND METHODS | 27 |
| 2.2.1 Materials | 27 |
| 2.2.2 Method | 28 |
| 2.3 RESULTS AND DISCUSSION | 30 |
| 2.3.1 Effect of SDS Concentration on IFT | 30 |
| 2.3.2 Characterization of Precipitate | 34 |
| 2.3.3 Effect of AOT Concentration on IFT | 36 |
| 2.3.4 IFT Model | 38 |

| | |
|--|-----------|
| 2.4 CONCLUSIONS | 47 |
| Chapter 3 | 49 |
| EFFECT OF LOW SALINITY SURFACTANT NANOFLUIDS ON SANDSTONE AT ALKALINE CONDITION | 49 |
| 3.1 INTRODUCTION | 49 |
| 3.2 MATERIALS AND METHODS | 52 |
| 3.2.1 Materials | 52 |
| 3.2.2 Method | 54 |
| 3.3 RESULTS AND DISCUSSION | 59 |
| 3.3.1 Effect of SNP concentration on surfactant adsorption | 59 |
| 3.3.2 Effect of the divalent cation-sulphate ion ratio on surfactant adsorption | 61 |
| 3.3.3 Effect of SNPs on wettability of Berea sandstone core plugs | 63 |
| 3.4 CONCLUSIONS | 67 |
| Chapter 4 | 69 |
| EFFECT OF LOW SALINITY SURFACTANT NANOFLUIDS ON QUARTZ AT ACIDIC CONDITION | 69 |
| 4.1 INTRODUCTION | 69 |
| 4.2 MATERIALS AND METHODS | 71 |
| 4.2.1 Materials | 71 |
| 4.2.2 Method | 73 |
| 4.3 RESULTS AND DISCUSSION | 76 |
| 4.3.1 Effect of ZNP Concentration on IFT of low salinity surfactant nanofluids | 76 |
| 4.3.2 Effect of divalent cation-sulfate ion ratio on IFT of low salinity surfactant nanofluids | 78 |

| | | |
|--|--|------------|
| 4.3.3 | Effect of ZNP concentration on the contact angle of low salinity surfactant nanofluids | 79 |
| 4.3.4 | Effect of the divalent cation-sulfate ion ratio on the contact angle of low salinity surfactant nanofluids | 83 |
| 4.4 | CONCLUSIONS | 84 |
| Chapter 5 | | 86 |
| X-RAY MICRO-TOMOGRAPHY CORE FLOOD INVESTIGATION | | 86 |
| 5.1 | INTRODUCTION | 86 |
| 5.2 | MATERIALS AND METHODS | 88 |
| 5.2.1 | Materials | 88 |
| 5.2.2 | Method | 89 |
| 5.3 | RESULTS AND DISCUSSION | 92 |
| 5.3.1 | Initial saturation and condition | 92 |
| 5.3.2 | Coreflooding results | 93 |
| 5.3.3 | Mechanism of oil recovery | 95 |
| 5.3.4 | Oil phase cluster statistics | 102 |
| 5.3.5 | Implications | 105 |
| 5.4 | CONCLUSIONS | 105 |
| Chapter 6 | | 107 |
| CONCLUSION AND FUTURE RECOMMENDATIONS | | 107 |
| REFERENCES | | 110 |
| APPENDIX | | 133 |
| PUBLICATIONS | | 140 |

LIST OF FIGURES

| | |
|--|----|
| Figure 1.1 Enhanced oil recovery methods..... | 14 |
| Figure 1.2 Oil component detachment from clay due to pH increase by low salinity water... 17 | 17 |
| Figure 1.3 Nanoparticles and surfactants as additives | 22 |
| Figure 2.1 Experimental values on γ for n-heptane - (NaCl + SDS) aqueous solution at 313.15 \pm 0.1 K, ■, 17.110 mM NaCl + SDS; ●, 59.890 mM NaCl + SDS; ▲, 119.780 mM NaCl + SDS; ●, Tichelkamp et al. (2014) | 32 |
| Figure 2.2 Experimental values on γ for n-heptane - (CaCl ₂ + SDS) aqueous solution at 313.15 \pm 0.1 K, ■, 9.010 mM CaCl ₂ + SDS; ●, 31.530 mM CaCl ₂ + SDS; ▲, 63.070 mM CaCl ₂ + SDS; ●, Tichelkamp et al. (2014) | 32 |
| Figure 2.3 (a) SEM image of precipitate formed from an aqueous solution containing 1.730 mM SDS and 63.070 mM CaCl ₂ at 313.15 K; (b) XRD pattern of precipitate (PPT), SDS and CaCl ₂ | 35 |
| Figure 2.4 Experimental values on γ for n-heptane - (NaCl + AOT) aqueous solution at 313.15 \pm 0.1 K, ■, 17.110 mM NaCl + AOT; ●, 59.890 mM NaCl + AOT; ▲, 119.780 mM NaCl + AOT..... | 37 |
| Figure 2.5 Experimental values at 313.15 \pm 0.1 K and model for $\Delta\gamma$ of (a) n-heptane - (NaCl + SDS) aqueous solution: ■, 17.110 mM NaCl + SDS; ●, 59.890 mM NaCl + SDS; ▲, 119.780 mM NaCl + SDS; ●, Tichelkamp et al. (2014); (b) n-heptane - (CaCl ₂ + SDS) aqueous solution; ■, 9.010 mM CaCl ₂ + SDS; ●, 31.530 mM CaCl ₂ + SDS; ▲, 63.070 mM CaCl ₂ + SDS; ●, Tichelkamp et al. (2014); (c) n-heptane - (NaCl + AOT) aqueous solution: ■, 17.110 mM NaCl + AOT; ●, 59.890 mM NaCl + AOT; ▲, 119.780 mM NaCl + AOT; Model predictions are shown as solid lines. | 43 |
| Figure 2.6 Model for regressed ΔG_{ads} vs (a) SDS concentration for n-heptane - (NaCl + SDS) aqueous solution at 313.15 \pm 0.1 K, —, 17.110 mM NaCl + SDS; —, 59.890 mM NaCl + | |

| | |
|---|----|
| SDS; —, 119.780 mM NaCl + SDS; (b) SDS concentration for n-heptane - (CaCl ₂ + SDS) aqueous solution at 313.15 ± 0.1 K, —, 9.010 mM CaCl ₂ + SDS; —, 31.530 mM CaCl ₂ + SDS; —, 63.070 mM CaCl ₂ + SDS; (c) AOT concentration for n-heptane - (NaCl + AOT) aqueous solution at 313.15 ± 0.1 K, —, 17.110 mM NaCl + AOT; —, 59.890 mM NaCl + AOT; —, 119.78 mM NaCl + AOT. | 46 |
| Figure 3.1 XRD pattern of muscovite and associated clay mineral..... | 53 |
| Figure 3.2 Experimental values for AOT adsorption on clay against SNP concentration: ●, LSS1; ●, LSS2; ●, LSS3; ●, LSS4..... | 61 |
| Figure 3.3 Experimental values for AOT adsorption on clay against divalent cations to sulphate ions ratio (M ²⁺ /SO ₄ ²⁻): ■, 0 mg/L SNP; ■, 1000 mg/L SNP; ■, 2000 mg/L SNP; ■, 3000 mg/L SNP..... | 63 |
| Figure 3.4 Hysteresis loop of capillary pressure curves for (a) B2, High pH low salinity surfactant solutions of LSS1 + 0% SNP: ●, primary drainage; ●, secondary drainage; ●, imbibition; (b) B3, High pH low salinity surfactant solutions of LSS1 + 0.1% SNP: ●, primary drainage; ●, secondary drainage; ●, imbibition; (c) B4, High pH low salinity surfactant solutions of LSS1 + 0.2% SNP: ●, primary drainage; ●, secondary drainage; ●, imbibition. | 66 |
| Figure 3.5 Schematic of surfactant adsorption on sandstone surface. | 66 |
| Figure 3.6 Schematic of nanoaggregates co-adsorption on sandstone surface..... | 67 |
| Figure 4.1 Experimental values for LSS nanofluid/scCO ₂ IFT against the ZNP concentration: ●, LSS1; ●, LSS2; ●, LSS3; and ●, LSS4..... | 76 |
| Figure 4.2 Schematic of nanoaggregate adsorption at the nanofluid/scCO ₂ interface. | 78 |
| Figure 4.3 Experimental values for LSS nanofluid/scCO ₂ IFT against the divalent cation/sulfate ion ratio (M ²⁺ /SO ₄ ²⁻): ■, 0 mg/L ZNP; ■, 100 mg/L ZNP; ■, 1000 mg/L ZNP; and ■, 2000 mg/L ZNP..... | 79 |

Figure 4.4 Variation of standard free energy of adsorption ΔG°_{ads} of n-alkanes on silica surface (●; Papirer, 2018) and the ratio of density of the n-alkanes at the n-alkane/silica interface to bulk density (ρ/ρ_b) (●; De Almeida and Miranda, 2016) with their number of carbon atoms.81

Figure 4.5 Experimental values for LSS nanofluid/quartz contact angles [Advancing (θ_a) and Receding (θ_r)] against the ZNP concentration: ■, LSS1 θ_a ; ■, LSS2 θ_a ; ■, LSS3 θ_a ; ■, LSS4 θ_a ; ●, LSS1 θ_r ; ●, LSS2 θ_r ; ●, LSS3 θ_r ; and ●, LSS4 θ_r82

Figure 4.6 Schematic of nanoaggregate co-adsorption on the quartz surface.83

Figure 4.7 Experimental values for LSS nanofluid/quartz contact angle [Advancing (θ_a) and Receding (θ_r)] against the divalent cation/sulfate ion ratio (M^{2+}/SO_4^{2-}): ■, 0 mg/L ZNP θ_a ; ■, 100 mg/L ZNP θ_a ; ■, 1000 mg/L ZNP θ_a ; ■, 2000 mg/L ZNP θ_a ; ●, 0 mg/L ZNP θ_r ; ●, 100 mg/L ZNP θ_r ; ●, 1000 mg/L ZNP θ_r ; and ●, 2000 mg/L ZNP θ_r84

Figure 5.1 Schematic of the experimental setup to run the μ -CT core flooding experiments, black lines: injection or collection line.....91

Figure 5.2 Schematic of wedge film formed at three-phase contact regions. The red curve represents the oscillatory decay of the structural disjoining pressure with the thickness of the wedge film.95

Figure 5.3 LSS + 0.01% ZNP – XZ plane (orange line) (a) Initial saturation (b) 10PV injection98

Figure 5.4 Schematic of the oil in water Pickering emulsion.99

Figure 5.5 LSS + 0.01% ZNP – XY plane (orange line) (a) Initial saturation (b) 30PV Injection99

Figure 5.6 LSS injection. (a) oil saturation profile (b) grain distribution profile (c) grain fraction difference profile 100

| | |
|---|-----|
| Figure 5.7 LSS + 0.01%NP (a) oil saturation profile (b) grain distribution profile (c) grain fraction difference profile..... | 100 |
| Figure 5.8 LSS + 0.1%NP (a) oil saturation profile (b) grain distribution profile (c) grain fraction difference profile..... | 102 |
| Figure 5.9 Oil phase cluster size distribution for (a) LSS (b) LSS + 0.01 % ZNP (c) LSS + 0.1 | 104 |

LIST OF TABLES

| | |
|--|----|
| Table 2.1 List of Chemicals Used in This Study | 27 |
| Table 2.2 Concentration of Salts and Surfactants Used in the Aqueous Solution..... | 30 |
| Table 2.3 Compositional Data of Precipitate From Energy Dispersive Spectroscopy | 36 |
| Table 2.4 Model Parameters and Derived Quantities for Several Exemplary Surfactant Concentrations at 313.15 K: Component specific parameter (α), Maximum Surface Excess (NS_{max}), and Gibbs Free Energy of Adsorption (ΔG_{ads}) ⁺ | 44 |
| Table 2.5 Derived Quantities for for ΔG_{ads} (J/mol) fit for Several Exemplary Surfactant Concentrations at 313.15 K: Slope (RT _m) and Constant (RT _c) | 47 |
| Table 3.1 Chemicals Used in This Study..... | 54 |
| Table 3.2 Compositions of the Brines..... | 55 |
| Table 3.3 Compositions of the Nanofluids | 56 |
| Table 3.4 Berea Sandstone Core Plugs Properties..... | 58 |
| Table 3.5 Wettability Index of Berea Sandstone Core Plugs..... | 64 |
| Table 4.1 Wettability Based on Contact Angle of Aqueous Phase-rock system..... | 71 |
| Table 4.2 List of Chemicals Used in This Study | 72 |
| Table 4.3 Compositional Data of the Substrate From Energy Dispersive Spectroscopy | 73 |
| Table 4.4 Compositions of the Brines..... | 73 |
| Table 4.5 Compositions of the Nanofluids | 75 |
| Table 5.1 List of Chemicals Used in This Study | 89 |
| Table 5.2 Compositions of the Brines..... | 90 |
| Table 5.3 Saturation Profile and oil Recovery | 93 |
| Table 5.4 Aqueous Phase Saturation Segmented 3D Images | 94 |

ORGANIZATION OF THE THESIS

Chapter 1 briefs about the background and the introduction to low salinity water injection enhanced oil recovery technique, proposed mechanisms with supporting and contrary evidence in the available literature, and the use of additives.

Chapter 2 presents the contribution of surfactants and salts in oil and aqueous phase interfacial tension behavior at low salinity conditions, inherent mechanisms, and model development to capture the overall interfacial behavior.

Chapter 3 discusses the effects of the addition of nanoparticles in low salinity surfactant aqueous solution with various divalent cations to sulphate ratio in alkaline condition to the wettability alteration of oil-saturated sandstone core plugs and surfactants adsorption by clays.

Chapter 4 discusses the effects of the addition of nanoparticles in low salinity surfactant aqueous solution with various divalent cations to sulphate ratio in supercritical CO₂ loading condition to the wettability alteration of oil-wet quartz surface at high temperature.

Chapter 5 presents the oil recovery performance and inherent mechanisms by low salinity surfactant nanofluids injection into sandstone porous media by X-ray micro-computed tomography coreflood technique.

Chapter 6 concludes and summarizes the use of additives to augment the effect of low salinity water as a new class of injection fluids in the oil recovery performance for enhanced oil recovery processes in a sandstone subsurface oil reservoir, and future recommendations.

CHAPTER 1

INTRODUCTION

1.1 INTRODUCTION

After primary recovery of crude oil from earth’s subsurface petroleum reservoirs, a large part of it remains trapped inside the pores of the reservoir rocks. The primary recovery method (natural flow, artificial lift) generally recovers oil less than 30% of oil in place (Stosur, 2003; Stosur et al., 2003). Various methods are being applied for the improvement in the recovery of those trapped oil. These recovery methods are technically and economically intensive. Secondary recovery, which utilizes the technique of water flooding and pressure maintenance, are responsible for up to 50% of the oil recovery (Stosur, 2003; Stosur et al., 2003). Some of the established tertiary methods, however, not restricted to any particular phase of the production life cycle of the reservoir (Sheng, 2010), utilizes the injection of water containing polymers, alkali, surfactant, foam, and even microbes (Figure 1.1).

Low salinity water injection (LSWI) is emerging as a new technique of enhanced oil recovery (EOR)/improved oil recovery (IOR) from subsurface petroleum reservoirs (Al-Shalabi and Sepehrnoori, 2016). Seawater or saline aquifers after modification of its chemical

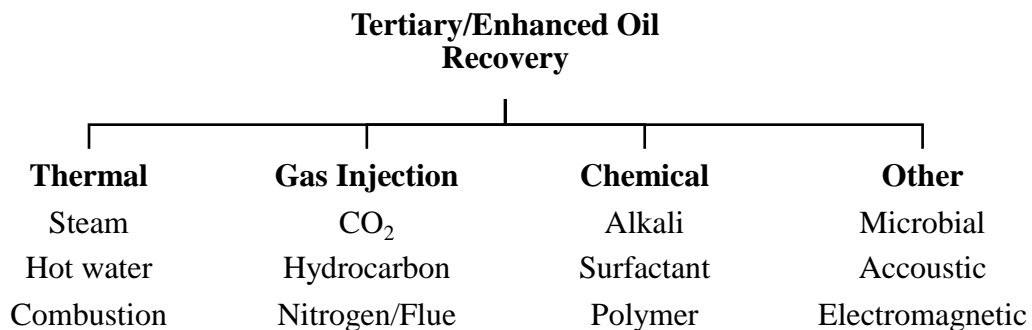


Figure 1.1 Enhanced oil recovery methods

and physical properties are generally used for the injection purpose (Tang and Morrow, 1999). They are known by various proprietary names such as LoSal™ by British Petroleum, Designer Waterflood by Shell, Smart WaterFlood by Saudi Aramco, and Advanced Ion Management (AIM™) by Exxon Mobil (Jackson et al., 2016). Many studies show Low Salinity Effect (LSE) both in case of clastic and carbonate rocks. Significant number of studies shows its successful application at laboratory as well as field scale. On the contrary there are several other published works that shows no effect. Studies on LSWI both from laboratory and field scale suggests that additional recovery of light to medium gravity crude oil is possible at favorable economics as compared to other IOR/EOR methods. These studies also suggest that this environmentally friendly recovery technique could be used in both secondary and tertiary mode. However, by and large, despite having several hundreds of publications in this area, researchers worldwide remain inconclusive over the mechanism of the enhanced oil recovery due to LSWI (Chavez-Miyauchi et al., 2016).

The following section describes the mechanisms which have widely been proposed and contradictions for low salinity effect during the LSWI process.

1.1.1 Proposed mechanisms for LSWI effect on sandstone rocks

The various mechanisms have been suggested for the LSWI effect on sandstone rocks, however, due to the complex nature of the crude oil-brine-rock (COBR) interaction, researchers remained inconclusive on the main mechanism. Some of them are as follows:

(a) Fines migration

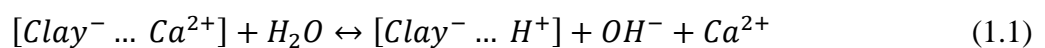
Swelling of clay by LSW which can limit the space for oil and water or formation of new channels due to blocking of established channels by clay dispersion can be the reason for the increase in oil recovery (Al-Shalabi and Sepehrnoori, 2016). Tang and Morrow highlighted

that low salinity effect results from (i) adsorption of polar components from crude oil onto fines-coated mineral surfaces, (ii) stripped mixed-wet fines during LSWI, and (iii) oil-bearing fines accumulation at the oil-water interface (Tang and Morrow, 1999). Tang and Morrow reported increased oil recovery, increased pH, and increased pressure drop due to the injection of diluted formation brine (<1550 mg/L Total Dissolved Solids) into the sandstone cores containing kaolinite clay, both in secondary and tertiary mode (Tang and Morrow, 1999). Contrary to this, the firing of the cores, injection of Ca^{2+} ions during successful LSWI, no initial water saturation, and with the use of refined oil, low salinity effect ceased to act (Tang and Morrow, 1999).

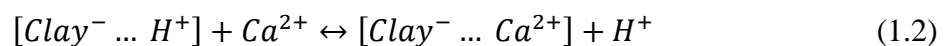
However, other researchers did not observe the production of fines, although the low salinity effect was prominent (Jackson et al., 2016; Lager et al., 2008). whereas several others reported fines production with no low salinity effect. Fine migration is not considered as the main mechanism but an auxiliary one.

(b) pH Increase

LSWI disturbs the thermodynamic chemical equilibrium causing interaction between brine and rock (initially at reservoir conditions of pH 5-6) to compensate for the loss of divalent cations (Austad et al., 2010), Figure 1.2. This creates an increase in the pH close to clay surface which leads to reactions between adsorbed basic and acidic material. The following mechanism was proposed:



Reversibility of pH can also occur by injection of high salinity brine by the following mechanism:



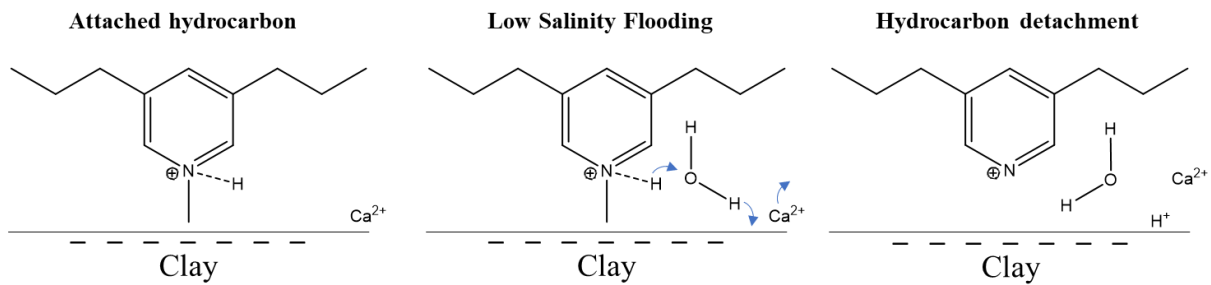


Figure 1.2 Oil component detachment from clay due to pH increase by low salinity water

This increase in pH causes surfactant generation from the residual oil by saponification of acidic components of the crude oil (McGuire et al., 2005). The surfactant generation leads to oil/water interfacial tension reduction as well as the wettability alteration of the rock surface to more water-wet conditions (McGuire et al., 2005). For a saponification reaction to occur, a high acid number of crude oils is required, however, low salinity effect has also been observed in low acid numbers (Jackson et al., 2016). Thus, a direct correlation of pH with acid number could be established (Jackson et al., 2016).

(c) Multi-Ion exchange

Multi-ion exchange (MIE) mechanism was proposed by Lager et al. (2006). They stated that the interaction between surface-active components of the crude oil and clay minerals controlled by the presence of divalent ion such as Ca^{2+} and Mg^{2+} is affected by the exchange of ions and thus there is an increase in oil recovery. They further argued that clay minerals are responsible for ion exchange and those with high cation exchange capacity (CEC) are optimal. But evidence also shows that kaolinite, which has low CEC, also shows a low salinity effect. Also, there is very little evidence that shows MIE and low salinity effects are closely linked (Jackson et al., 2016). Whereas despite the conditions of MIE were met in some coreflooding tests, low salinity effects were not observed (Jackson et al., 2016). Therefore, it was briefly

concluded that MIE alone does not explain the low salinity effect and thus the oil recovery by this process.

(d) Salting-in

RezaeiDoust et al. (2009), in their work, proposed that the decrease in the salinity below a critical ionic strength can increase the solubility of organic material in the aqueous phase. Organic materials, using hydrogen bonds around the hydrophobic part, are solvated in water. The presence of cations in a large amount in high salinity formation water breaks this water structure which prevents organic materials from dissolution. However, this effect remains under-investigated.

(e) Wettability alteration

The wettability alteration in sandstone rocks using low salinity water through mechanisms including fine migration, pH increase could cause IFT reduction, MIE and double layer expansion. McGuire et al. (2005), in their work on wettability alteration, reported that this mechanism in the case of LSWI is similar to those occurring during alkaline and surfactant waterflooding. They reported pH increase up to 9 during LSWI (1500 mg/L) in sandstone core causing generation of surfactant, which lowered the IFT between oil and water and increased the water wettability which leads to higher oil recovery. A similar mechanism was suggested by Zhang and Morrow (2006), and they reported an increase in the effluent brine pH. In their work, Nasralla and Nasr-El-Din (2011) reported the wettability alteration to be the reason for oil recovery due to change in the electrical charge for both oil/brine and rock/brine interfaces to highly negative promoting repulsive electrical forces in the double layer and resulting in a more stable water film. They also reported the dominance of cation type in oil recovery through LSWI. Moreover, the presence of clay minerals was supposed to promote wettability alteration

by low salinity effect. Contrary to the requirement of clay minerals, wettability alteration has also been observed in clean sandstone, sandpack, and quartz surface (Jackson et al., 2016). Most studies support the wettability alteration of rock surface to the more water-wet state by low salinity water injection and the initial condition of the rock is mixed-wet. Despite the broad agreement, some evidence still contradicts that low salinity effect relates to more-water wet or the initial mixed-wet condition of the rock (Jackson et al., 2016).

(f) Double layer expansion

With low salinity water injection, electrical double layer expansion takes place at the mineral-brine interface. This is well established that at the low to moderate salinity, the diffuse part of the electrical double layer expands (thickness of the layer increases) with the decrease in ionic strength. This expansion results in detachment of adsorbed polar oil components due to the increase in electrostatic repulsion between those components and the charged mineral surfaces, making the surface more water wet (Jackson et al., 2016). Further reduction in the ionic strength below a threshold value can cause the detachment of clay particles too which leads to fines migration and formation damage (Jackson et al., 2016).

The double layer expansion model assumes that the oil/brine interface or the polar oil components and the mineral surface have the same polarity at the reservoir pH. However, this assumption is inconsistent with the mineral surface scale adhesion tests which indicate increased adhesion of oil when salinity is decreased but the pH is fixed (Jackson et al., 2016). Also, for low salinity effect to take place effectively (and thus oil recovery in tertiary recovery mode), these double layers need to be continuous at the reservoir conditions which is not the case when the reservoir has been depleted by secondary recovery mode. This discrepancy in the continuity of the oil phase where there is residual oil by itself would not allow the formation of a continuous double layer.

Based on the above review, it has widely been observed that researchers remain inconclusive over the mechanism of oil recovery by LSWI which necessarily means that low salinity effect does not always occur. Thus, there is a need to augment the effect of low salinity water using additives and/or by changing the composition of the brine itself. Earlier, a few attempts have been made to use a low dosage of surfactants in combination with low salinity water. It was proposed that residual oil recovery (tertiary mode) will be effective when a suitable type of surfactant is mixed with the low salinity brine in an appropriate concentration. The use of surfactant, which is already known to be effective in tertiary recovery by surfactant flooding, can compensate for the discrepancies caused due to discontinuity of the electric double layer. The use of additives such as nanoparticles has also gained attention recently due to its effectiveness in rock surface wettability control, which, however, has never been investigated in a low salinity water injection scenario. Thus, the effect of additives in oil recovery through IFT reduction, surfactant adsorption control, wettability alteration, multi-ion exchange in low salinity conditions will be of the prime focus throughout this research.

Water salinity plays an important role and a common point in both surfactant and low salinity water flooding. At an optimal salinity, the surfactant solution has ultralow interfacial tension with oil phase (Alagic and Skauge, 2010; Khanamiri et al., 2016; Tichelkamp et al., 2014) and the degree of solubility of oil in the aqueous phase is equal to the degree of water solubility in the oil phase. Surfactants are the surface-active agents that reduce the interfacial tension (IFT) at the interface of the two fluids by their spontaneous self-assembly. They have been applied in various engineering, science, and technological applications. One of their important applications of surfactants is in subsurface enhanced oil recovery (EOR) process for matured crude oil reservoirs which have been so far successfully applied all over the world (Babadagli, 2007; Iglauer et al., 2010; Sharma et al., 2016, 2015). Their amphiphilic nature governed by their structure enables them to get dissolved in aqueous and various non-aqueous

phases. Their affinity and preference for phases is related to their critical packing parameter (CPP) which is a value relating the structure of a surfactant [volume of the hydrophobic tail (V_L), chain length (l_c) of the hydrophobic tail and area occupied at interface by its head group (a_s)] to the shape of its aggregates (Wang, 2010). Hydrophile-lipophile balance (HLB) is also a well-known structural parameter of surfactants. Surfactants are categorized into four main groups: anionic, cationic, zwitterionic and non-ionic based on the charge of the hydrophilic group. The surfactant solution has ultralow interfacial tension with an oil phase at optimal salinity. While the degree of solubility of oil in the aqueous phase is equal to the degree of water solubility in the oil phase. In a work reported in 2010 by Algaic and Skauge, it was found that surfactant injection after low salinity flooding in a core flooding experiment gives high oil recovery by tertiary method (Alagic and Skauge, 2010). In a work by Khanamiri et al. (2016), they too reported a similar recovery by low salinity surfactant (LSS) and optimal salinity surfactant. It was found that rock-fluid interaction in LSS had a stronger role than in optimal salinity surfactant flooding.

Several researchers have investigated the effect of salinity in combination with ionic surfactants on IFT of the hydrocarbon/brine system. Some of them found that in the presence of ionic surfactants in solution, an increase in salinity decreases the IFT (Hamouda and Karoussi, 2008). They proposed several mechanisms for this effect. The decrease in IFT may be due to the increase in the activity coefficient of the surfactant with an increase in the ionic strength (Gurkov et al., 2005). Enhancement in the adsorption of surfactants at the interface due to the increase in salt concentration can decrease the IFT (Prosser and Franses, 2001). However, these investigations were mostly carried out at high salinity conditions. Although surfactant can reduce the interfacial tension between oil and water to a very low value, its loss due to adsorption on the rock surface may occur (Iglauer et al., 2011). The reduction of surfactant adsorption on the reservoir rock surface is detrimental to the success of the oil

recovery technique (Ahmadall et al., 1993; Wu et al., 2017). Some work in the last few years has been reported that shows that reduction of surfactant adsorption is possible by using different additives (Figure 1.3) (Ahmadi and Shadizadeh, 2012; Shamsijazeyi et al., 2013).

Research and development related to nanoparticle use in an upstream application are gaining attention recently (Boul and Ajayan, 2020). The nanomaterials developments for their application in the domain of well construction, oil and gas production and reservoir management is advancing in steps (Boul and Ajayan, 2020). Nanoparticles are being considered in the chemical flooding process (Mohajeri et al., 2015) while researchers have also investigated the effect of nanoparticles on surfactant adsorption (Wu et al., 2017). Nanoparticles are also being considered a wettability modifier, but this research is in a very nascent stage. Moreover, nanoparticles application in the low salinity context will gradually be discussed as this thesis progress.

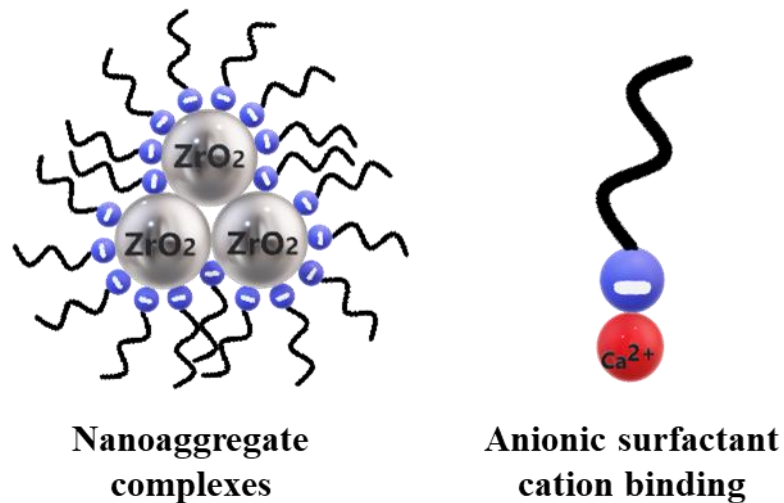


Figure 1.3 Nanoparticles and surfactants as additives

1.2 OBJECTIVE OF THE WORK

The objective of this research is to improve the performance of low salinity water injection (LSWI) using low-cost additives and investigate the mechanism of recovery through the scrutiny of oil-brine rock interactions.

1.3 SCOPE OF THE THESIS

The scope of the work is provided below.

- Formulation of low salinity injection fluid containing a surfactant, nanoparticles, and determination of IFT between the liquid and model oil under varying concentrations at low salinity. Qualitative and quantitative information was gathered to see the effect of additives to reduce the IFT of the injection fluid and model oil (at IIT Madras).
- To investigate wettability studies using rock representative substrate by the centrifuge method for various advanced LSWI flood system (at IIT Madras).
- To investigate oil-brine-rock interaction for determination of wettability alteration, additives adsorption by clay, the effect of pH and effect of salinity through analytical and coreflood methods at ambient/reservoir conditions (at IIT Madras and Curtin University, Australia).
- To carry core/microscale flood experiments to determine the recovery efficiency of this method both in secondary and tertiary mode (at Curtin University, Australia).
- To understand the pore structure of reservoir core plugs, multi-phase fluid saturation profile, and physics of flow within the pore network by flow visualization utilizing a micro-CT scan (at Curtin University, Australia).

CHAPTER 2

EFFECT OF SALT TYPE ON THE INTERFACIAL TENSION BETWEEN OIL AND AQUEOUS PHASE

2.1 INTRODUCTION

Surfactants reduce the interfacial tension (IFT) at the interface of two immiscible fluids, and these surface-active properties of surfactants have been exploited in various engineering, scientific and technological applications (Binks, 2002; Hunter et al., 2008; ShamsiJazeyi et al., 2014). One important application of surfactants is subsurface enhanced oil recovery (EOR), where additional oil is extracted from matured crude oil reservoirs (Babadagli, 2007; Iglauer et al., 2010; Sharma et al., 2015; Li et al., 2016; Nwidee et al., 2016; Sharma et al., 2016; Guo et al., 2017). The amphiphilic (having both hydrophilic and lipophilic part) nature of the surfactants, which is governed by their chemical structure enables them to dissolve in aqueous and various non-aqueous phases (Tichelkamp et al., 2014). Surfactant affinity and preference for specific phases is related to their critical packing parameter (CPP), which again is a value relating the structure of the surfactant [i.e., volume of the hydrophobic tail (V_L), chain length (l_c) of the hydrophobic tail, and area occupied at the interface by its head group (a_s)] to the shape of its aggregates (Wang, 2010).

$$CPP = \frac{V_L}{a_s l_c} \quad (2.1)$$

The hydrophile-lipophile balance (HLB) is also a well-known structural parameter classifying surfactants (Wang, 2010). Generally, surfactants are categorized into four main groups: anionic, cationic, zwitterionic and non-ionic based on their charge of the hydrophilic group. Although a large amount of work has been carried out (Tang and Morrow, 1999; Morrow and

Buckley, 2011; Hadia et al., 2012, 2013; Tichelkamp et al., 2014; Chavez-Miyauchi et al., 2016; Hosseinzade Khanamiri, et al., 2016a; Tavassoli et al., 2016), there is a lack of data for low salinity floods, which are a relatively new development (Chavez-Miyauchi et al., 2016; Hamon, 2016).

In this context water salinity plays a key role in both surfactant and LSW flooding (Al-Shalabi and Sepehrnoori, 2016). At optimal salinity, the aqueous surfactant solution has an ultralow interfacial tension (IFT) with the oil phase (Iglauer et al., 2009, 2011; Alagic and Skauge, 2010; Wu et al., 2010; Tichelkamp et al., 2014; Hosseinzade Khanamiri et al., 2016a) and the solubility of oil in the aqueous phase is equal to the water solubility in the oil phase (Tichelkamp et al., 2015).

However, the IFT behavior between low salinity water and an oleic phase in presence of low surfactant concentrations is a lesser known phenomenon (Hamon, 2016). As per our knowledge there are rare directly relevant data available in the present context. However, there is some evidence suggesting that IFT reduction by surfactants at the non-polar oleic (such as n-heptane) phase – aqueous solution interface is similar in many aspects to surface tension reduction at the air – aqueous solution interface as the air contains mainly non-polar molecules (Rosen and Kunjappu, 2012). Historically, in the context of low salinity systems, Jones and Ray published several papers during 1935-42 related to the surface tension of aqueous electrolyte solutions at dilute concentrations (Jones and Ray, 1935, 1937, 1941a, 1941b, 1942). They measured the minimum in the surface tension for 13 different salts near a very low salt concentration for respective measurements. This observation was first reported by them which is widely known as the ‘Jones-Ray effect’ (Petersen and Saykally, 2005). In each of the experiment, initially a decrease in surface tension was observed until a minimum followed by an increase in surface tension with increase in salt concentration. This implies a net surface excess of the ions and decrease in the surface tension till the minimum surface tension in the

surface tension-aqueous salt concentration curve is reached. Dole (Dole, 1938) was the first who presented a model for this surface tension dependence; his model explained the negative slope and minimum in the surface tension-aqueous salt concentration curve. He concluded that the Onsager equations (Onsager and Samaras, 1934) may be applicable over a limited concentration range (for concentrations above the salt concentration at which minimum surface tension in the surface tension-aqueous salt concentration curve is reached), while there were no theories which were sufficiently adequate to explain the ‘Jones-Ray effect’. However, Petersen and Saykally (Petersen and Saykally, 2005) reported the most relevant study by demonstrating the ‘Jones-Ray effect’. Their model captured the effect by re-defining the Langmuir adsorption isotherm; this is thus a variation of Dole’s model. In this work, a similar IFT effect between low salinity water (9.010 – 119.780 mM salinity) formulated with lowly concentrated anionic surfactants (0.141 – 2.167 mM) and n-heptane as oleic phase and identified minimum IFTs have been shown. Importantly, this IFT effect was not reported earlier for such low salinity-surfactant formulations. It is widely accepted that the minimum IFT is found at the vicinity of the critical micellar concentration (CMC) (Rosen and Kunjappu, 2012; Nwidae et al., 2016; Fu et al., 2017). Evidence also suggests that a middle phase microemulsion may form when cosurfactants are used, which reduces IFT to a very low value (Iglauer et al., 2009, 2011). The surface pressure at this point is the suitable measure of the effectiveness of a surfactant in terms of reducing IFT. If the solubility of a surfactant is below the CMC at a specific, constant temperature, then the minimum IFT is achieved at the point of maximum solubility. If the maximum solubility of an ionic surfactant becomes equal to that of CMC at a given temperature, then this temperature is known as Krafft point. For all practical purpose, here anionic surfactant is used above this Krafft point.

In addition it has been demonstrated that anionic surfactant can react with divalent cations and precipitate (Rodriguez et al., 2001; Maneedaeng and Flood, 2016), which

negatively impacts on IFT. The precipitate was thoroughly characterized using XRD and SEM analysis. Moreover, the Petersen and Saykally model discussed above, with a suitable modification was used to determine the thermodynamic parameters required for IFT calculation and verified with the experimental IFT values measured. The model was subsequently used to determine the maximum interface coverage by surfactant molecules with increasing salt concentration in the low concentration range.

2.2 MATERIALS AND METHODS

2.2.1 Materials

Sodium chloride (NaCl, ≥ 99 % mass fraction) and Calcium chloride (CaCl₂, ≥ 98 % mass fraction) were used as mono- and divalent background salts. Sodium dodecyl sulphate (SDS, ≥ 99 % mass fraction) and dioctyl sulphosuccinate sodium salt (AOT, ≥ 97 % mass fraction) were the two anionic surfactants used, and n-heptane (99 % mass fraction purity) was used as an oleic phase (Tichelkamp et al., 2014), Table 2.1.

Table 2.1 List of Chemicals Used in This Study

| Chemical Name | Source | Purity (mass fraction) | CAS Number |
|--|---|------------------------|------------|
| Sodium chloride (NaCl) | Merck Specialities Private Limited, Mumbai, India | ≥ 0.99 | 7647-14-5 |
| Calcium chloride (CaCl ₂) | Alfa Aesar, England | ≥ 0.98 | 10043-52-4 |
| n-heptane | Alfa Aesar, England Sisco Research Laboratories Pvt. Ltd., Taloja, Maharashtra, India | 0.99 | 142-82-5 |
| SDS | Sigma-Aldrich, USA | ≥ 0.99 | 151-21-3 |
| AOT | Sigma-Aldrich, USA | ≥ 0.97 | 577-11-7 |

Aqueous solutions of individual salts and surfactants were prepared using ultrapure water of 18.2 M Ω .cm resistivity, 71.6 mN/m surface tension measured against air, and 6.6-7.1 pH measured using a pH meter (PC 2700, EUTECH Instruments, USA) at 298.15 K.

2.2.2 Method

All salt solutions were prepared gravimetrically using a LC GC RADWAG AS/X 220 analytical balance with ± 0.00004 mass fraction uncertainty. The IFT between different salt solutions containing surfactants and n-heptane were measured by the Wilhelmy plate method (Wilhelmy, 1863) using a tensiometer (DCAT 11EC, Dataphysics, Germany). 80 ml of salt solution of varying surfactant concentrations and 40 ml of n-heptane were prepared as described earlier (Sakthivel et al., 2015a, 2015b; Kakati and Sangwai, 2017). The aqueous phase solutions were prepared using a magnetic stirrer (IKA[®] big squid, Germany) at 400-600 rpm at 298.15 K. In the Wilhelmy plate technique the gravitational force of the lamella that forms when the Wilhelmy plate (type PT 11, made of platinum-iridium, thickness of 0.2 mm and length 19.9 mm) stands at the interface between the two liquids is measured. The plate itself is located inside the upper (lighter) phase where it experiences a buoyancy force. To compensate for this effect, the Wilhelmy plate is initially submerged completely in the lighter phase in a separate vessel and in this state, the weighing balance (inbuilt) is tared automatically. Once the buoyancy effect is compensated, the vessel with the lighter phase is replaced with a vessel with the heavier phase. To form the interfacial lamella, the Wilhelmy plate is then partially submerged into the heavier phase and pulled back to the heavier phase-air interface. On top of the heavier phase, a layer of the lighter phase is carefully filled until the Wilhelmy plate is submerged completely. Now the measured weight is equal to the gravitational force of the interfacial lamella and the IFT can be calculated according to the Wilhelmy equation. The measured weight of the interfacial lamella (and the calculated IFT) is continuously monitored

over the display panel and logged throughout the elapsed experimental time. The measured weight of the interfacial lamella oscillates initially due to disturbance caused at the interface when a layer of the lighter phase is filled. The period of no variation in measured weight is considered stable. In this work, IFT measurements were taken to collect 30-40 data points in the stable region over a 60-90-minute time span. Precautions were taken to avoid evaporation of the volatile hydrocarbon liquids. For this, the tensiometer door was kept closed and a small volume of hydrocarbon liquid was introduced inside the tensiometer to saturate the air. Humidity was controlled with a silica gel (60-120 mesh). The reported IFT values are average values along with their uncertainty which is provided in a separate supporting document (provided in Tables S1, S2 and S3 in the Supporting Information).

Sodium chloride (NaCl) and calcium chloride (CaCl₂), i.e., monovalent and divalent cations, and anionic surfactants as secondary salts [sodium dodecyl sulfate (SDS) and dioctyl sulfosuccinate sodium salt (AOT), commonly known as aerosol OT or docusate], were used for the formulation of aqueous solutions. SDS [Scheme 1(a)] is the most commonly used surfactant (molecular weight of 288.38 g/mol), and its use dates back to the 1940 (Putnam and Neurath, 1944). AOT [Scheme 1(b)] has a molecular weight of 444.56 g/mol and its micelle has a special counterion binding effect suitable for IFT reduction (Dey et al., 2010). This special counterion binding effect of AOT in the presence aqueous NaCl solutions increases twofold abruptly for NaCl concentration above 0.015 mol/kg; this is related to a shape change of the micelle formed by AOT (Dey et al., 2012). AOT is thus considered to be the only anionic surfactant whose micelle undergoes a shape change in the presence of sodium ions, while for other anionic surfactants such a shape change can only take place in the presence of multivalent counterions at low concentrations (Alargova et al., 2003; Petkov et al., 2010).

Table 2.2 Concentration of Salts and Surfactants Used in the Aqueous Solution

| NaCl conc. (mM) | CaCl ₂ conc. (mM) | SDS conc. (mM) | AOT conc. (mM) |
|--------------------|---------------------------------|-------------------|-------------------|
| 17.110 | 9.010 | 0.217 | 0.141 |
| 59.890 | 31.530 | 0.433 | 0.562 |
| 119.780 | 63.070 | 0.867 | 0.844 |
| | 126.150 | 1.300 | 1.125 |
| | | 1.730 | 1.406 |
| | | 2.167 | |

Standard uncertainty is $u(\text{conc.}) = 0.001 \text{ mM}$

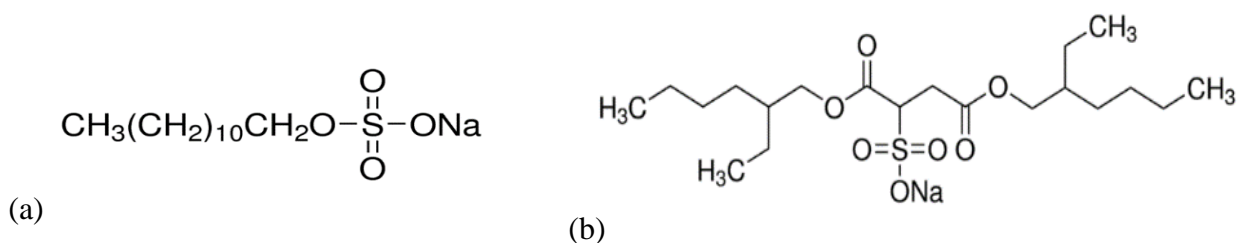
**Scheme 1.** Chemical structures of (a) SDS; (b) AOT.

Table 2.2 summarizes salts and anionic surfactants concentration used in aqueous solutions. Krafft point of SDS and AOT is 280.65 K and 304.15 K, respectively (Fu et al., 2017). So, all IFT measurements in this work were carried out at $313.15 \pm 0.1 \text{ K}$.

2.3 RESULTS AND DISCUSSION

2.3.1 Effect of SDS Concentration on IFT

Initially, the IFTs between aqueous NaCl solutions (17.110 mM NaCl) formulated with varying SDS concentrations against n-heptane were measured, Figure 2.1 (and Table S1, supporting information). A minimum IFT ($= 4.840 \text{ mN/m}$) was observed at 1.730 mM SDS concentration. The IFT measurements were repeated for the same SDS concentrations at

59.890 mM NaCl concentration; now the minimum IFT (3.562 mN/m) was observed at 0.867 mM SDS concentration. Similarly, the experiments were carried out for 119.780 mM NaCl concentration and a minimum IFT value of 3.180 mN/m at 0.433 mM SDS concentration was measured (Table S1). This indicates that as brine salinity increases, the SDS concentration required to achieve minimum IFT decreases. These points were much below the literature reported CMC value (8 mM) of SDS (Zhang et al., 1999).

The minima in the IFT curve is due to an increase in interface excess surfactant concentration. As the availability of counterions increases, an increase in counterion binding neutralizing the negatively charged micellar surface (Maneedaeng et al., 2012) results in a smaller electrical repulsion between already adsorbed surfactant ions and surfactant ions moving towards the interface. Mechanistically, a decrease in electrical repulsion between the similarly charged hydrophilic heads of the surfactant molecules permits closer packing at the interface (Connor and Ottewill, 1971; Rosen and Kunjappu, 2012). Salinity increase increases counterion binding and decreases the surfactant head group area (Asakawa et al., 2001). The slope of the respective curves for each salt solution gradually increases with an increase of bulk phase surfactant concentration, which is caused by an increase in the surfactant interface excess, until the point of minimum IFT (Rosen, 1976; Sandoval et al., 2014) (Figure 2.1). Thus, the experimental IFT data are in good agreement with the literature data on n-heptane – [20 mM NaCl + 1.25 mM sodium dodecylbenzenesulfonate (SDBS)] aqueous solution (pH range of 2.25 – 10.19) which were in the range of 1.648 – 2.905 mN/m at 298.15 K and 2.603 mN/m (at 8.24 pH) at 333.15 K (Tichelkamp et al., 2014). However, variation of surfactant and salt concentrations in the aqueous solution resulted in a minimum on the IFT curve. It has been observed that the IFT change depended more on a change in salt concentration than on a change in surfactant concentration for lower surfactant concentrations.

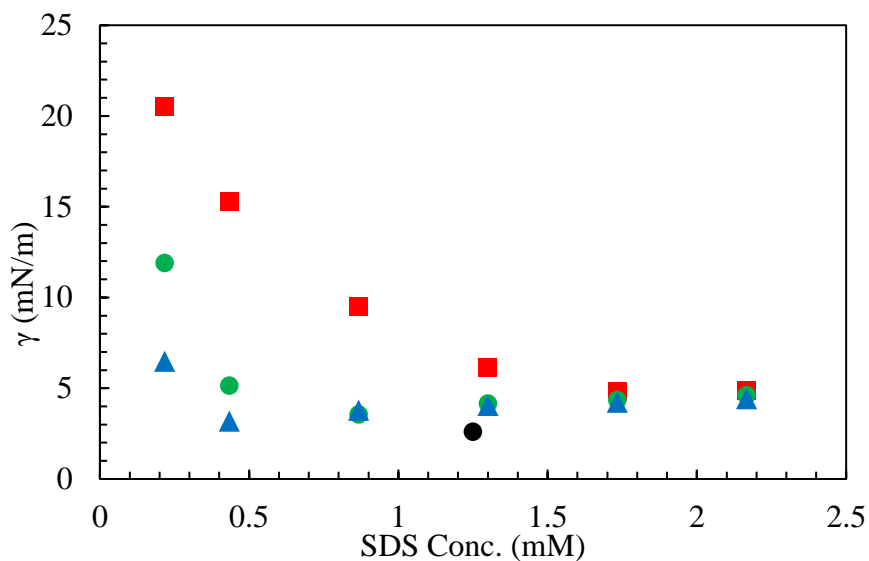


Figure 2.1 Experimental values on γ for n-heptane - (NaCl + SDS) aqueous solution at 313.15 ± 0.1 K, ■, 17.110 mM NaCl + SDS; ●, 59.890 mM NaCl + SDS; ▲, 119.780 mM NaCl + SDS; ●, Tichelkamp et al. (2014)

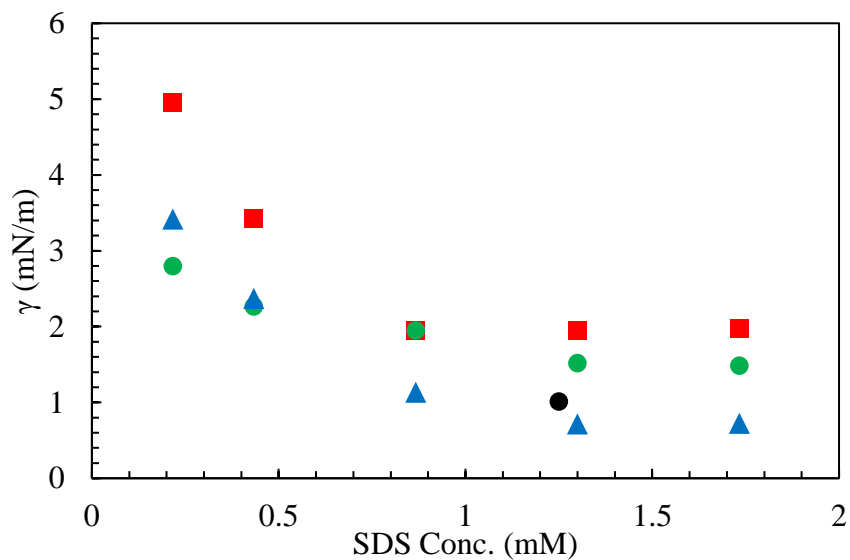
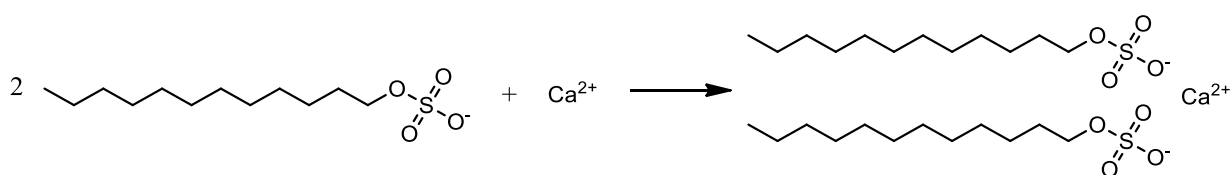


Figure 2.2 Experimental values on γ for n-heptane - (CaCl₂ + SDS) aqueous solution at 313.15 ± 0.1 K, ■, 9.010 mM CaCl₂ + SDS; ●, 31.530 mM CaCl₂ + SDS; ▲, 63.070 mM CaCl₂ + SDS; ●, Tichelkamp et al. (2014)

In another set of experiments, aqueous (CaCl₂ - SDS)/n-heptane IFTs were measured, Figure 2.2 (and Table S2, supporting information). As expected, IFT decreased significantly with increasing SDS concentration (0.867 mM, 1.730 mM and 1.300 mM at 9.010 mM, 31.530 mM and 63.070 mM CaCl₂ concentrations, respectively), but also with an increase in CaCl₂ concentration (except at 0.217 mM and 0.433 mM SDS concentration). In addition, experiments at 126.150 mM CaCl₂ concentration (at 0.217 mM, 0.867 mM and 1.730 mM SDS) have been carried out to systematically test the influence of CaCl₂ concentration; clearly an increasing CaCl₂ concentration increases IFT.

The IFT data obtained are in good agreement with the literature data on n-heptane – aqueous solution which were in the range of 0.961 – 1.447 mN/m at 298.15 K and 1.011 mN/m at 333.15 K (Tichelkamp et al., 2014). The addition of Ca²⁺ ions into the aqueous phase causes more counterion binding to the surfactant micelles permitting an increase in adsorption of surfactant molecules at the interface (Rosen and Kunjappu, 2012). Since Ca²⁺ ions carries a greater charge and is more polarizable than a sodium Na⁺ ion, it can strongly bind to the surfactant micelles.⁵⁴ This phenomenon neutralizes surfactant micelles more effectively, thereby moving surfactant molecules to the interface from the bulk due to a decrease in repulsion (Rosen and Kunjappu, 2012). However, a chemical reaction also occurs; the DS⁻ molecules and Ca²⁺ ions react to calcium dodecyl sulphate, Ca(DS)₂, which has a low solubility product and thus precipitates (Maneedaeng and Flood, 2016), (Scheme 2):



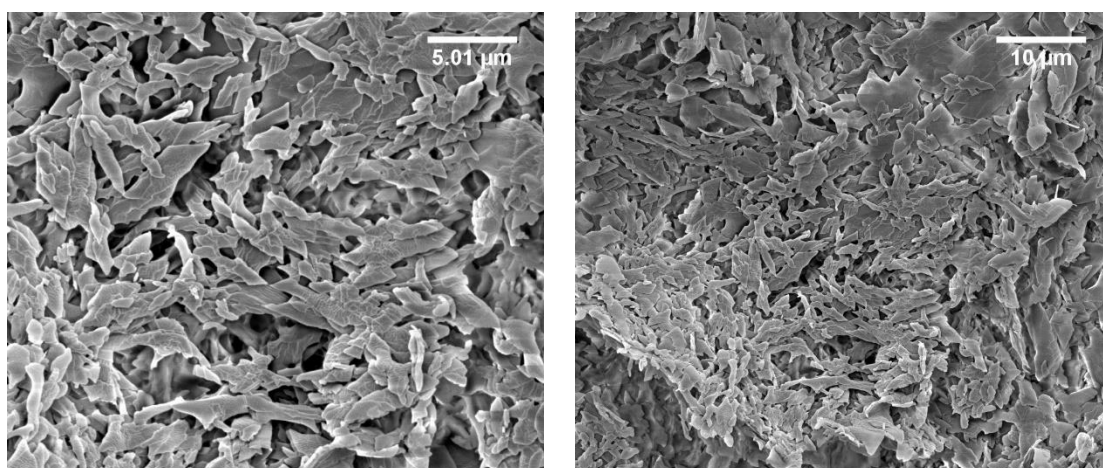
Scheme 2. Reaction scheme of DS⁻ molecules and Ca²⁺ ions.

Thus, addition of CaCl_2 into the solution was more effective in terms of IFT reduction than the addition of NaCl ; however, in presence of excess SDS (≥ 1.300 mM at 31.530 mM and 63.070 mM CaCl_2), precipitate formed which resulted in an IFT increase as surfactant molecules were removed from the interface. This precipitate was characterized as follows.

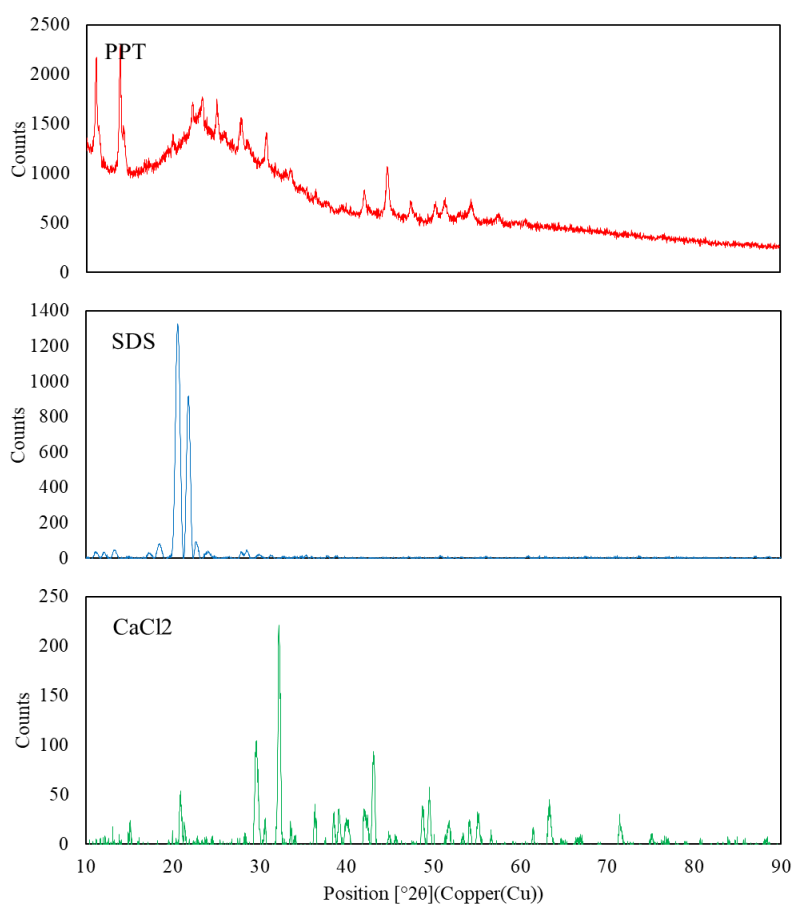
2.3.2 Characterization of Precipitate

The SDS- CaCl_2 precipitate was separated out using a 2.7 μm cellulose filter paper (Whatman 542) from the aqueous solution (initially containing 1.730 mM SDS and 63.070 mM CaCl_2). The precipitate was rinsed with deionized cold water and dried over silica gel for 24 hours. Then the precipitate was characterized by X-ray powdered diffraction (XRPD) using a X'Pert Pro PANalytical diffractometer with $\text{Cu K}\alpha$ (30 mA/45 kV) radiation to determine its structure. The instrument was operated with a step size of 0.017 $^\circ 2\theta$ angle while the data collection was from 10-90 $^\circ 2\theta$ angle. XRD analysis was also carried out for SDS and CaCl_2 at the same setting for comparison. Furthermore, a scanning electron microscope (SEM) (FEI Inspect F50) was used to examine the morphology of the precipitate, [Figure 2.3(a)]. Energy dispersive spectroscopy (EDS) was also performed to determine the composition of the precipitate.

The precipitated crystals were not fully grown, and later it was revealed by XRD that it was of semi-crystalline nature. Elongated flat plates, mostly trapezoidal and rhombic in shape were observed that are consistent with literature reported morphology of $\text{Ca}(\text{DS})_2$ (Rodriguez et al., 2001; Maneedaeng and Flood, 2016). EDS analysis (Table 2.3) showed that sodium ions had no role in the precipitation due to its replacement by Ca^{2+} ions in the surfactant molecules. The XRD pattern of the precipitate resembled that of a semi-crystalline material as the hump in the background with peaks could be clearly seen (Ostrowski et al., 2015), [Figure 2.3(b)].



(a)



(b)

Figure 2.3 (a) SEM image of precipitate formed from an aqueous solution containing 1.730 mM SDS and 63.070 mM CaCl_2 at 313.15 K; (b) XRD pattern of precipitate (PPT), SDS and

CaCl_2

Table 2.3 Compositional Data of Precipitate From Energy Dispersive Spectroscopy

| Element | w | Error % |
|---------|-------|------------|
| C | 0.651 | 7.7 |
| O | 0.170 | 10 |
| S | 0.100 | 3.5 |
| Cl | 0.001 | 61.6 |
| Ca | 0.074 | 6.3 |

On contrary, clear and sharp peaks were visible for SDS due to its crystalline nature. CaCl_2 got hydrated during the XRD run but showed diffraction peaks after removal of noise using a Fourier filter incorporated in the XRD interpretation tool. However, no quantitative information could be gathered from the XRD pattern of the precipitate.

2.3.3 Effect of AOT Concentration on IFT

Several aqueous (AOT- NaCl) - n-heptane IFT measurements were conducted to study the effect of AOT and salinity on IFT. Initially, a minimum IFT of 0.631 mN/m (at 17.110 mM NaCl) at 1.406 mM AOT was measured, Figure 2.4, while IFT decreased with increasing AOT concentration. Further, the minimum IFTs (0.161 mN/m and 0.302 mN/m) were at 1.406 mM AOT (at 59.890 mM NaCl) and at 0.281 mM AOT (at 119.780 mM NaCl) concentrations, respectively (Table S3). An IFT of 0.161 mN/m was the lowest value observed in this work (Figure 2.4). Literature CMC values of AOT in presence of NaCl in aqueous solution at 298.15 K are 1.070 mM, 0.470 mM and 0.280 mM at 0.0197 mol/kg, 0.0612 mol/kg and 0.1188 mol/kg NaCl concentrations, respectively (Umlong and Ismail, 2005). Further, these data are in good agreement with the literature IFT data on n-heptane – (20 mM NaCl + 2.47 mM AOT) aqueous solution which were 0.140 mN/m (at 6.2 pH) at 298.15 K and 1.1 ± 0.1 mN/m (at 6.5 pH) at 333.15 K, respectively (Tichelkamp et al., 2014). Besides, on contrary, minima was observed

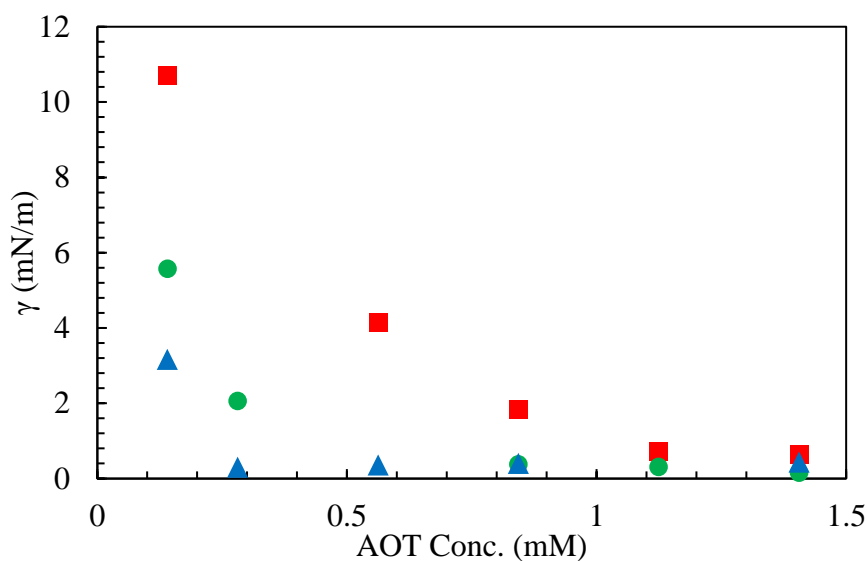


Figure 2.4 Experimental values on γ for n-heptane - (NaCl + AOT) aqueous solution at 313.15 ± 0.1 K, ■, 17.110 mM NaCl + AOT; ●, 59.890 mM NaCl + AOT; ▲, 119.780 mM NaCl + AOT in two IFT curves for (AOT- NaCl) - n-heptane at 59.890 mM and 119.780 mM NaCl concentration. Also, unlike the CaCl_2 -SDS combination, no precipitation occurred due to ion interactions.

The lowest IFT value reflects the balance between the hydrophilic and hydrophobic nature of AOT. It has been shown that HLB is related to the structural parameter, CPP, of the surfactant (Wang, 2010). When CPP is close to 1, a tight packing of surfactant molecules at the oil-water interface leads to a minimum IFT value (Tichelkamp et al., 2014). For other salt concentrations, it has either a dominating hydrophobic or hydrophilic nature, thus the IFT increases as CPP deviates from unity, which indicates unfavorable packing at the interface. At 119.780 mM NaCl concentration, the minimum IFT increased again to 0.300 mN/m at 0.281 mM AOT concentration. AOT is found to have special counterion binding behavior in aqueous salt solution (Umlong and Ismail, 2005; Dey et al., 2010; Dey, Thapa and Ismail, 2012; Pang et al., 2016). The addition of counterions reduces the electrostatic repulsion between different

AOT headgroups. Thus, AOT molecules are expected to be closely packed at the oil-water interface and increase their degree of order at points of minimum IFT. Literature IFT data on n-heptane – (18.78 mM NaCl + 0.41 mM NaCl + 2.47 mM AOT) aqueous solutions were 0.029 mN/m (at pH 6.2) at 298.15 K and 0.004 mN/m (at 7 pH) at 333.15 K, respectively (Tichelkamp et al., 2014). However, in this work, both surfactant and ion concentration in aqueous solution were varied to observe minima in the various IFT curves. Furthermore, as for the aqueous (NaCl – SDS)/n-heptane combination, it was observed that the IFT change depended more on a change in salt concentration than on a change in surfactant concentration for lower surfactant concentrations.

2.3.4 IFT Model

Petersen and Saykally (2005), with slight modification of Dole's (Dole, 1938) model, derived a surface tension model which was verified by Jones and Ray (Jones and Ray, 1935, 1937, 1941a, 1941b, 1942) experimental data. Petersen and Saykally's model uses water, cation and anion density profiles adapted from molecular dynamics (MD) simulations, (Jungwirth and Tobias, 2002) in which the interfacial boundaries, including the Gibbs dividing surface are defined. One major theoretical issue that has been dominating the development of isotherm equations are specific assumptions which are either preferentially selected or often ignored while choosing and applying adsorption equations (Liu, 2009; Michalkova et al., 2011). Thus, selection bias is a potential concern because of the complex adsorption mechanism (Liu, 2009). Thus, the model developed here, after further modification, has a limited application to low salinity and low surfactant concentration ranges only and cannot not be generalized. Assuming that the interfacial region between the organic and aqueous phase is fully occupied by anionic surfactant molecules, a slightly modified Petersen and Saykally model is used here to fit the experimental IFT data (water/n-heptane in presence of surfactant and salts) and to evaluate IFT

variations with salt and surfactant concentrations. In Petersen and Saykally's model interface anion adsorption is represented by the Langmuir adsorption isotherm:

$$N_S = \frac{N_S^{max} \times KC}{C_w + KC} \approx \frac{N_S^{max} \times C}{C + 55.5M \times e^{(\Delta G_{ads}/RT)}} \quad (2.2)$$

where, N_S is the surface concentration of the anion, N_S^{max} is the maximum obtainable surface concentration, K is the equilibrium constant for occupying a surface site, C_w is the water concentration (which is 55.5 M), C is the bulk surfactant concentration, T is temperature (K), and ΔG_{ads} is the Gibbs free energy of adsorption. The equation for surface excess (Γ) of the anion is then given by,

$$\Gamma_- = N_S - dCv_- = \frac{N_S^{max} K' C v_-}{1 + K' C v_-} - dCv_- \quad (2.3)$$

where, d is the interfacial depth and v_- is the stoichiometric number of anions in the surfactant.

The Langmuir constant K' is given by,

$$K' = \frac{K}{55.5M} = \frac{1}{55.5M \times e^{(-\Delta G_{ads}/RT)}} \quad (2.4)$$

Thus, by neglecting the second term of the right-hand side of the equation (3) due to the introduction of a parameter a and the large value of the first term, the modified Γ equation is,

$$\Gamma_- = \frac{aN_S^{max} K' C v_-}{1 + K' C v_-} \quad (2.5)$$

where, a is a surfactant-salt pair specific constant.

The interfacial region is electrically neutral (Petersen and Saykally, 2005), i.e., $v_- \Gamma_-$ equals $v_+ \Gamma_+$ (v_+ is the stoichiometric number of cations). Thus, the surface excess cation is,

$$\Gamma_+ = \frac{aN_S^{max} K' C v_+}{1 + K' C v_-} \quad (2.6)$$

The IFT difference, $\Delta\gamma$, between the hydrocarbon-low salinity aqueous surfactant solution IFT and, γ and the hydrocarbon-water interfacial IFT, γ_o was found by integrating the Gibbs adsorption (Petersen and Saykally, 2005):

$$\Delta\gamma = \gamma - \gamma_o = RT \int_0^C (\sum_i \Gamma_i) d \ln C \quad (2.7)$$

where, R is the universal gas constant. γ_o (49.38 mN/m) was taken from the literature (Tong et al., 2010; Zhang et al., 2014). The net interface excess can then be substituted (Petersen and Saykally, 2005):

$$\sum_i \Gamma_i = \Gamma_- + \Gamma_+ = \frac{aN_S^{max} K' C (v_- + v_+)}{1 + K' C v_-} \quad (2.8)$$

Thus, from equations (4), (7) and (8),

$$\Delta\gamma = -RT a N_S^{max} \left(\frac{v_- + v_+}{v_-} \right) \ln \left(1 + \frac{1}{55.5 M \times e^{(-\Delta G_{ads}/RT)}} C v_- \right) \quad (2.9)$$

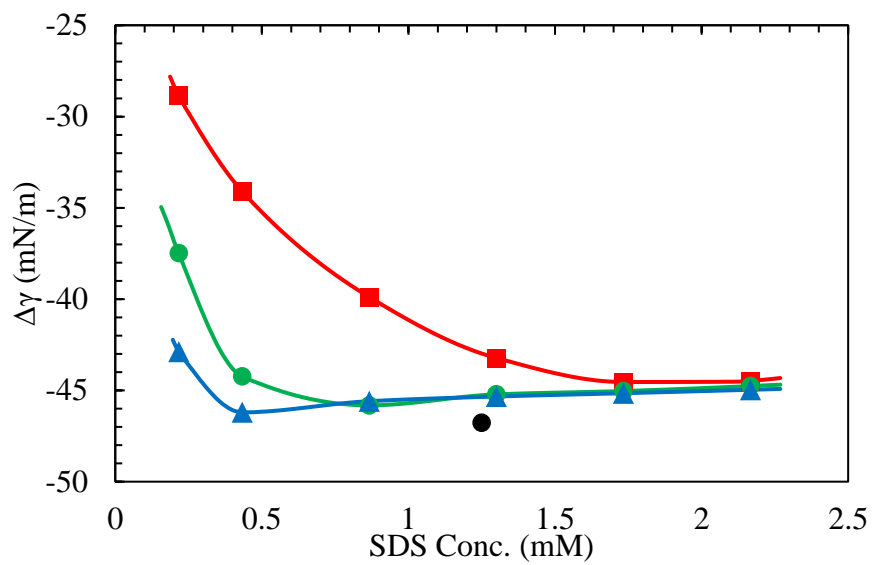
This model has three adjustable parameters: a , N_S^{max} and ΔG_{ads} .

In the calculation of the Langmuir constant K' from equation (4), the value of ΔG_{ads} is to be adjusted, as it is a function of concentration of chemical species at the interface

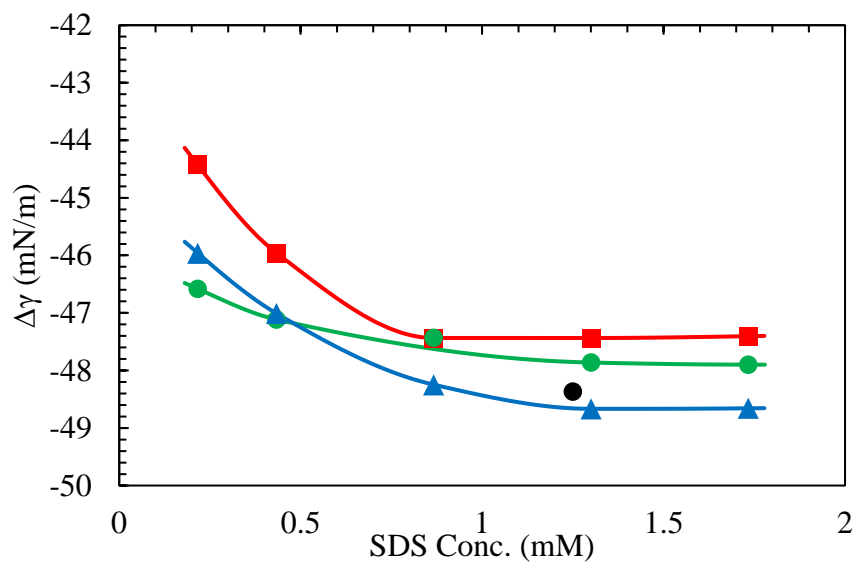
(Michalkova et al., 2011). Derived equation (9), the model, by non-linear regression of those three adjustable parameters, is used to calculate the $\Delta\gamma$ data. The values of the parameters a , N_S^{max} and ΔG_{ads} obtained are shown in Table 2.4. From this, a N_S^{max} value in the range of $2.7\text{-}3.6 \times 10^{-10}$ mol/cm², and a value of a in the range of $3.22\text{-}9.24 \times 10^8$ is obtained, depending on the type of anionic surfactant-salt combination used. Regressed ΔG_{ads} values are found to be in logarithmic relation with surfactant concentration (C),

$$\Delta G_{ads} = -RT(m \ln C + c) \quad (2.10)$$

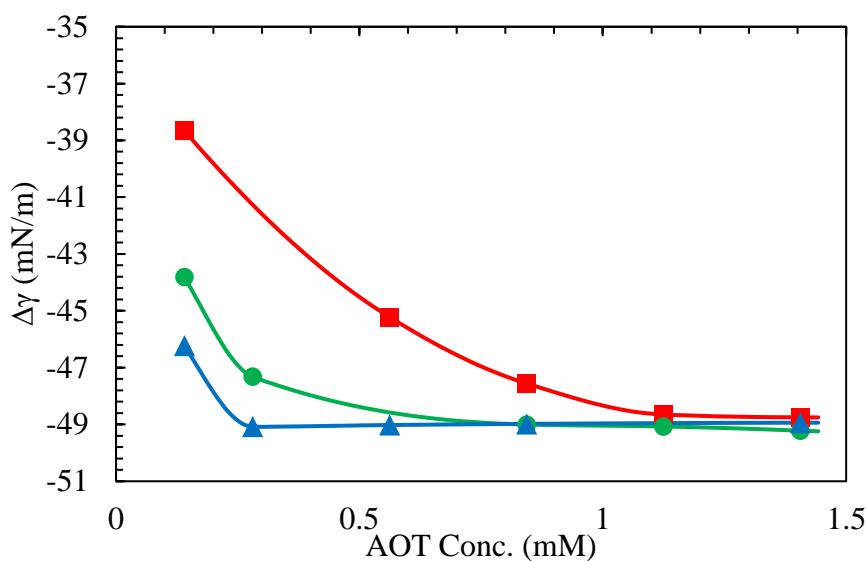
where, ΔG_{ads} is in J/mol, C is concentration in M, $-RTm$ is slope and $-RTc$ is constant (where, m is in M⁻¹ and c is dimensionless). Figure 2.5 represents the model (equation 9) for $\Delta\gamma$ which adequately captures the experimental $\Delta\gamma$ values. The model is only applicable at dilute concentrations as it does not account for the deviation due to ion activities (Petersen and Saykally, 2005). It is to be noted here that equations 9 and 10 entail a total of 4 adjustable parameters. With only about 6 data sets per surfactant + salt concentration, the model values show best fit with most of the experimental data. Figure 2.6 shows the fitted curve for the relation derived by the regressed ΔG_{ads} . A crossover in the ΔG_{ads} curve could be seen at the vicinity of 0.867 mM SDS concentration showing larger ΔG_{ads} values for aqueous (17.11 mM NaCl - SDS)/n-heptane at relatively higher SDS concentrations [Figure 2.6(a)]. ΔG_{ads} values for the aqueous (9.010 mM CaCl₂ - SDS)/n-heptane combination remained higher for the given SDS concentration range [Figure 2.6(b)]. The other two ΔG_{ads} curves for the aqueous CaCl₂ – SDS/n-heptane system nearly overlapped for the given SDS concentration range. All three ΔG_{ads} curves overlapped below 0.281 mM AOT concentrations but ΔG_{ads} values remained higher for aqueous (17.110 mM NaCl – AOT)/n-heptane combination (for > 0.281 mM AOT concentrations).



(a)



(b)



(c)

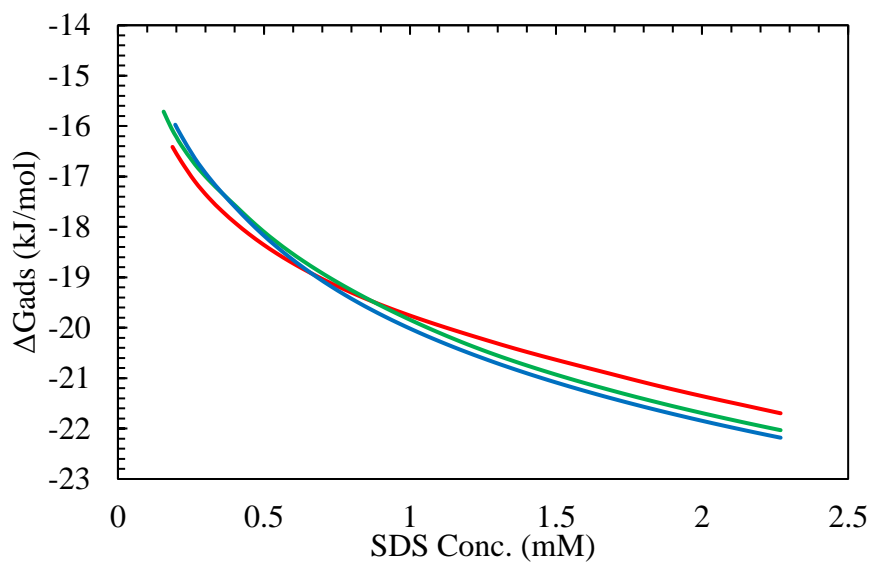
Figure 2.5 Experimental values at 313.15 ± 0.1 K and model for $\Delta\gamma$ of (a) n-heptane - (NaCl + SDS) aqueous solution: ■, 17.110 mM NaCl + SDS; ●, 59.890 mM NaCl + SDS; ▲, 119.780 mM NaCl + SDS; ●, Tichelkamp et al. (2014); (b) n-heptane - (CaCl₂ + SDS) aqueous solution; ■, 9.010 mM CaCl₂ + SDS; ●, 31.530 mM CaCl₂ + SDS; ▲, 63.070 mM CaCl₂ + SDS; ●, Tichelkamp et al. (2014); (c) n-heptane - (NaCl + AOT) aqueous solution: ■, 17.110 mM NaCl + AOT; ●, 59.890 mM NaCl + AOT; ▲, 119.780 mM NaCl + AOT; Model predictions are shown as solid lines.

Table 2.5 summarizes the derived quantities for ΔG_{ads} and shows excellent fits ($R^2 \sim 1$). ΔG_{ads} values can either be obtained from the derived quantities (Table 2.5) or can be seen from the plotted curves (Figure 2.6) to calculate the IFT values from the model for intermediate surfactant concentrations.

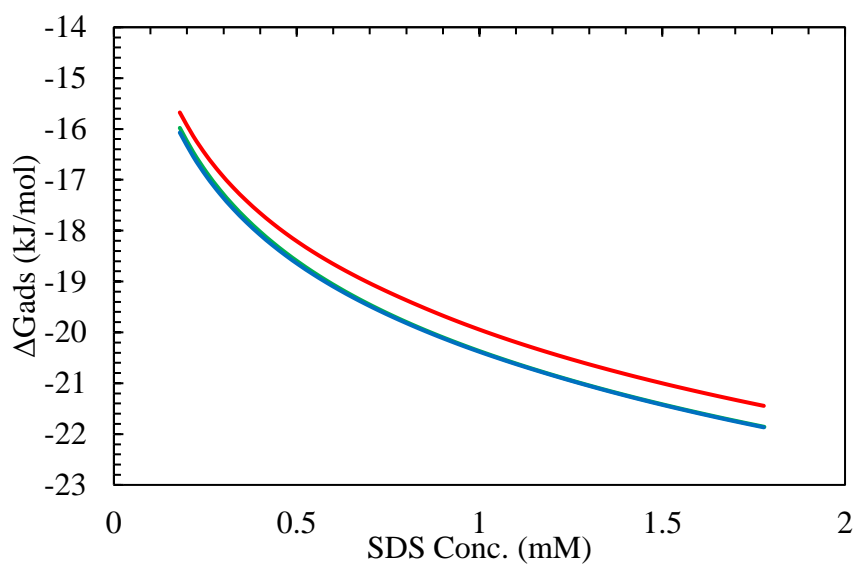
Table 2.4 Model Parameters and Derived Quantities for Several Exemplary Surfactant Concentrations at 313.15 K: Component specific parameter (a), Maximum Surface Excess (N_S^{max}), and Gibbs Free Energy of Adsorption (ΔG_{ads})⁺

| Salt | Salt conc. (mM) | Surfactant | Surfactant conc. (mM) | a (10^8) | N_S^{max} (10^{-10} mol/cm ²) | ΔG_{ads} (kJ/mol) |
|-------------------|-----------------|------------|-----------------------|----------------|--|---------------------------|
| NaCl | 17.110 | SDS | 1.730 | 3.22 | 2.70 | -20.98 |
| NaCl | 59.890 | SDS | 0.867 | 3.22 | 3.10 | -19.46 |
| NaCl | 119.780 | SDS | 0.433 | 3.22 | 3.30 | -17.80 |
| CaCl ₂ | 9.010 | SDS | 0.867 | 3.72 | 2.90 | -19.57 |
| CaCl ₂ | 31.530 | SDS | 1.730 | 3.72 | 3.30 | -21.79 |
| CaCl ₂ | 63.070 | SDS | 1.300 | 3.72 | 3.50 | -21.05 |
| NaCl | 17.110 | AOT | 1.406 | 9.24 | 3.10 | -23.30 |
| NaCl | 59.890 | AOT | 1.406 | 9.24 | 3.50 | -23.59 |
| NaCl | 119.780 | AOT | 0.281 | 9.24 | 3.60 | -19.49 |

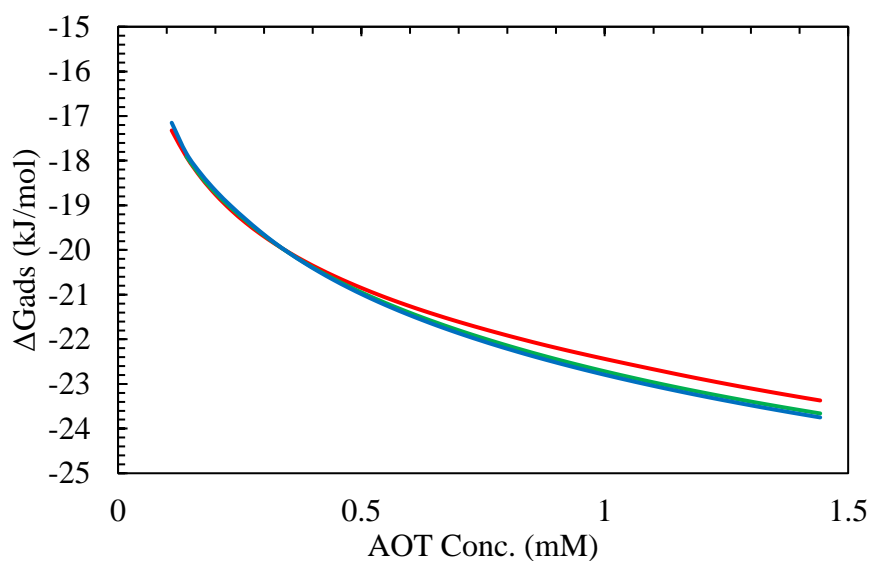
⁺Standard uncertainties are: $u(a) = 0.002 \times 10^8$, $u(N_S^{max}) = 0.003 \times 10^{-10}$ mol/cm², $u(\Delta G_{ads}) = 0.1$ kJ/mol



(a)



(b)



(c)

Figure 2.6 Model for regressed ΔG_{ads} vs (a) SDS concentration for n-heptane - (NaCl + SDS) aqueous solution at 313.15 ± 0.1 K, —, 17.110 mM NaCl + SDS; —, 59.890 mM NaCl + SDS; —, 119.780 mM NaCl + SDS; (b) SDS concentration for n-heptane - (CaCl₂ + SDS) aqueous solution at 313.15 ± 0.1 K, —, 9.010 mM CaCl₂ + SDS; —, 31.530 mM CaCl₂ + SDS; —, 63.070 mM CaCl₂ + SDS; (c) AOT concentration for n-heptane - (NaCl + AOT) aqueous solution at 313.15 ± 0.1 K, —, 17.110 mM NaCl + AOT; —, 59.890 mM NaCl + AOT; —, 119.78 mM NaCl + AOT.

Table 2.5 Derived Quantities for for ΔG_{ads} (J/mol) fit for Several Exemplary Surfactant Concentrations at 313.15 K: Slope (RTm) and Constant (RTc)

| Salt | Surfactant | Salt conc. (mM) | RTm | RTc |
|-------------------|------------|--------------------|-------|-------|
| | | 17.110 | 2106 | 34374 |
| NaCl | SDS | 59.890 | 2430 | 36715 |
| | | 119.780 | 2588 | 37911 |
| | | 9.010 | 2524 | 37396 |
| CaCl ₂ | SDS | 31.530 | 2566 | 38098 |
| | | 63.070 | 2527 | 37848 |
| | | 17.110 | 2319 | 38479 |
| NaCl | AOT | 59.890 | 2506 | 40027 |
| | | 119.780 | 2572 | 40560 |

2.4 CONCLUSIONS

The present study was designed to determine the low salinity surfactant effect on the IFT between n-heptane and aqueous solution. Surfactants by spontaneous self-aggregation at the interface causes the IFT reduction. The results of this investigation show that addition of salts into the aqueous solution further helps in reducing the IFT. Binding of counterion with the surfactant molecules helps in tight surfactant packing due to electrostatic repulsion between the head groups of the surfactant molecules. This phenomenon was responsible for additional IFT reduction due to the divalent nature and larger size of the Ca^{2+} ions when SDS-CaCl₂ combination were used. Strong counterion binding even caused the precipitation of Ca(DS)₂ molecules when a surfactant solution containing relatively high concentration (63.070 mM) of CaCl₂ was used, which was later confirmed by its morphology and compositional analysis. Semi-crystalline nature of the precipitate was quite visible from the diffraction pattern. However, the optimum concentration combination of 59.890 mM NaCl – 1.406 mM AOT in

aqueous solution was most effective in reducing the IFT which gave the minimum value of 0.161 mN/m.

Through multiple regression analysis, the generated data were adequately reproduced with the modified Petersen and Saykally model which is based on the “Jones-Ray” effect. Three parameters a , N_S^{max} and ΔG_{ads} were adjusted in the model to estimate the IFT values. The relevance of these parameters is clearly supported by the current findings. Estimated IFT values are found to be in good agreement with the experimental values. Regressed ΔG_{ads} values are showing a consistent logarithmic relation with the surfactant concentration for all n-heptane – salt-surfactant aqueous solutions. The results obtained in this work shows that a minimum IFT is possible at low salinity-low surfactant combination depending on the type and concentration of salt ions and surfactants even without the loss of surfactant through precipitation. This study shows that the low salinity-low surfactant injection fluid’s composition can effectively be tuned to lower IFT between oil/aqueous solution to a minimum to maximize oil recovery from the subsurface reservoirs through mobilization.

CHAPTER 3

EFFECT OF LOW SALINITY SURFACTANT NANOFLUIDS ON SANDSTONE AT ALKALINE CONDITION

3.1 INTRODUCTION

Wettability alteration is one of the important factors in enhanced oil recovery (EOR) (Al-Anssari et al., 2016, 2017; Nwideo et al., 2017a). The degree of wettability alteration of a porous rock can be quantified in terms of wettability indices. One such method, the USBM method, was developed by Donaldson et al. (1969). In this method, the area under the secondary capillary pressure curves are measured to estimate the wettability. Note that the USBM wettability index is measured as a value throughout the range from complete water-wet ($+\infty$) to complete oil-wet ($-\infty$) and 0 for neutral wettability (Tiab and Donaldson, 2012). Usually, these curves are measured in centrifuges (Tiab and Donaldson, 2012). The rate of oil recovery and the residual oil saturation, which is the target of enhanced oil recovery technology is highly dependent on the wettability (Tiab and Donaldson, 2012). Low salinity water injection (LSWI) also helps in the wettability alteration (Tang and Morrow, 1999; Berg et al., 2010; Morrow and Buckley, 2011; Hadia et al., 2013; Mahani et al., 2015; Mahani et al., 2015; Al-Shalabi and Sepehrnoori, 2016; Hosseinzade Khanamiri et al., 2016a; Kakati and Sangwai, 2017; Chapter 2). However, how precisely wettability is linked to LSWI is only poorly understood (Hamon, 2016). Furthermore, surfactant can reduce interfacial tension between oil and water to an ultra-low value (Iglauer et al., 2011), but surfactant can also be adsorbed on the rock surface. Such surfactant adsorption on the reservoir rock surface detrimentally influences oil recovery (Ahmadall et al., 1993; Wu et al., 2017). However, some works in the last few years have reported that the control of surfactant adsorption on the rock surface is possible by using different additives (Ahmadi and Shadizadeh, 2012; Shamsijazeyi et al.,

2013). One such additive, nanoparticles, are now being considered for chemical flooding (Hendraningrat et al., 2013; Mohajeri et al., 2015; Wu et al., 2017; Kuang et al., 2018). Mechanistically, the effect of nanoparticles on surfactant adsorption has not yet been investigated at low salinity conditions or in the presence of alkali ions; despite alkali being known to reduce surfactant adsorption as well as to produce in-situ soap in the presence of active oil (Olajire, 2014; Sharma et al., 2015), which has been widely used in alkali/surfactant/polymer (ASP) flooding (Guo et al., 2017). Thus the motivation of the present work is how addition of additives (surfactant augmented nanoparticles stabilized at high pH) to a low salinity water can help in wettability alteration of the sandstone cores.

Mechanisms of oil recovery from LSWI in sandstone reservoirs have also widely been debated and reported in literatures which mainly hover around wettability alteration through complex formation by multi-ion exchange (MIE) and double-layer expansion (DLE) due to salinity reduction (Al-Shalabi and Sepehrnoori, 2016). The key process of MIE has been reported to be affected by divalent cations, and the divalent to monovalent ion ratio (Hosseinzade Khanamiri et al., 2016). Divalent cations are proposed to act as bridging ions between negatively charge rock surface sites and acidic components in the crude oil promoting their binding. Since the clay in the rock covers most of the rock surface, clay imparts an overall negative charge to the surface. In one of the works, it was shown that retention of dodecyl benzenesulphonate on kaolinite clay increases with increase in H^+ concentration, i.e., at acidic pH ranges (Hanna and Somasundaran, 1979). The role of ion types (divalent and monovalent) has also been investigated in terms of the recovery performance and their influence on oil/brine/rock interfacial behaviour at low salinity conditions. Wei et al. (2017) have highlighted the roles of HCO_3^- , Mg^{2+} , and SO_4^{2-} as they constructed the most viscoelastic oil-water interfaces as compared to other ions. This viscoelasticity of the oil-water interface rendered the stability of the interface, prevented snap-off of oil (Iglauer et al., 2010), improved

relative permeability and thus increased oil recovery. However, the role of these ions in wettability alteration resulting in detachment of polar species from the sandstone rock surface could not be explained. Earlier research suggests that chromate and sulphate can be adsorbed on kaolinite surfaces when the pH value is in the range of 5-7. This phenomenon was explained by a site-binding model of the kaolinite edge, where the edge is viewed as composite layers of Al and Si oxide which are typically positively charged (Zachara et al., 1988).

It has been observed from the existing literature that adsorption of surfactants and/or other ionic species can have effect on the wettability of the rock surface. Hammond and Unsal (2012), by dynamic pore network modelling, showed how wettability alteration of a mixed-wet rock surface towards a more water-wet condition can mobilize trapped oil, which migrates towards larger pores and can thus reduce the trapped oil saturation in the displacement process. Thus, it is the matter of interest of the present work that how adsorption of surfactants and/or other ionic species on the rock surface affect its wettability and how it could be controlled by varying the proportion of ionic species and/or using nanoparticles in low salinity condition. Thus, in this work, the effect of divalent ion to SO_4^{2-} ratio on surfactant adsorption on clay at low salinity-high pH aqueous nanofluids in the presence of SiO_2 nanoparticles (SNP) has been investigated. Since the pH of the solutions (using NaOH) is high, it has been observed that the ratio of divalent cations to monovalent cations for all the solutions are negligible. Surfactant augmented nanofluids proved to be strong wettability modifier for reservoir rock representative samples (Al-Anssari et al., 2016, 2017, 2018; Nwidee et al., 2017a, 2017b, 2018; Kuang et al., 2018) due to co-adsorption of nanoaggregates over the rock's surface, thus this work is of further interest to low salinity cases in sandstone core plugs. Therefore, in the present work, the aqueous solution (high pH low salinity surfactant solutions, LSS) which showed the maximum average surfactant adsorption on the clay was chosen for the imbibition process with

varying SNP concentrations (wt%), i.e., LSS1+0%SNP, LSS1+0.1%SNP and LSS1+0.2%SNP, respectively.

3.2 MATERIALS AND METHODS

3.2.1 Materials

Table 3.1 provides the list of chemicals used in this study. Sodium chloride (NaCl , $\geq 99\%$ mass fraction) and sodium sulphate (Na_2SO_4 , $\geq 99\%$ mass fraction) were used as monovalent background salts. Calcium chloride (CaCl_2 , $\geq 98\%$ mass fraction) and magnesium sulphate heptahydrate ($\text{MgSO}_4 \cdot 7\text{H}_2\text{O}$, $\geq 99\%$ mass fraction) were used as divalent background salts. Dioctyl sulfosuccinate sodium salt (AOT, $\geq 97\%$ mass fraction) was the anionic surfactant used, and light paraffin oil (saturates $> 99\%$ mass fraction) was used as an oleic phase. Silica nanoparticles (SNPs) (average particle size = 15 nm) were used to prepare nanofluids. Aqueous solutions of individual salts and surfactants were prepared using ultrapure water of $18.2 \text{ M}\Omega \cdot \text{cm}$ resistivity and 6.6–7.1 pH of the fluids was measured using a pH meter (PC 2700, EUTECH Instruments, USA) at 298.15 K. Light paraffin oil used in this study is having API gravity of 38.98 (830 kg/m^3) and kinematic viscosity of 28.07 cS at 298.15 K.

Berea sandstone with the permeability less than 200 mD are known to contain feldspars and muscovite in the range of 7-8% (Kareem et al., 2017). Clay powder was heated in an oven at $120 \text{ }^\circ\text{C}$ for two hours to remove water and any other adsorbed materials (Wu et al., 2011). The powder was analysed by X-ray powdered diffraction (XRPD) using a Bruker D8 Discover powder diffractometer with $\text{Cu K}\alpha$ (40 mA/40 kV) radiation for phase identification by determining peaks associated with various phases present in it, Figure 3.1. The instrument was operated with a step size of 0.017° 2θ angle while the data collection was from $10\text{-}90^\circ$ 2θ angle. The data was processed and analysed using PANalytical X'Pert High Score Plus software to

determine the phases and their composition. Clay powder mainly contained Muscovite (76.2% wt) and Pyrophyllite (23.8% wt). Muscovite is the most common mineral in the family of mica.

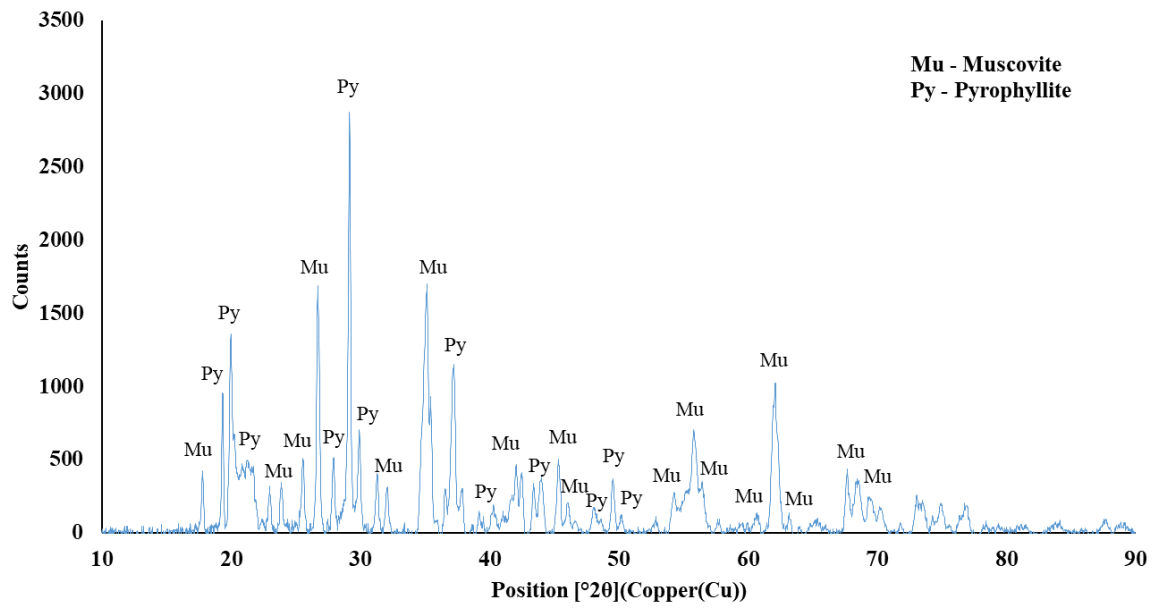


Figure 3.1 XRD pattern of muscovite and associated clay mineral.

Table 3.1 Chemicals Used in This Study

| Chemical | Supplier | Purity (mass fraction) | CAS Number |
|--|---|-----------------------------------|-----------------------|
| Sodium chloride (NaCl) | Merck Specialties, Mumbai, India | ≥ 0.99 | 7647-14-5 |
| Calcium chloride (CaCl ₂) | Alfa Aesar, England | ≥ 0.98 | 10043-52-4 |
| Magnesium sulphate heptahydrate (MgSO ₄ ·7H ₂ O) | Rankem, Mumbai, India | ≥ 0.99 | 10034-99-8 |
| Sodium sulphate (Na ₂ SO ₄) | Merck Specialities, Mumbai, India | ≥ 0.99 | 7757-82-6 |
| Sodium hydroxide (NaOH) | Sisco Research Laboratories, Mumbai, India | ≥ 0.98 | 1310-73-2 |
| Silicon dioxide nanopowder (SiO ₂) | Sisco Research Laboratories, Mumbai, India | ≥ 0.99 | 7631-86-9 |
| Diocetyl sulfosuccinate sodium salt (AOT) | Sigma-Aldrich, USA | ≥ 0.97 | 577-11-7 |
| Light paraffin liquid | S. D. Fine Chemicals, Mumbai, India The Pioneer | | 8012-95-1 |
| Clay powder | Chemical Company, Delhi, India | | |

3.2.2 Method

All salt solutions were prepared gravimetrically using a LC GC RADWAG AS/X 220 analytical balance with ± 0.00004 mass fraction uncertainty. The aqueous phase solutions were prepared using a magnetic stirrer (IKA[®] big squid, Germany) at 400-600 rpm at 298.15 K,

Table 3.2. High salinity brine (HSW) was prepared and later diluted 10 times to make low salinity brine (LSW1). NaOH was mixed with LSW1 to increase its pH to 12.5. Later, low salinity brines (LSW2, LSW3 and LSW4) with 12.5 pH were prepared in ultrapure water, separately. Further, high pH low salinity brines containing AOT (11.247 mM) were prepared and from here onward labelled as high pH low salinity surfactants (Hosseinzade Khanamiri et al., 2016a) as LSS1, LSS2, LSS3 and LSS4, respectively (prepared using low salinity water LSW1, LSW2, LSW3 and LSW4, respectively). High pH low salinity surfactants were used to prepare 12 combinations of nanofluids with 1000 (0.1% wt), 2000 (0.2% wt) and 3000 mg/L (0.3% wt) SNPs by homogenizing (IKA® Digital-Turrax T 25, Germany) at speed of 10000 rpm for 15 minutes for each combination before mixing it with nanoparticles and then by sonication (Roustaei and Bagherzadeh, 2015; Al-Anssari et al., 2017). Table 3.3 gives the combinations of the prepared aqueous solutions with and without SNPs used in this work.

Table 3.2 Compositions of the Brines

| Brine | Na⁺ [mg/L] | Ca²⁺ [mg/L] | Mg²⁺ [mg/L] | Cl⁻ [mg/L] | SO₄²⁻ [mg/L] | M²⁺/SO₄²⁻ |
|--------------|----------------------------------|-----------------------------------|-----------------------------------|----------------------------------|---|---|
| HSW | 11494.9 | 601.2 | 36.5 | 18790.1 | 144.1 | 4.424 |
| LSW1 | 1149.5 | 60.1 | 3.6 | 1879.0 | 14.4 | 4.424 |
| LSW2 | 1207.7 | 37.1 | 0 | 1928.1 | 14.4 | 2.576 |
| LSW3 | 1252.8 | 11 | 0 | 1951.4 | 14.4 | 0.764 |
| LSW4 | 1271.6 | 0 | 0 | 1961.0 | 14.4 | 0.000 |

Table 3.3 Compositions of the Nanofluids

| LSS | SNP [0 mg/L] | SNP [1000 mg/L] | SNP [2000 mg/L] | SNP [3000 mg/L] |
|------|-----------------|--------------------|--------------------|--------------------|
| LSS1 | LSS1+0% | LSS1+0.1% | LSS1+0.2% | LSS1+0.3% |
| LSS2 | LSS2+0% | LSS2+0.1% | LSS2+0.2% | LSS2+0.3% |
| LSS3 | LSS3+0% | LSS3+0.1% | LSS3+0.2% | LSS3+0.3% |
| LSS4 | LSS4+0% | LSS4+0.1% | LSS4+0.2% | LSS4+0.3% |

2.2.1. Surfactant retention measurements.

Clay powder and prepared LSS + SNP solution were mixed at a 1:20 weight ratio in a test tube and then shaken for 4 hours at 298.15 K in an electrical shake (Wu et al., 2011). The mixture was aged for two weeks at 298.15 K and atmospheric pressure; the tests tubes containing the aged mixtures were then centrifuged for at least 30 minutes at 6000 rpm to separate the supernatant from the clay. The separated supernatant was analysed to determine the remaining surfactant concentration; the change in solution surfactant concentration was assumed to be equal to the amount of surfactant retained on clay. Specifically, an aliquot of the supernatant solution was analysed by UV absorption using a spectrophotometer (JASCO V-630, USA) to obtain the absorbance values for various wavelengths until the equilibrium concentration was reached to determine surfactant concentration based on known standards. The difference between the initial and remaining surfactant concentration provided the total surfactant retention by the clay powder. AOT adsorption on the clay surface were calculated in terms of milligrams of AOT adsorbed per gram of clay powder. Each adsorption data presented in this work is the average value of three measurements.

2.2.2. Wettability index measurements.

Berea core plugs obtained from Kocurek Industries, Inc. USA were cut into appropriate size suitable for the drainage/imbibition cell of the automated centrifuge system (ACES-300, Corelab, USA), Table 3.4. Core plugs were then cleaned from free sand particles by dipping them into methanol and sonicated (90 W and 35 kHz) for 30 minutes in two sessions. Cleaned core plugs were left to dry in a hot air oven at 100 °C for 24 hours. Porosity and permeability of the cores were measured at 298.15 K by a helium gas expansion porosimeter and permeameter (Coreval 30, Vinci-Technologies, France) with pressure transducer accuracy of 0.1% of full scale. Dried cores were left to saturate with HSW for another 24 hours in a high-pressure saturator (Vinci-Technologies, France) at pressure of 13.79 MPa and 298.15 K. Subsequently, HSW saturated core plugs were fixed into the drainage cell and filled with light paraffin oil. Centrifugal force was then applied stepwise to the plugs by rotation (1000-10000 rpm) to obtain the capillary pressure curves against average water saturation. A mounted automated video camera (EO Edmund Optics, USA), pre-calibrated for the initial oil/aqueous phase interface, was used to measure the change in the fluid level by change in pixels with step-up of rotational speed. This pixel change with known cell dimensions, was used to calculate the cumulative fluid production and thus water saturation automatically for each angular velocity. Centrifugation was stopped at a point when further water production stopped, and plugs were partially saturated by oil. This process gave the primary drainage capillary pressure data against average water saturation as well as the connate water saturation for each plug. The plugs were then fixed into imbibition cells and filled with high pH low salinity surfactant solutions with and without SNPs. Then, imbibition capillary pressure curves were generated against average water saturation by centrifugation. The drainage processes were repeated for core plugs to obtain secondary drainage capillary pressure curves against average water saturation. The data obtained for primary imbibition and secondary drainage were

processed numerically with a curve fitting tool application of Matlab (Version R2017a) software to obtain functions ($R^2 > 0.98$) to capture the curve trend in the given domain of saturations and range of capillary pressures. These equations were further integrated for limits of end point saturations (Table S4, Supporting Information) to obtain the areas under the curves. The logarithm of the ratio of area under the secondary drainage curve (A_1) and imbibition curve (A_2) were taken to give USBM wettability index (I).

$$I = \log \frac{A_1}{A_2}$$

The method, however, cannot be compared to other methods such as contact-angle measurement (Iglauer et al., 2014; Iglauer, 2017; Kakati and Sangwai, 2018) and Amott method when the wettability of native or restored-state core is measured (Anderson, 1986). Suitable for plug-size cores, the USBM test contrasts the work necessary for displacement of one fluid by the other (Anderson, 1986; Tiab and Donaldson, 2012). The work required for the displacement of non-wetting phase by the wetting phase is less due to favourable free-energy change when compared to the work required for the opposite displacement (Anderson, 1986; Tiab and Donaldson, 2012). This phenomenon is attributed to the proportionality of required work to the area under the capillary pressure curve (Donaldson et al., 1969; Anderson, 1986; Tiab and Donaldson, 2012). Besides, as per our information, the method has never been applied for determination of wettability alteration in sandstone core plugs due to nanofluids injection.

Table 3.4 Berea Sandstone Core Plugs Properties

| Plug ID | Length [cm] | Diameter [cm] | Porosity [%] | Permeability [mD] |
|----------------|------------------------|--------------------------|-------------------------|------------------------------|
| B2 | 2.395 | 2.555 | 20.926 | 203.04 |
| B3 | 2.367 | 2.558 | 20.526 | 193.08 |
| B4 | 2.481 | 2.558 | 20.939 | 202.18 |

3.3 RESULTS AND DISCUSSION

3.3.1 Effect of SNP concentration on surfactant adsorption

The average surfactant adsorption (49.75 mg/g) was highest for LSS1 when compared against LSS2 (44.50 mg/g), LSS3 (38.57 mg/g) and LSS4 (42.87 mg/g), Figure 3.2. The largest decline (i.e. highest to lowest) (55.59%) in surfactant adsorption with increase in SNP concentration was measured for LSS3, which otherwise showed the highest adsorption (55.56 mg/g at 0 SNP) among all solutions. LSS3 and LSS4 (27.28% decrease from highest to lowest) showed a continuously decreasing trend in surfactant adsorption with increasing SNP concentration (from 0-3000 mg/L). This can be attributed to the decrease of the adsorption area due to the adsorbance of silica nanoparticles on clay platelets in the presence of salt. Baird and Walz (2006) observed that, in the presence of salt and SNP, a microscopic ordering begins to develop which otherwise is randomly arranged. This microscopic ordering took place where a small "sponge-like" structure was visible. Whereas, for LSS1, surfactant adsorption increased (54.23 mg/g at 1000 mg/L SNP) and then showed a maximum decrease (13.95%) with increase in SNP concentration. The reported value of AOT adsorption on kaolinite surface is 51.3 mg/g at neutral pH condition (Wu et al., 2011) whereas kaolinite shows no adsorption of AOT at high pH condition (pH 11) (Suzzoni et al., 2018). However, LSS2 showed a declining trend in surfactant adsorption initially and then increased with increasing SNP concentration. Thus, it can be clearly observed that there is a reversal in the surfactant adsorption trend between LSS1 and LSS2 with increase in SNP concentration (Figure 3.2). Interestingly, surfactant adsorption tended to converge at 1000 mg/L SNP concentration for LSS2, LSS3 and LSS4, respectively. Moreover, this phenomenon was unique in terms of LSS2, LSS3 and LSS4 not containing Mg^{2+} , whereas, Mg^{2+} is present in LSS1.

In a molecular dynamics simulation study, Kobayashi et al. (2017) showed that cation bridging can take place between the muscovite surface and the negatively charged sulphonate

group of the AOT molecules; while Ca^{2+} formed cation bridges, Mg^{2+} caused water bridging and thus Ca^{2+} plays a larger role in wettability alteration. Furthermore, as for LSS2/LSS3/LSS4, it was observed that the change in surfactant adsorption depends more on the change in the ratio of divalent cations to sulphate ions than on a change in SNPs concentration for higher SNPs concentrations (>1000 mg/L SNP). The isoelectric point (IEP), which is the pH value where the zeta potential is zero, of muscovite is reported at pH 3.5 (Marion et al., 2015). Muscovite, a non-swelling clay, has a negative overall (i.e. for basal planes and edges in which edges account for 5-10% of the overall surface charge) surface potential at higher pH (zeta potential > -100 mV at pH > 10) (Marion et al., 2015). Adsorption of surfactants and/or other ionic species are greatly affected by the surface charges of minerals. Moreover, pyrophyllite often accompanied with muscovite also shows an overall negative potential at higher pH (zeta potential > -60 mV at pH > 10) with IEP in the acidic range (pH in the range of 2.35 – 3.07) (Liu and Bai, 2017). Thus, the charge density of the cations will facilitate the adsorption behaviour of the surfactant by cation bridging. Further, Allen et al. (2017) investigated, using neutron reflection approach, that monovalent cations can also act as bridge between negatively charged mica and negatively charged surfactant depending on hydration effect. It was explained that cations which are smaller and highly charged are more hydrated and reluctant to bind to the mineral surface or the surfactant head group (Allen et al., 2017). However, hydration effect was not fully understood but proposed to be a consideration when the valency of two ions (such as Ca^{2+} and Mg^{2+}) are same (Allen et al., 2017). Our hypothesis implies that preferential adsorption of negatively charged SNP by negatively and densely charged (structural) clay surface, facilitated by divalent cation bridging, decreases the surfactant adsorption. Silica surface charge (IEP at pH 2 approximately) is pH dependent and needs counterion binding due to its negative surface charge at higher pH (Griffin et al., 2016).

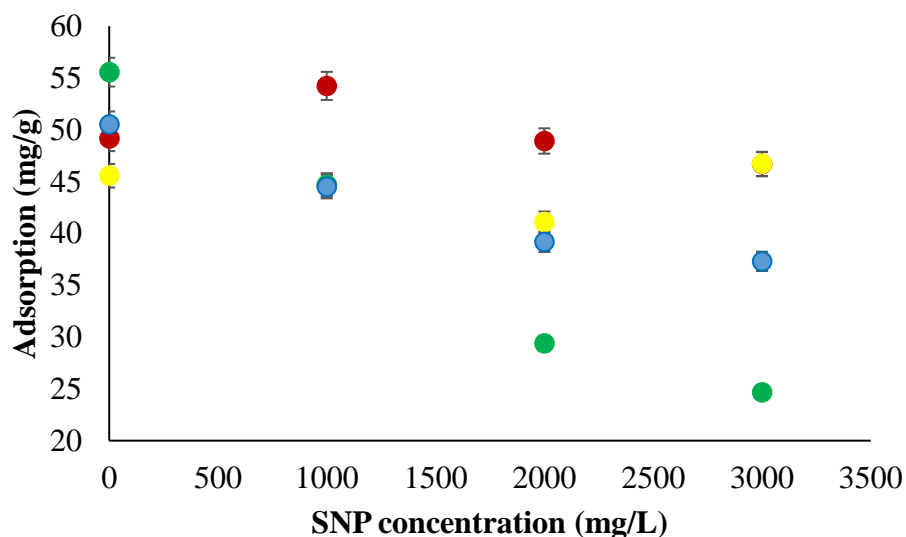


Figure 3.2 Experimental values for AOT adsorption on clay against SNP concentration: ●, LSS1; ●, LSS2; ●, LSS3; ●, LSS4.

This further implies that AOT adsorption on SNP surface, however, lesser than adsorbed by clay surface, also occurs by divalent cation bridging as monovalent cation like Na^+ does not act as bridge due to strong hydration effect. In this process, possibly, precipitation of CaSO_4 can also take place (Al-Shalabi and Sepehrnoori, 2016). The next section will thus focus on the dependency of surfactant adsorption on clay surfaces and how this is related to the divalent cation-sulphate ion ratio.

3.3.2 Effect of the divalent cation-sulphate ion ratio on surfactant adsorption

Figure 3.3 shows the surfactant adsorption on the clay surface as a function of the divalent cation to sulphate ion ratio ($\text{M}^{2+}/\text{SO}_4^{2-}$) at varying SNPs concentrations. Average surfactant adsorptions were 50.20 mg/g (at 0 SNP), 47.02 mg/g (at 1000 mg/L SNP), 39.64 mg/g (at 2000 mg/L SNP) and 38.84 mg/g (at 3000 mg/L SNP), respectively. This shows that average surfactant adsorption decreased with increasing SNPs concentration in the aqueous solutions. Moreover, there is a reversal in trend of the surfactant adsorption against $\text{M}^{2+}/\text{SO}_4^{2-}$ curve between at 0 SNP and 3000 mg/L SNP. Interestingly, both the highest (55.56 mg/g at 0

SNP) and lowest (24.68 mg/g at 3000 mg/L SNP) obtained surfactant adsorption values were measured at 0.763 M^{2+}/SO_4^{2-} . However, it was observed that the change in surfactant adsorption depends more on the change in SNP concentration than on the change in the divalent cation to sulphate ion ratio for lower M^{2+}/SO_4^{2-} values (< 2.575). Furthermore, there was a dramatic increase in surfactant adsorption (89.29 % for 3000 mg/L SNP at 4.427 M^{2+}/SO_4^{2-} and 66.50 % for 2000 mg/L SNP at 4.427 M^{2+}/SO_4^{2-}) with an increase in M^{2+}/SO_4^{2-} values > 0.763 . At 1000 mg/L SNP concentration, surfactant adsorption remained constant for $0 \leq M^{2+}/SO_4^{2-} \leq 2.575$ but increased thereafter.

These trends in the surfactant adsorption curve can be attributed to the interplay of availability of cations (depending on their concentrations) for cation bridging between the negatively charged muscovite surface and the head group of the anionic surfactant, between the negatively charged muscovite surface and the negatively charged SNP surface, between the negatively charged SNP surface and the head group of the anionic surfactant, and for precipitation by SO_4^{2-} ions, respectively, at constant SO_4^{2-} ions concentration (14.4 mg/L). When no SNP is present (red squares, Figure 3.3), the introduction of cations (at 0.763 M^{2+}/SO_4^{2-}) increases surfactant adsorption while further increase in cation concentration (37.1 and 60.1 mg/L) decreases the surfactant adsorption due to precipitation of cations by SO_4^{2-} ions which prevent further adsorption of surfactant on the muscovite surface. At 0.2 and 0.3% (wt) SNP, the introduction of cations (at 0.763 M^{2+}/SO_4^{2-}) decreases the adsorption of surfactants on the muscovite surface as they preferentially facilitate bridging between SNPs and the muscovite surface while further increase in cation concentration also facilitates surfactant adsorption directly by the muscovite surface and/or already adsorbed SNP. For 0.1% (wt) SNP, surfactant adsorption is nearly constant until the cation concentration has increased to 37.1 mg/L. Furthermore, based on the evidence from the work of Baird and Walz (2006), it can be explained that preferential adsorption of SNP facilitated by cation bridging at 0.763 M^{2+}/SO_4^{2-}

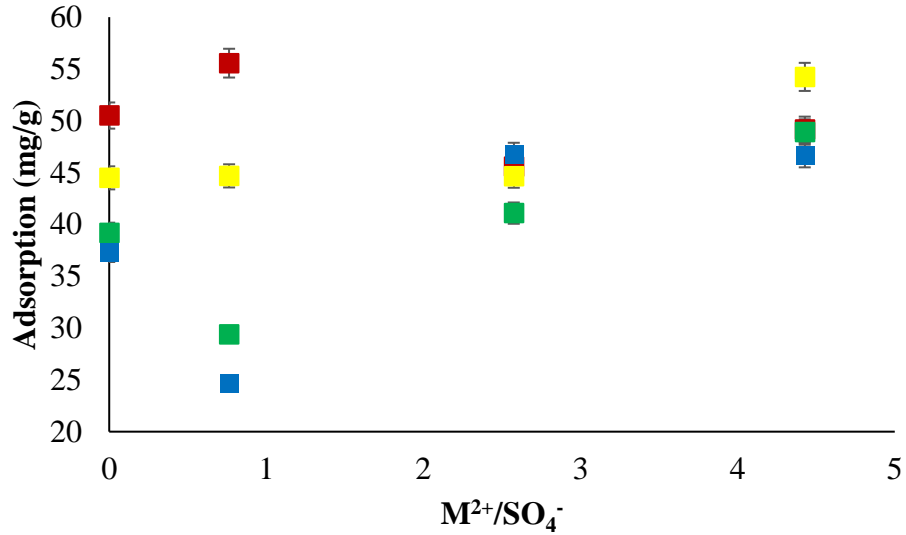


Figure 3.3 Experimental values for AOT adsorption on clay against divalent cations to sulphate ions ratio (M^{2+}/SO_4^{2-}): ■, 0 mg/L SNP; ■, 1000 mg/L SNP; ■, 2000 mg/L SNP; ■, 3000 mg/L SNP.

is increased due to the increase in SNP concentration from 0.1 to 0.3% (wt) thereby decreasing the surfactant adsorption.

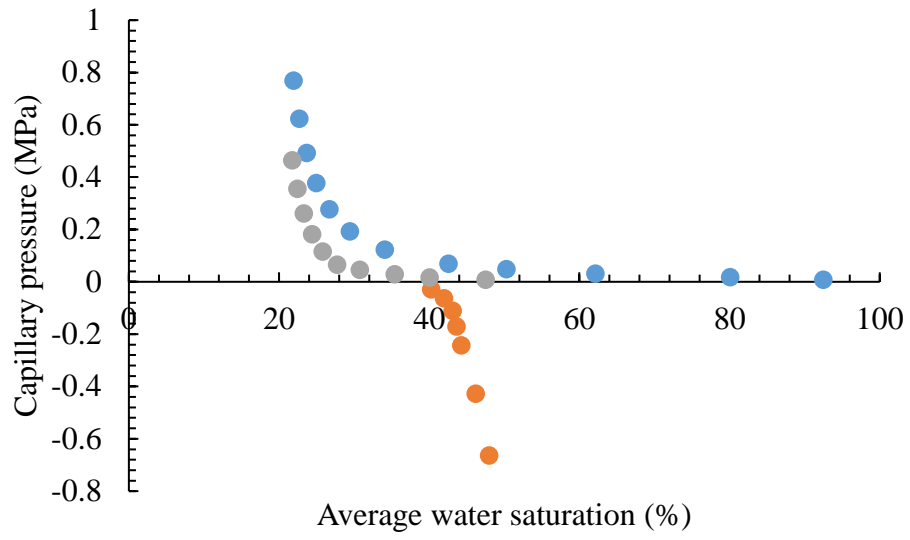
3.3.3 Effect of SNPs on wettability of Berea sandstone core plugs

Figure 3.4 (a-c) shows the capillary pressure hysteresis loops for three core plugs. The loops were obtained by displacing HSW by light paraffin oil, these fluids by imbibition fluids and all fluids were again displaced by light paraffin oil. Table 3.5 gives wettability index. Clearly, when exposed to anionic surfactant only, Berea core was mixed-wet. However, the wettability of the Berea core changed from mixed-wet to water-wet (Iglauer et al., 2014) when SNP were used, Table 3.5.

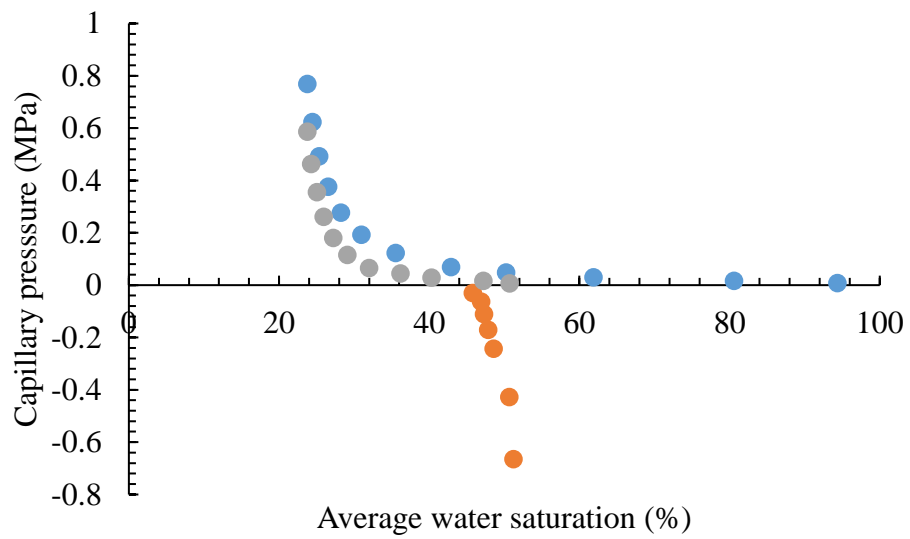
Table 3.5 Wettability Index of Berea Sandstone Core Plugs

| Plug ID | Imbibition Fluids | Wettability Index |
|---------|-------------------|-------------------|
| B2 | LSS1+0%SNP | -0.07 |
| B3 | LSS1+0.1%SNP | 0.35 |
| B4 | LSS1+0.2%SNP | 0.16 |

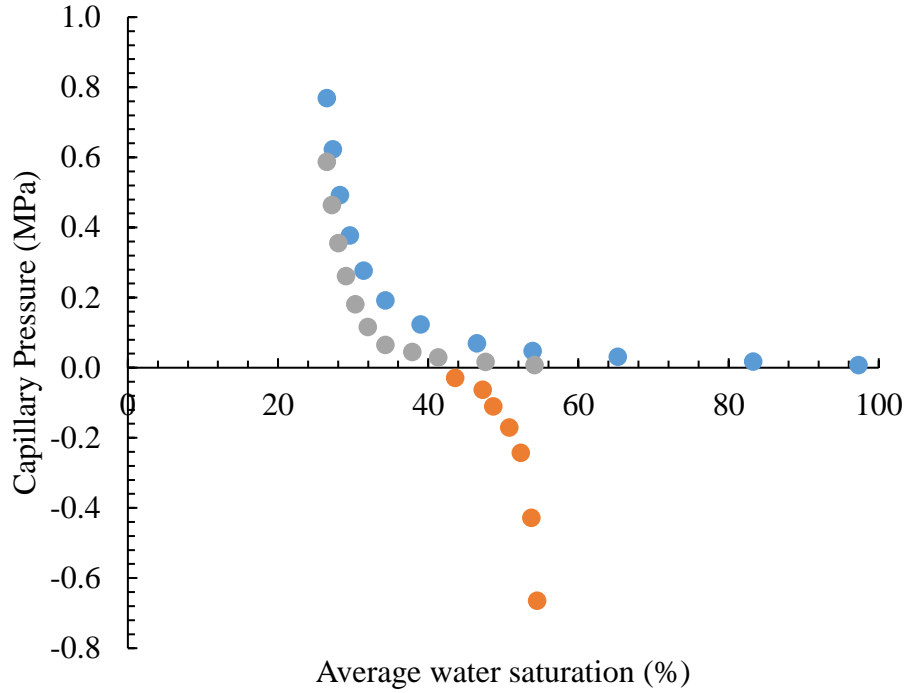
However, despite of the fact that surfactant adsorption for LSS1 on clay surfaces were similar for surfactant adsorption (49.17 mg/g adsorption for 0 and 48.92 mg/g adsorption for 2000 mg/L SNP concentration), increasing the concentration of SNP from 1000 mg/L to 2000 mg/L did not significantly increase water wettability. This implies that the wettability alteration in the Berea sandstone may not be due to surfactant adsorption itself, Figure 3.5, but the adsorption of SNP in presence of surfactant at high pH and low salinity. Furthermore, facilitated by high pH and low salinity, formation of nanoaggregates may occur due to availability of more surfactant molecules in the aqueous phase; subsequently co-adsorption of the formed nanoaggregates on sandstone surface takes place which might be responsible for wettability alteration towards the water-wet condition, Figure 3.6. On the contrary, increasing the SNP concentration can cause repulsion between the initially co-adsorbed (with surfactants adsorbed directly to sandstone surface) and additionally formed SNP-surfactant nanoaggregate complexes preventing them from further co-adsorption at the negatively charged sandstone surface.



(a)



(b)



(c)

Figure 3.4 Hysteresis loop of capillary pressure curves for (a) B2, High pH low salinity surfactant solutions of LSS1 + 0% SNP: ●, primary drainage; ●, secondary drainage; ●, imbibition; (b) B3, High pH low salinity surfactant solutions of LSS1 + 0.1% SNP: ●, primary drainage; ●, secondary drainage; ●, imbibition; (c) B4, High pH low salinity surfactant solutions of LSS1 + 0.2% SNP: ●, primary drainage; ●, secondary drainage; ●, imbibition.

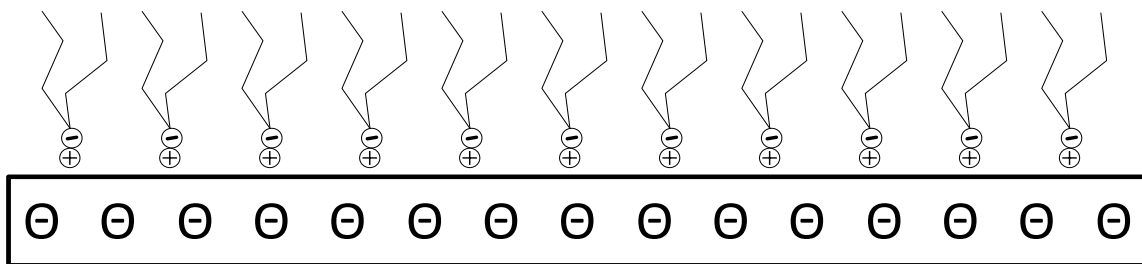


Figure 3.5 Schematic of surfactant adsorption on sandstone surface.

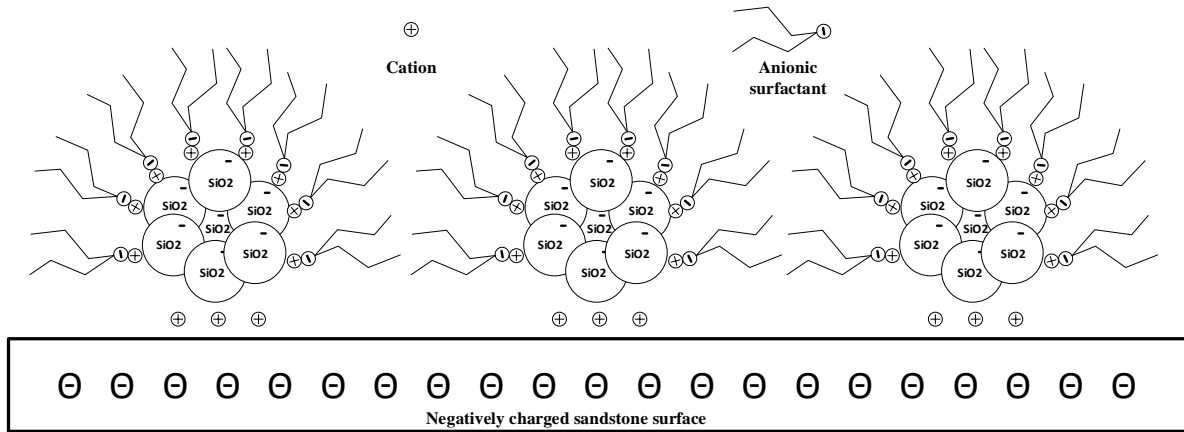


Figure 3.6 Schematic of nanoaggregates co-adsorption on sandstone surface.

3.4 CONCLUSIONS

The effect of the divalent cation-sulphate ion ratio on anionic surfactant adsorption on clay in presence of nanoparticles at high pH and low salinity condition was investigated, for its potential use in high pH low salinity surfactant nanofluids EOR. The formulations which gave the maximum average adsorption of surfactant on clay were used for imbibition experiments in Berea sandstone to measure the wettability alteration effect due to the high pH low salinity surfactant nanofluids. Clearly, the divalent cation-sulphate ion ratio played a prominent role in surfactant adsorption on the clay when used in combination with silica nanoparticles. The effect of silica nanoparticles concentration on anionic surfactant adsorption was pronounced when used in higher concentrations (>1000 mg/L). Whereas, the effect of the divalent cation-sulphate ion ratio with respect to surfactant adsorption was pronounced for low ratios (M^{2+}/SO_4^{2-} values < 2.575). High pH low salinity surfactant solutions of LSS1 (0-2000 mg/L SNP) were used for USBM wettability index measurements in light paraffin oil saturated Berea sandstone core plugs. The 1000 mg/L SNP with LSS1 turned the rock surface water-wet and can thus be used as a strong wettability modifier. Further increasing SNP concentration had no or minimal effect on the sandstone wettability. This wettability effect can be attributed to the co-adsorption of

nanoaggregates surfactant complexes and surfactant molecules on the sandstone surface which can be prominent at an optimal SNP concentration. Besides, our hypothesis is that there is an interplay of availability of divalent cations for bridging between clay/sandstone surface and SNP, SNP and anionic surfactant or between clay surface and anionic surfactant. Facilitated by cation bridging, co-adsorption of nanoaggregates and surfactants takes place over the clay containing sandstone surface and can alter its wettability, possibly, favourably towards oil recovery by low salinity surfactant nanofluids injection.

CHAPTER 4

EFFECT OF LOW SALINITY SURFACTANT NANOFLUIDS ON QUARTZ AT ACIDIC CONDITION

4.1 INTRODUCTION

Low salinity water injection has emerged as a new enhanced oil recovery technique, and it is often considered as a cost-effective and environmentally friendly oil recovery method (Al-Shalabi and Sepehrnoori, 2016; Chapter 2; Chapter 3). The importance of the technique is evidently more highlighted with the decline in conventional resources and the need for efficient tertiary recovery methods (Pouryousefy et al., 2016; Roshan et al., 2016; Zhang et al., 2018). One of the areas of interest is the use of additives such as surfactants or nanoparticles in combination with low salinity water to enhance its performance. (Hendraningrat et al., 2013; Mohajeri et al., 2015; Wu et al., 2017; Hosseinzade Khanamiri et al., 2016a; Kuang et al., 2018). Beside implications of these techniques in CO₂ enhanced oil recovery (Jha et al., 2015; Karimaie and Lindeberg, 2017; Namani et al., 2017; Al-Bayati et al., 2018), they can be used for CO₂ geosequestration (Al-Anssari et al., 2018; Al-Khdheewi et al., 2018; Iglauer, 2018; Jha et al., 2018) and hybrid water alternating gas injection (WAG) processes (Al-Bayati et al., 2018; Al-Khdheewi et al., 2018).

It has been observed that presence of ionic species (such as Ca²⁺, Na²⁺, Mg²⁺, HCO₃⁻, SO₄²⁻) (Al-Shalabi and Sepehrnoori, 2016; Chapter 2; Chapter 3; Hosseinzade Khanamiri et al., 2016b; Hosseinzade Khanamiri et al., 2016c; Jackson, et al., 2016; Kakati and Sangwai, 2017; Wei et al., 2017; Kakati and Sangwai, 2018) can play an important role in oil recovery by low salinity water injection. The mechanisms are essentially linked to interfacial tension (IFT) reduction, electric double layer expansion, fines migration, multi-ion exchange (MIE), and pH increase (Al-Shalabi and Sepehrnoori, 2016). While some studies showed that the

concentration of divalent and monovalent cations in low salinity aqueous solutions could affect IFT between oil and water in a unique way depending on their ratio (Hosseinzade Khanamiri et al., 2016c) other argued that cation bridging takes place and alters the wettability of the rock surface as the predominant mechanism (Kobayashi et al., 2017; Chapter 3). Wettability of geological minerals and its effect on the CO₂ trapping process during geosequestration is also highly affected by physiochemical interactions of CO₂ and brine (Fauziah et al., 2019).

Wettability of rock surfaces in an aqueous/non-aqueous (oleic)/rock three-phase system is related to the hydrophilicity or hydrophobicity of the aqueous phase and its preference to cover or not to cover the rock surface (Iglauer et al., 2014; Iglauer, 2017). Table 4.1 presents the wettability classification of the aqueous phase-rock system used in this study (Iglauer et al., 2014). Electric double layer expansion (DLVO theory) (Xie et al., 2016), is also supposed to increase the rock surface water wetness by providing a stable water film (Nasralla and Nasr-El-Din, 2011). For DLVO theory to be effective, however, the oil layer needs to be continuous that may not be a case of residual oil in rock pores, i.e. where it exists in blobs non-uniformly distributed in microporous space (Iglauer et al., 2010; Al-Shalabi and Sepehrnoori, 2016; Iglauer and Wulling, 2016).

Divalent cations and SO₄²⁻ are known to build the most viscoelastic oil-water interfaces as compared to other ions and are favorable to oil recovery (Wei et al., 2017). Interestingly though, the role of these ions in wettability alteration resulting in detachment of polar species from the sandstone rock surface could not be explained. The role of SO₄²⁻ in oil recovery has been investigated for carbonate, chalk and dolomite reservoirs (Al-Shalabi and Sepehrnoori, 2016); however, sandstone chemistry has rarely been investigated.

Moreover, divalent cation to SO₄²⁻ ratio can play a key role in the adsorption of anionic surfactant and surfactant augmented nanoparticles by the clay bound rock surface thus affecting the wettability of sandstone surfaces (Chapter 3). The role of cations in cation bridging

Table 4.1 Wettability Based on Contact Angle of Aqueous Phase-rock system

| Wettability State | Water contact angle θ (°) |
|--------------------------|--|
| Complete water-wet | 0 |
| Strongly water-wet | 0-50 |
| Weakly water-wet | 50-70 |
| Intermediate water-wet | 70-100 |

contributing towards physico-chemical interactions between different negatively charged species by rendering all the surface negatively charged using high pH was further observed (Chapter 3). The major contribution towards the adsorption of surfactants are known to be affected by the presence of 1:1 (Wu et al., 2011; Suzzoni et al., 2018) and 2:1 Dioctahedral clay minerals (Chapter 3).

In spite of recent efforts, there is a considerable lack of experimental data and understanding of the physical phenomena affecting the macro-scale processes. In this study, therefore to investigate in detail the role of divalent cations to SO_4^{2-} ratio on the wettability alteration of weak water-wet quartz surfaces by low salinity sodium dodecylbenzenesulfonate (SDBS, 1.435 mM) (Hosseinzade Khanamiri et al., 2016b), ZrO_2 (0-2000 mg/L) (Nwidee et al., 2017b) nanofluids was augmented at high pressure (20 MPa) and temperature (343.15 K) conditions in presence of CO_2 .

4.2 MATERIALS AND METHODS

4.2.1 Materials

Sodium chloride (NaCl , $\geq 99\%$ mass fraction) and sodium sulfate (Na_2SO_4 , $\geq 99\%$ mass fraction) were used as monovalent background salts and Calcium chloride (CaCl_2 , $\geq 99\%$ mass

fraction) and magnesium sulfate ($\text{MgSO}_4 \geq 99\%$ mass fraction) were used as divalent background salts. The anionic surfactant used in the study was Sodium dodecylbenzenesulfonate (SDBS $\geq 99\%$ mass fraction) and Decane (99% mass fraction purity) was used as an oleic phase. Zirconium dioxide nanoparticles (ZNPs) (average particle size ≤ 100 nm) was also used to prepare the nanofluids. Aqueous solutions of individual salts and surfactants were prepared using ultrapure water of 17.65 M Ω cm resistivity. Table 4.2 provides the list of chemicals used in this study.

The composition of the quartz plate, Table 4.3, was measured by energy dispersive spectroscopy (EDS) technique using a scanning electron microscope (Phenom XL, Netherlands).

Table 4.2 List of Chemicals Used in This Study

| Chemical | Supplier | Purity (mass fraction) | CAS Number |
|--|---|-------------------------------|-------------------|
| Sodium chloride (NaCl) | Rowe Scientific, Western Australia, Australia | ≥ 0.99 | 7647-14-5 |
| Calcium chloride (CaCl ₂) | Rowe Scientific, Western Australia, Australia | ≥ 0.99 | 10043-52-4 |
| Magnesium sulfate (MgSO ₄) | Merck, Australia | ≥ 0.99 | 7487-88-9 |
| Sodium sulfate (Na ₂ SO ₄) | Merck, Australia | ≥ 0.99 | 7757-82-6 |
| Zirconium dioxide nanopowder (ZrO ₂) | Merck, Australia | ≥ 0.99 | 1314-23-4 |
| SDBS | Merck, Australia | ≥ 0.99 | 25155-30-0 |
| Decane | Merck, Australia | ≥ 0.99 | 124-18-5 |
| Carbon dioxide | BOC Gas | ≥ 0.99 | |

Table 4.3 Compositional Data of the Substrate From Energy Dispersive Spectroscopy

| Element | Atomic Composition | Weight Composition |
|-----------|--------------------|--------------------|
| | [%] | [%] |
| Oxygen | 68.29 | 52.67 |
| Silicon | 17.35 | 23.49 |
| Sodium | 9.23 | 10.23 |
| Magnesium | 1.93 | 2.26 |
| Calcium | 0.98 | 1.89 |

Table 4.4 Compositions of the Brines

| Brine | Na ⁺ [mg/L] | Ca ²⁺ [mg/L] | Mg ²⁺ [mg/L] | Cl ⁻ [mg/L] | SO ₄ ²⁻ [mg/L] | M ²⁺ /SO ₄ ⁻ |
|-------|---------------------------|----------------------------|----------------------------|---------------------------|---|---|
| HSW | 11494.9 | 601.2 | 36.5 | 18790.1 | 144.1 | 4.424 |
| LSW1 | 1149.5 | 60.1 | 3.6 | 1879.0 | 14.4 | 4.424 |
| LSW2 | 1207.7 | 37.1 | 0 | 1928.1 | 14.4 | 2.576 |
| LSW3 | 1252.8 | 11 | 0 | 1951.4 | 14.4 | 0.764 |
| LSW4 | 1271.6 | 0 | 0 | 1961.0 | 14.4 | 0.000 |

4.2.2 Method

All salt solutions were prepared gravimetrically using an analytical balance (CP224S, Sartorius AG, Germany) with repeatability of ≤ 0.1 mg (standard deviation). The aqueous phase solutions were prepared using a magnetic stirrer at 400-600 rpm at 20 °C, Table 4.4. High salinity brine (HSW) was prepared and later diluted ten times to make low salinity brine (LSW1). Later, brines with lower salinity (LSW2, LSW3, and LSW4) were prepared with

ultrapure water. Furthermore, the low salinity brines containing SDBS (1.435 mM) were prepared and onwards from here labeled as low salinity surfactants as LSS1, LSS2, LSS3, and LSS4 respectively. Low salinity surfactants were used to prepare 12 combinations of nanofluids with 100, 1000 and 2000 mg/L ZNPs using ultrasonication (300VT Ultrasonic Homogenizer/BIOLOGICS, using a sonication power of 240 W), each batch were sonicated for 4 periods of 15 min with 5 min rest to avoid overheating (Roustaei and Bagherzadeh, 2015; Al-Anssari et al., 2017). Quartz samples were cleaned with de-ionized water, acetone, methanol and then using air plasma to remove all organic and inorganic contaminations (Iglauer et al., 2014). These samples were then aged in decane for three weeks at 293.15 K and atmospheric pressure. Quartz samples were then air dried for 15 minutes using pressurized pure air before contact angle measurements. Unique surface behavior and physicochemical properties depending on chain length make alkanes suitable candidates for wetting and 2-dimensional ordering studies (Holzwarth et al., 2000). Table 4.5 gives the combination of the prepared aqueous solutions with and without ZNPs used in this study.

Contact angle and interfacial tension measurements

Wettability measurements were carried out at reservoir conditions (i.e., 343.15 K at 20 MPa) by contact angle method using a tilted plate goniometric setup (Arif et al., 2016; Ali et al., 2019). The setup consisted of a cell designed to operate at high pressure and high-temperature conditions. A stage tilted at an angle of 17° was placed inside the cell to hold the substrate (Arif et al., 2017). Two separate high precision syringe pumps (Teledyne D-500, pressure accuracy of 0.1%) were used to adjust the CO₂ pressure, and to drive (using de-ionized water) the low salinity surfactant solutions. At the pressure and temperature maintained in this study, CO₂ is in supercritical phase (scCO₂).

The aged substrate was placed on the stage inside the cell and heated to 343.15 K, and the CO₂ pressure was then raised to 20 MPa. Subsequently, a droplet (average volume of $6 \pm 1 \mu\text{L}$) of low salinity surfactant solutions was dispensed onto the quartz surface through a needle (Ali et al., 2019). The advancing (θ_a , at the leading edge) and receding (θ_r , at trailing edge) contact angles of the droplet were then measured as soon as the drop started to move. This process was filmed using a high-resolution video camera (Basler scA 640–70 fm, pixel size = $7.4 \mu\text{m}$; frame rate = 71 fps; Fujinon CCTV lens: HF35HA-1B; 1:1.6/35 mm) and images were extracted to obtain θ_a and θ_r (Ali et al., 2019). The standard deviation of the measurements was $\pm 3^\circ$ based on replicated measurements (Ali et al., 2019). The pendant drop method has been used for measuring interfacial tension (IFT) of low salinity surfactant nanofluids in the presence of CO₂. Image analysis of the captured image of a pendant drop for IFT calculations was carried out by drop profile fitting using pendant drop plugin of Image J software (Siddiqui et al., 2018).

Table 4.5 Compositions of the Nanofluids

| LSS | ZNP [0 mg/L] | ZNP [100 mg/L] | ZNP [1000 mg/L] | ZNP [2000 mg/L] |
|------------|-------------------------|---------------------------|----------------------------|----------------------------|
| LSS1 | LSS1+0% | LSS1+0.01% | LSS1+0.1% | LSS1+0.2% |
| LSS2 | LSS2+0% | LSS2+0.01% | LSS2+0.1% | LSS2+0.2% |
| LSS3 | LSS3+0% | LSS3+0.01% | LSS3+0.1% | LSS3+0.2% |
| LSS4 | LSS4+0% | LSS4+0.01% | LSS4+0.1% | LSS4+0.2% |

4.3 RESULTS AND DISCUSSION

4.3.1 Effect of ZNP Concentration on IFT of low salinity surfactant nanofluids

Figure 4.1 shows the experimental data on IFT of low salinity surfactant nanofluids as a function of ZNP concentration. From this figure, it is seen that the IFT decreases with increase in ZNP concentration for LSS1. For LSS2 and LSS3, however, IFT increases with the ZNP increase; whereas for LSS3 it increases and then decreases. Thus, it is observed that there is a reversal in the IFT trend between LSS1 and LSS2/LSS3 with an increase in ZNP concentration. Interestingly, for LSS2, LSS3, LSS4, IFT values at approximately 100 mg/L of ZNP concentration are very close to each other.

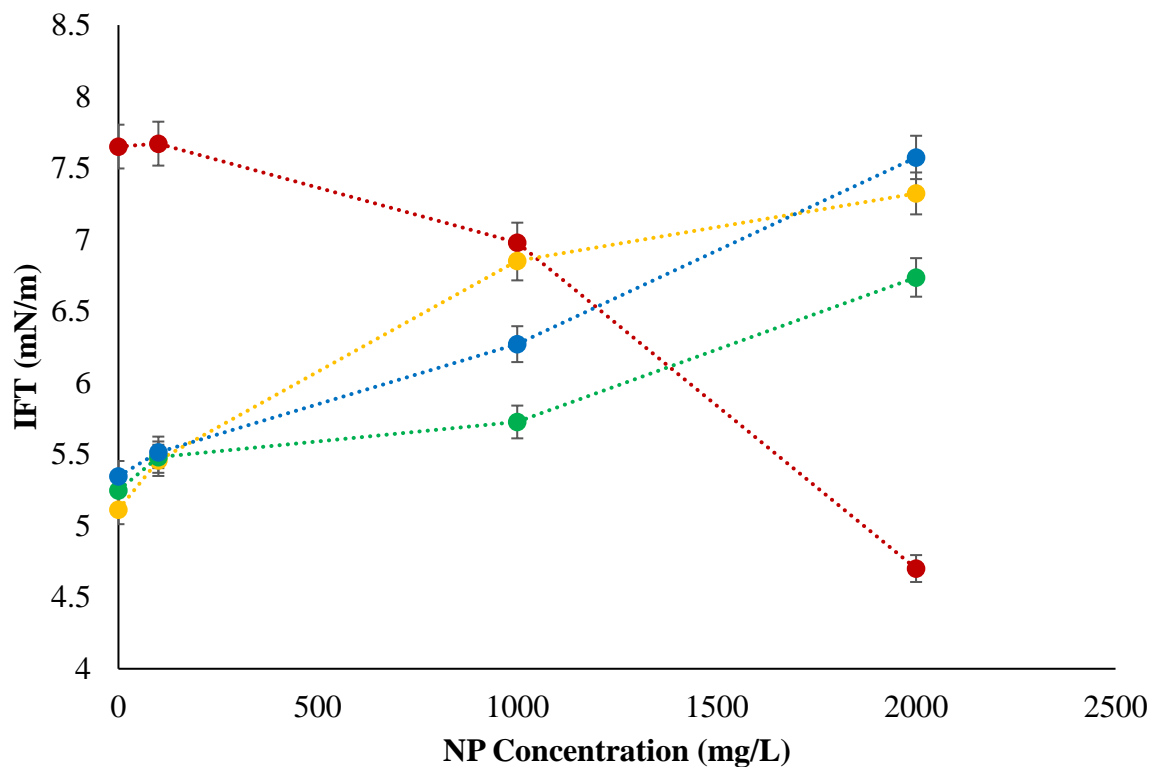


Figure 4.1 Experimental values for LSS nanofluid/scCO₂ IFT against the ZNP concentration:

●, LSS1; ●, LSS2; ●, LSS3; and ●, LSS4.

Considering LSS2/LSS3/LSS4, it is observed that for higher ZNPs concentrations (>100 mg/L ZNP) the IFT change depends more on the change in the ratio of divalent cations to sulfate ions than on a change in ZNPs concentration. Iso-electric point (IEP) of ZNPs is at pH 6 (Wamkam et al., 2011). Any pH above and below this IEP affects the average particle size (large cluster of nanoparticles of equivalent diameter 100-1600 nm formed from individual ZrO₂ particles of diameter 20-30 nm) (Wamkam et al., 2011). Because CO₂ dissolution and reaction with the water acidifies (pH < 3) the aqueous phase (Chen et al., 2019), the zeta potential of ZNPs is slightly positive (rendering them weakly positively charged) (Wamkam et al., 2011). In the acidic condition (pH < 3), the average particle size of ZNPs is 100 nm (Wamkam et al., 2011). The charge associated with the ZNPs makes them suitable for counterion binding from available negatively charged species including the negatively charged head group of an anionic surfactant. Anionic surfactant head group are also exposed to counterion binding by cations having high charge density. Allen et al. (2017) explained that the cations having high charge density (i.e., smaller and highly charged) are more hydrated and reluctant to bind to the surfactant head group or the mineral surface (Allen et al., 2017). On the other hand, hydration effect was proposed to be only significant when the valency of two ions (such as Ca²⁺ and Mg²⁺) are the same, mostly on account of immature understanding of this effect (Allen et al., 2017). Dugyala et al. investigated the role of electrostatic interactions in the adsorption kinetics of nanoparticles at fluid-fluid interfaces (Dugyala et al., 2016). They found that the water/decane IFT decrease was higher when the particles were weakly charged as higher numbers of particles adsorbed to the interface, which was attributed to image charge effect (Dugyala et al., 2016). With their model using modified Ward and Tordai theory (Ward and Tordai, 1946), they showed that the effective diffusivity of the particles is determined by their energy barrier when the particles approach near the interface (Dugyala et al., 2016). A high net energy barrier prevents the adsorption of particles to the interface when the particles

are highly charged which can be resolved with screening the particles by salt addition (Dugyala et al., 2016).

It is similarly postulated that the measured IFT in this study is also based on the availability of positively charged species (Ca^{2+} , Mg^{2+}) for binding with either the head group of SDBS or other negatively charged species (SO_4^{2-}). Head group of SDBS and/or SO_4^{2-} may get attached to the ZNPs surface, Figure 4.2, and contribute towards the effective diffusivity and enhance the availability of nanoaggregates at the interface to reduce IFT. However, the formed nanoaggregates can also have an effective net charge which might be responsible for IFT increase in other cases as seen for LSS2, LSS3 and partly for LSS4.

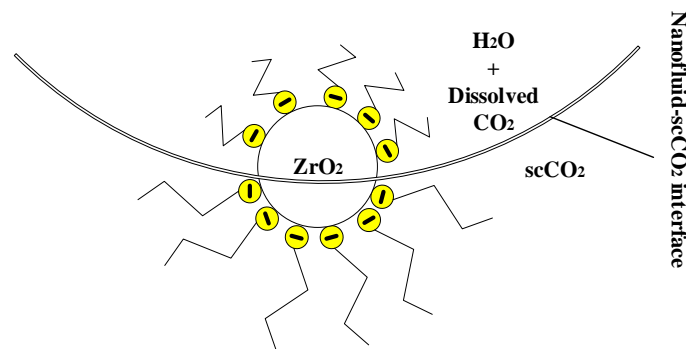


Figure 4.2 Schematic of nanoaggregate adsorption at the nanofluid/ scCO_2 interface.

4.3.2 Effect of divalent cation-sulfate ion ratio on IFT of low salinity surfactant nanofluids

Figure 4.3 presents the experimental IFT data for low salinity surfactant nanofluids as a function of divalent cation-sulfate ion ratio ($\text{M}^{2+}/\text{SO}_4^{2-}$). For 0/100/1000 mg/L ZNP concentration, IFT decreases then increases with increase in $\text{M}^{2+}/\text{SO}_4^{2-}$, whereas, this trend reverses for 2000 mg/L ZNP concentration. The highest and lowest IFT values are both experienced at $4.427 \text{ M}^{2+}/\text{SO}_4^{2-}$. This phenomenon can be attributed to the effect of counterion binding by divalent cations to partially deplete SDBS molecules at the interface causing high

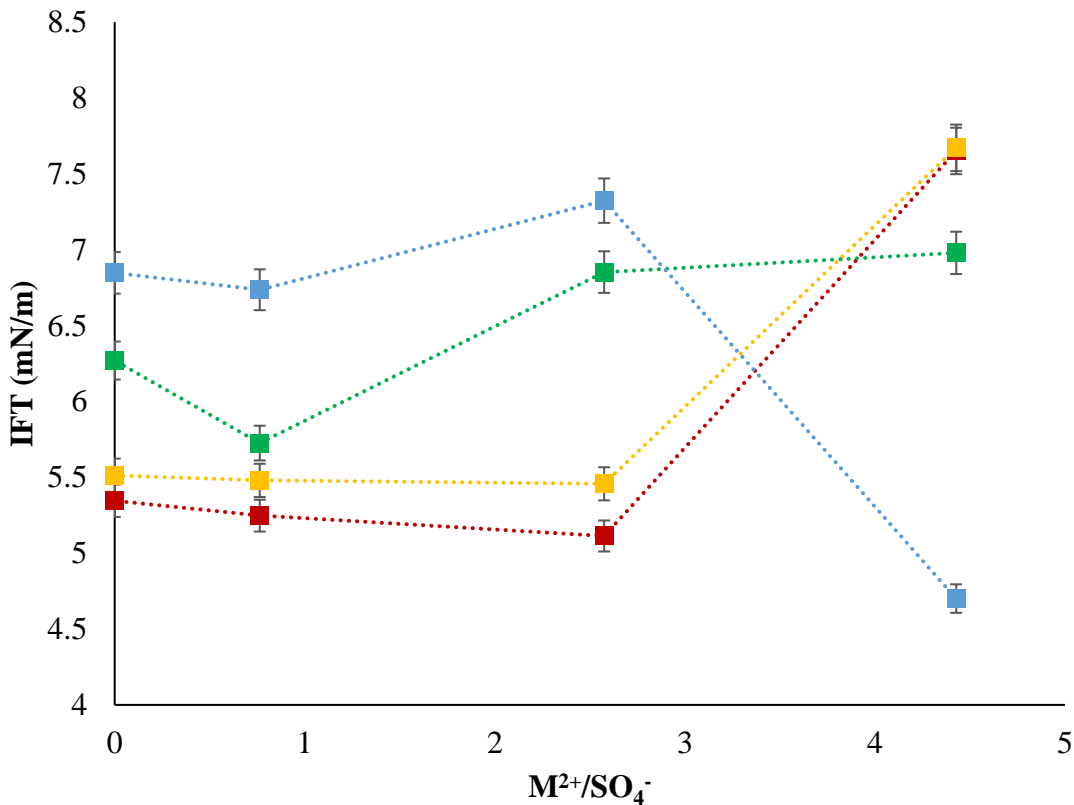


Figure 4.3 Experimental values for LSS nanofluid/scCO₂ IFT against the divalent cation/sulfate ion ratio (M^{2+}/SO_4^{2-}): ■, 0 mg/L ZNP; ■, 100 mg/L ZNP; ■, 1000 mg/L ZNP; and ■, 2000 mg/L ZNP.

IFT at 0/100 mg/L of ZNPs. Whereas, the SDBS adsorption at the ZNPs surface enhances the availability of nanoaggregates at the interface, thereby causing the low IFT at 2000 mg/L ZNP.

4.3.3 Effect of ZNP concentration on the contact angle of low salinity surfactant nanofluids

The consistencies in the data based on replicate measurements and their trend represent weak or intermediate water wetness of the quartz substrate due to aging in decane, followed by

drying in compressed pure air and brief heating (before CO₂ loading). Alkane molecules adsorbed to the silica surface can interact directly with the surface, and adjacent adsorbed molecules (Brindza et al., 2010). The interface formed between nonpolar alkane solvents and hydrophilic silica interfaces is polar (Brindza et al., 2010). Earlier gravimetric studies of medium-length (C₆ – C₁₂) alkane adsorption onto silica particles showed a linear relationship between the amount of alkane adsorbed and the relative alkane partial pressure (Schlangen et al., 1995; Schlangen and Koopal, 1996). This linear dependency implies monolayer adsorption (not multilayer; i.e. a thin liquid film) (Brindza et al., 2010). A brief heating of the substrate at 343.15 K in the IFT chamber before CO₂ loading elevates the vapour pressure of adsorbed n-decane to 3.4x10⁻³ MPa (NIST Chemistry WebBook, SRD 69) which is within the linear range. The thickness of the adsorbed n-alkanes which remains on the silica plate after draining (i.e., at the disjoining pressure of 3x10⁻⁵ MPa) for higher alkanes (octane onwards) ranges from 10-40 Å (Gee, Healy and White, 1989). In this study, the pressure of compressed air used for drying of substrate is 0.5 MPa i.e. before placing it inside the IFT cell for contact angle measurements. Further, reported values of standard adsorption free energy $\Delta G^{\circ}_{\text{ads}}$ of alkanes on silica surface show that $\Delta G^{\circ}_{\text{ads}}$ decreases with increase in alkane chain length in the range of -10 to -25 kJ/mol for hexane to nonane, Figure 4.4 (Nwidee et al., 2017a; Liu et al., 2019). The above discussion explains the wettability condition of quartz substrate ahead of the wettability alteration of its surface by the dispensed nanofluids.

Figure 4.5 indicates the low salinity surfactant nanofluids contact angles as a function of ZNP concentration. Clearly, both advancing (θ_a , at the leading edge) and receding (θ_r , at trailing edge) contact angles (Nwidee et al., 2017a, 2017b) of the droplet first decreases and then increases with increase in ZNP concentration. Least θ_a (44.48°) was observed for LSS1 (at 1000 mg/L ZNP) although the θ_a (45.85°) of LSS2 (at 100 mg/L ZNP) was also close to the lowest value. Similarly, θ_r were least for LSS1 and LSS2. Whereas, θ_a and θ_r both are highest

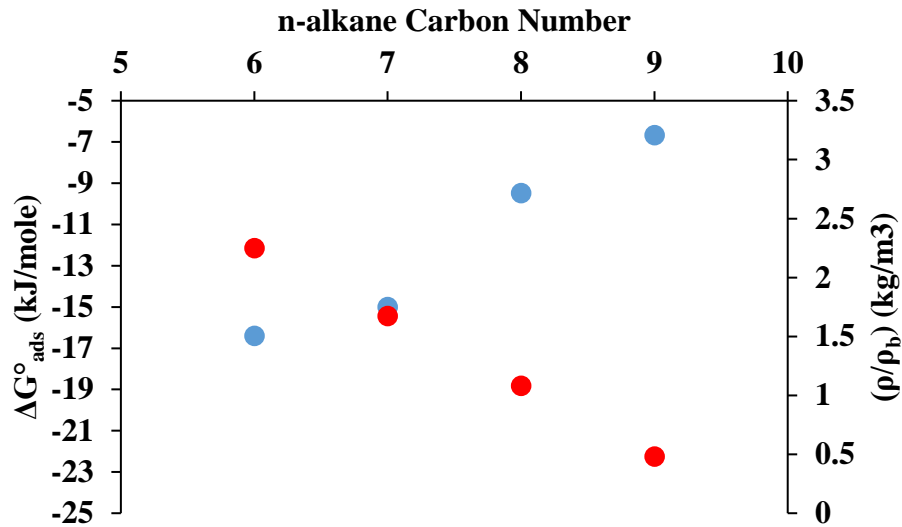


Figure 4.4 Variation of standard free energy of adsorption ΔG°_{ads} of n-alkanes on silica surface (●; Papirer, 2018) and the ratio of density of the n-alkanes at the n-alkane/silica interface to bulk density (ρ/ρ_b) (●; De Almeida and Miranda, 2016) with their number of carbon atoms.

for LSS4. This shows that quartz surface can be turned more water wet when surfactant augmented ZNP is used in the range of (100-1000 mg/L).

Further increasing ZNP concentration further reduces the water wettability. These results have been compared with the contact angle measurements from the study conducted by Giraldo et al. (2013), dispensed the water droplet on an alumina nanoparticle (particle size of 35 ± 4 nm, 0-10000 mg/L, dispersed in an anionic surfactant) treated oil-wet sandstone at room temperature and pressure. Also, Tola et al. (2017) dispensed aqueous solution droplets containing zinc oxide nanoparticles (particle size of 25 nm, 0-5000 mg/L) dispersed in 2500 mg/L SDS surfactant on crude oil saturated Berea sandstone plates to measure contact angles at ambient conditions. This shows that the wettability alteration of quartz is due to the adsorption of ZNP nanoaggregates at low salinity. Furthermore, at low salinity, the formation of nanoaggregates may occur due to the availability of more surfactant molecules in the

aqueous phase; thus, co-adsorption of the formed nanoaggregates on the quartz surface takes place altering the wettability towards more water-wet condition, Figure 4.6. On the contrary, increasing ZNP concentration causes repulsion between the initially co-adsorbed (with surfactants adsorbed directly to the quartz surface due to cation bridging) and additionally formed ZNP-surfactant nanoaggregate complexes preventing them from further co-adsorption at the quartz surface.

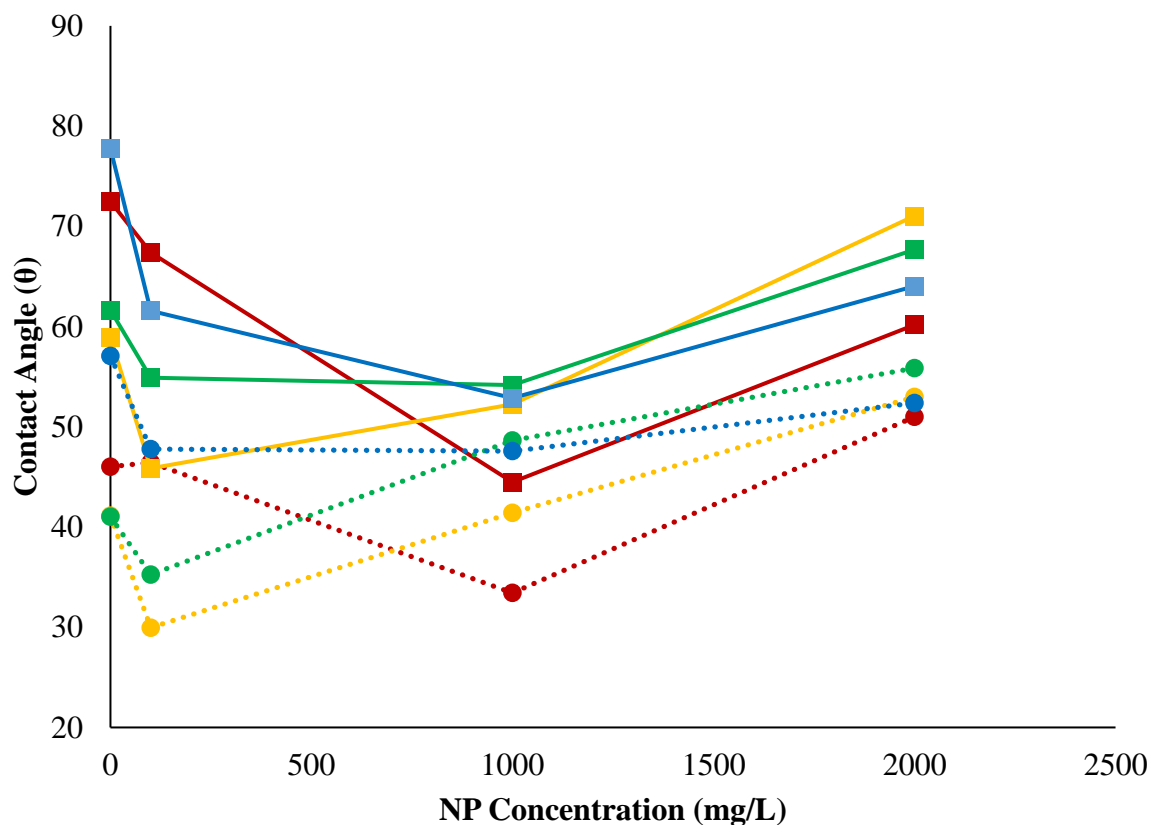


Figure 4.5 Experimental values for LSS nanofluid/quartz contact angles [Advancing (θ_a) and Receding (θ_r)] against the ZNP concentration: ■, LSS1 θ_a ; ■, LSS2 θ_a ; ■, LSS3 θ_a ; ■, LSS4 θ_a ; ●, LSS1 θ_r ; ●, LSS2 θ_r ; ●, LSS3 θ_r ; and ●, LSS4 θ_r .

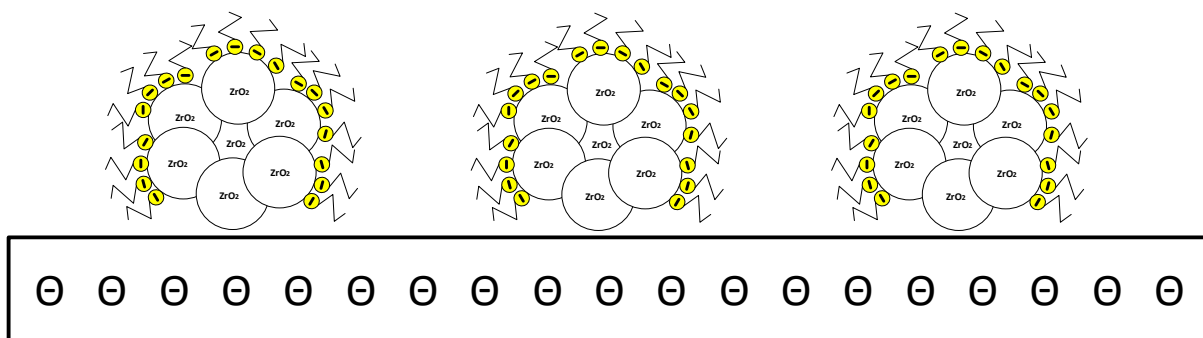


Figure 4.6 Schematic of nanoaggregate co-adsorption on the quartz surface.

4.3.4 Effect of the divalent cation-sulfate ion ratio on the contact angle of low salinity surfactant nanofluids

Figure 4.7 shows the contact angles of low salinity surfactant nanofluids as a function of divalent cation-sulfate ion ratio (M^{2+}/SO_4^{2-}). θ_a and θ_r both decrease and then increase for 0 and 100 mg/L ZNP concentrations with increase in M^{2+}/SO_4^{2-} . Whereas, interestingly, this trend reverses for 1000 and 2000 mg/L nanoparticle concentrations. θ_a and θ_r both are highest for 0 M^{2+}/SO_4^{2-} (at 0 mg/L ZNP) and lowest for 2.575 M^{2+}/SO_4^{2-} (at 100 mg/L ZNP). On the other hand, θ_a and θ_r both are also low for 1000 mg/L ZNP concentration at 4.427 M^{2+}/SO_4^{2-} . This shows that the optimum range of ZNP concentration and divalent cation-sulfate ion ratio are 100-1000 mg/L and 2.575-4.427, respectively, to render the surface more water wet. In addition, surfactant augmented ZNPs nanoaggregates co-adsorption facilitated by the divalent cation bridging, at an optimal condition is responsible for the change of the quartz surface, which becomes more water-wet at low salinity.

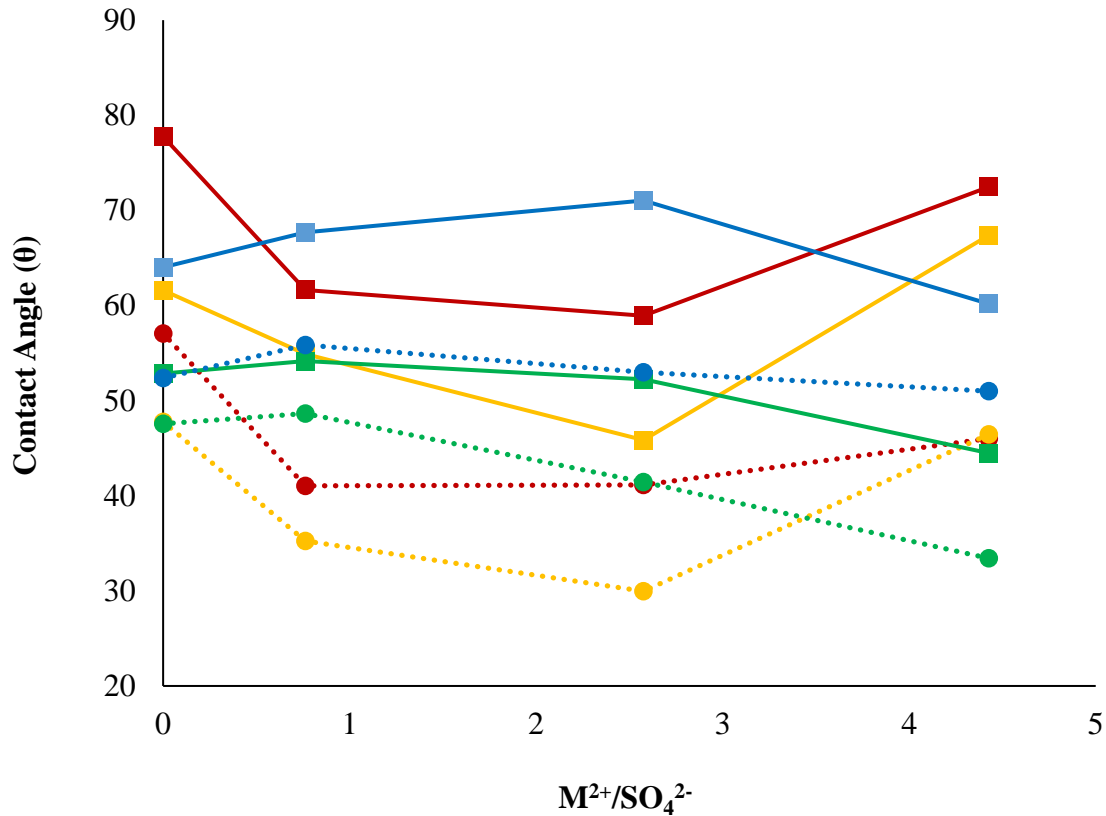


Figure 4.7 Experimental values for LSS nanofluid/quartz contact angle [Advancing (θ_a) and Receding (θ_r)] against the divalent cation/sulfate ion ratio (M^{2+}/SO_4^{2-}): ■, 0 mg/L ZNP θ_a ; ■, 100 mg/L ZNP θ_a ; ■, 1000 mg/L ZNP θ_a ; ■, 2000 mg/L ZNP θ_a ; ●, 0 mg/L ZNP θ_r ; ●, 100 mg/L ZNP θ_r ; ●, 1000 mg/L ZNP θ_r ; and ●, 2000 mg/L ZNP θ_r .

4.4 CONCLUSIONS

The effect of the ratio of divalent cations to sulfate ions on the advancing and receding contact angles of drops of low salinity surfactant nanofluids on weakly water wet quartz surface at a pressure of 20 MPa and temperature of 343.15 K was investigated in this study. The interfacial tension of low salinity surfactant nanofluids was also measured at the same temperature and pressure conditions. It was clearly observed that divalent cation to sulfate ion ratio has a prominent role in wettability alteration of weak water-wet quartz surfaces and on the CO₂-water interfacial tension of the system when used in combination with SDBS

surfactant augmented ZNPs at low salinity. Maximum change in the advancing and receding angle of a droplet of low salinity surfactant nanofluids was observed at M^{2+}/SO_4^{2-} values of 4.427 and 2.575, respectively. It was found that the wettability alteration is more pronounced when ZNP concentration ranges from 100 - 1000 mg/L for M^{2+}/SO_4^{2-} values in the range of 2.575-4.427. It is also interesting to observe that the interfacial tension of low salinity surfactant solutions (LSS2, LSS3 and LSS4) converge at a ZNP concentration of 100 mg/L and below which the change in IFT is independent of the M^{2+}/SO_4^{2-} ratio. However, the minimum interfacial tension value of 4.7 mN/m is obtained for a M^{2+}/SO_4^{2-} value of 4.427 (LSS1) for 2000 mg/L ZNP concentration. Importantly, it was observed that the ratio of divalent cations to sulfate ions plays a vital role in wettability alteration and interfacial tension change irrespective of the divalent to monovalent cations' ratio or presence of nanoparticles when sulfate ions are present in the solution. This study has its major implications in low salinity surfactant nanofluids EOR whereas results could also be used for the assessment of their potential use in CO₂ geosequestration/EOR/WAG.

CHAPTER 5

X-RAY MICRO-TOMOGRAPHY CORE FLOOD INVESTIGATION

5.1 INTRODUCTION

Low salinity surfactant nanofluids are yet to evolve to turn into acceptable formulations for injection in enhanced oil recovery (EOR) process (Chapter 4). Researchers have been investigating the role of low salinity surfactant nanofluids in the oil recovery by means of wettability alteration of the rock surface combined with interfacial tension (IFT) reduction of the fluid-fluid interface (Chapter 3, 4). The use of additives (such as surfactants and/or nanoparticles) combined with low salinity aqueous phase to enhance the performance of low salinity water injection has obtained a significant interest (Hosseinzade Khanamiri et al., 2016a, 2016b, 2016c; Chapter 2-4; Ivanova et al., 2019a). Although it has been briefly observed that wettability of sandstone pore surface could be altered using a low concentration of nanoparticles with low salinity surfactant (LSS) aqueous solutions, their interaction with the rock surface and fluid-fluid interface are poorly understood (Chapter 3, 4). Besides, the behavior of such low salinity surfactant nanofluids in porous rocks has not been investigated previously. Therefore, we investigate the behavior of these novel formulations in oil recovery of porous sandstone samples at ambient conditions, using high-resolution X-ray micro-computed tomography (Micro-CT) coreflooding technique. Micro-CT technique (Zhang et al., 2016; Yu et al., 2018; Yang, et al., 2019a, 2019b) is a non-destructive imaging method that has been used extensively for imaging three-dimensional pore structures as well as fluid saturation distribution in rock samples within the resolutions of a few microns. Microlevel visualization can be used to analyze mechanism of oil recovery at the scale of multiple pores and could be linked to or provide possible explanation of oil recovery at Darcy scale [9]. This work highlights the role of ZrO_2 nanoparticles in the oil phase recovery process at low salinity due

to its unique behavior as its surface potential can be altered at reservoir conditions (Bartels et al., 2017). As per our knowledge, our work is featuring the role of ZrO₂ nanoparticles in the oil phase recovery from porous sandstone media after nanoparticle surface modification by anionic surfactant adsorption for the first time at low salinity conditions. Furthermore, ZrO₂ nanoparticle has been shown to have the optimal wettability alteration performance (Nwidae et al., 2017b). Earlier experimental and theoretical studies suggest that wettability alteration and permeability change is achievable by the adsorption of nanoparticles on the surface of sandstone cores (Ju and Fan, 2009; Zhang et al., 2016). In their core flooding experiments, Ju et al. (2009) using lipophilic and hydrophilic polysilicon nanoparticles, observed that oil recovery could be improved by approximately 9% in the nanoparticle size range of 10-500 nm when compared to waterflooding only, whereas, due to the phenomena of the interfacial tension change and wettability alteration, hydrophobic-lipophilic as well as neutrally wet polysilicon nanoparticles were shown to be good EOR agent in water-wet formation, and lipophobic-hydrophilic nanoparticles shows poor recovery factor (Onyekonwu and Ogolo, 2010). A new extension in the theory of mechanism of wettability alteration, by nanoparticle structuring in the wedge film in the confined three-phase region (solid-oil-aqueous phase) inducing a structural disjoining pressure was proposed by Wasan and Nikolov (2003). Together with physicochemical factors, this phenomenon was shown to be a working mechanism in the cleansing dynamics of oil bound soil when the nanofluids were used (Wu et al., 2013). The shrinking of the three-phase region contact line towards the detachment of oil droplets was also attributed to the molecular diffusion of water molecules between the solid phase and the oil drop (Kralchevsky et al., 2005). Besides, mechanism such as emulsification and solubilization are also known to affect the cleaning of oil deposits from solid surfaces (Miller and Raney, 1993; Christian and Scamehorn, 1995). The formation of Pickering emulsions can take place too when nanoparticles are used (Chevalier and Bolzinger, 2013). The effect of salinity on the

solubility of polar organic components (salting-in and salting-out) of the oil phase is a well-known phenomenon (RezaeiDoust et al., 2009; Jackson et al., 2016). The diffusion of water molecules into the organic material causes its solvation by water structure formation around the hydrophobic part using hydrogen bonds (RezaeiDoust et al., 2009). Cations present in the aqueous phase can break the water structure that decreases the solubility of organic material (RezaeiDoust et al., 2009). Thus, reducing the salinity (salting-in) can increase its solubility if it is reduced below a critical ionic strength (RezaeiDoust et al., 2009). Diffusion based swelling of organic material could also be expected in this process (Ivanova et al., 2019b). During the process of oil recovery by low salinity water injection alone (i.e. without additives), wettability change is proposed to be a consequence and not a cause for recovery (Jackson et al., 2016). However, wettability controls fluid distribution in porous media, which in turn influences multiphase flow in an oil recovery process (Morrow, 1990; Tiab and Donaldson, 2012; Ivanova et al., 2019; Ali et al., 2020; Chapter 3, 4). Thus, this work targets to achieve higher recovery of oil phase by the injection of low salinity surfactant nanofluids by means of wettability alteration of oil-wet sandstone rock surface. A miniature core holder design suitable for micro-CT coreflood study at ambient conditions is developed and the same has been imaged at several stages of injection to find the saturation distribution and further analysis of associated effect due to injection.

5.2 MATERIALS AND METHODS

5.2.1 Materials

Doddington sandstone with porosity of 20.7% and brine permeability of 2178 md was used to drill four miniature core plugs of 15 mm length and 5 mm diameter. Details about Doddington sandstone used in this work could be found elsewhere (Iglauer et al., 2010). 1-Bromodecane (98% mass fraction purity) was used as a doping agent with the oil phase to give

Table 5.1 List of Chemicals Used in This Study

| Chemical | Supplier | Purity (mass fraction) | CAS Number |
|--|---|-------------------------------|-------------------|
| Sodium chloride (NaCl) | Rowe Scientific, Western Australia, Australia | ≥ 0.99 | 7647-14-5 |
| Calcium chloride (CaCl ₂) | Rowe Scientific, Western Australia, Australia | ≥ 0.99 | 10043-52-4 |
| Magnesium sulfate (MgSO ₄) | Merck, Australia | ≥ 0.99 | 7487-88-9 |
| Sodium sulfate (Na ₂ SO ₄) | Merck, Australia | ≥ 0.99 | 7757-82-6 |
| Zirconium dioxide nanopowder (ZrO ₂) | Merck, Australia | ≥ 0.99 | 1314-23-4 |
| Sodium dodecylbenzenesulfonate (SDBS) | Merck, Australia | ≥ 0.99 | 25155-30-0 |
| Decane | Merck, Australia | ≥ 0.99 | 124-18-5 |
| 1-Bromodecane | TCI, Australia | ≥ 0.98 | 112-29-8 |

a distinct CT signature. Zirconium dioxide (ZrO₂) nanoparticles (ZNPs) (average particle size ≤ 100 nm) was also used to prepare the nanofluids. Ultrapure water of 17.65 M Ω cm resistivity was used to prepare aqueous solutions of individual salts and surfactants. The list of chemicals used in this study is in Table 5.1.

5.2.2 Method

All salt solutions were prepared gravimetrically using an analytical balance (CP224S, Sartorius AG, Germany) with repeatability of ≤ 0.1 mg (standard deviation). A magnetic stirrer

was used to prepare the aqueous phase solutions (refer to Table 5.2) at 400-600 rpm at 20 °C. High salinity brine (HSW) was prepared and later diluted ten times to make low salinity brine (LSW). The ionic strength (I) of the brine is calculated by using the relation:

$$I = \frac{1}{2} \sum_j C_j z_j^2 \quad (5.1)$$

Where C is the molar concentration (M), and z is the valency of ionic species j . Thus, ionic strength of HSW and LSW are 0.53 M and 0.053 M, respectively. Furthermore, the low salinity brines, which contained SDBS (1.435 mM), were prepared and labeled as low salinity surfactants (LSS). LSS was used to make nanofluids with 100 and 1000 mg/L ZNPs using ultrasonication (300VT Ultrasonic Homogenizer/BIOLOGICS, using a sonication power of 240 W), each batch was sonicated for four periods of 15 min with 5 min rest to avoid overheating (Roustaei and Bagherzadeh, 2015; Al-Anssari et al., 2017; Ali et al., 2019).

Table 5.2 Compositions of the Brines

| Brine | Na⁺ [mg/L] | Ca²⁺ [mg/L] | Mg²⁺ [mg/L] | Cl⁻ [mg/L] | SO₄²⁻ [mg/L] | M²⁺/SO₄⁻ |
|--------------|--|---|---|--|---|--|
| HSW | 11494.9 | 601.2 | 36.5 | 18790.1 | 144.1 | 4.424 |
| LSW | 1149.5 | 60.1 | 3.6 | 1879.0 | 14.4 | 4.424 |

Doddington sandstone miniature plugs were coated with Teflon tape of approximately 100 mm length, and then it was held firmly under a heat shrink tube, Figure 5.1. A miniature core holder was designed to carry the sample with this arrangement with further coating, with epoxy resin and hardener, for approximately 15.7 mm diameter, Figure 5.1.

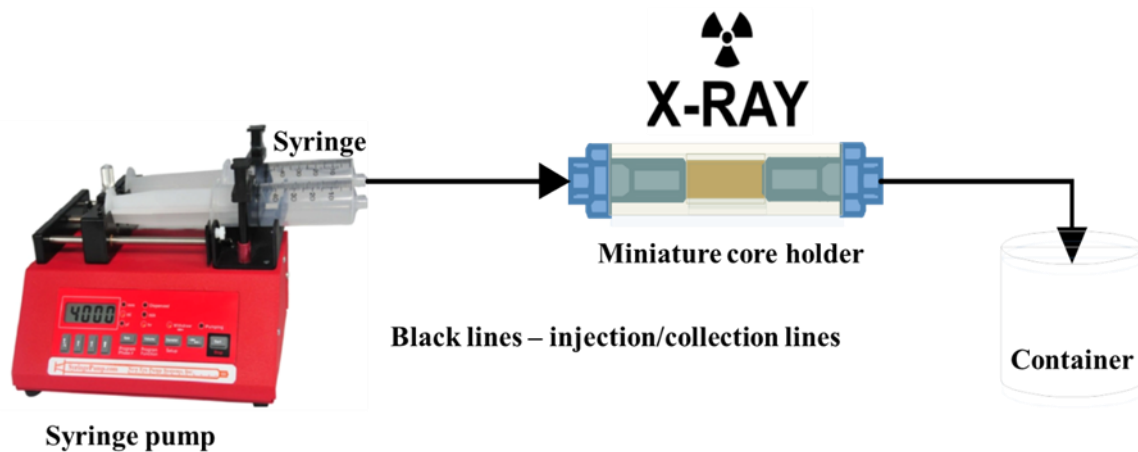


Figure 5.1 Schematic of the experimental setup to run the μ -CT core flooding experiments, black lines: injection or collection line.

Three miniature core plugs were saturated with high salinity brine under vacuum for 24 hours. Air bubbles trapped inside the pores did not appear coming out from the brine after a couple of hours of the saturation process itself, but to ensure full saturation 24 hours period was enough for the core plugs. It was then saturated with 1-bromodecane doped (35% by volume) n-decane using a syringe pump (NE-4000, Adelab Scientific, Australia) at a slow rate for 1 hour to attain connate water saturation, Figure 5.1. They were scanned (using Xradia VersaXRM instrument) at this stage at a resolution of $1.96 \mu\text{m}/\text{voxel}$ for a cylindrical volume of $2\text{mm} \times 2\text{mm}$ to get the image slices for 3D reconstruction. The purpose of the scan at this stage was to evaluate the saturation profile of both the fluids at initial condition before they could be flooded with LSS solution and LSS nanofluids. Moreover, the integrity of the design of core holders was also checked for any bypass of fluids during the saturation process; however, image analysis (using Avizo 2019.2 software, Thermofisher Scientific, USA) confirmed that no bypass occurred. Three core plugs were later flooded with LSS + 0.0% ZNP, LSS + 0.01% ZNP, and LSS 0.1% + ZNP, respectively, for up to 30 pore volumes (PV). The solutions were injected for 10 PV at the rate of 0.004 ml/min and the rate of 0.008 ml/min for additional 20 PV. They were scanned at the end of 10 PV and 30 PV, respectively, of solutions

injection. These rates were selected based on capillary number ($N_{cap} = v\mu/\gamma$, where v is the injected fluid Darcy velocity, μ is injected fluid viscosity, and γ is the fluid-fluid interfacial tension) in the order of 10^{-5} - 10^{-6} . IFT measurements between low salinity surfactant with 0%, 0.01% and 0.1% (by weight) ZNP, and doped oil phase using spinning drop tensiometer (Kruss SITE 100, Germany) at ambient condition when the equilibrium conditions were reached. The capillary tube was initially filled with the aqueous solutions, and a tiny drop using a syringe was dispensed carefully near to the middle of the capillary tube when it was still under rotation. With three repeat measurements, the IFT between LSS, LSS + 0.01% ZNP, LSS + 0.1% ZNP, and oil phase were measured to be $0.59 \pm 3.36e-3$ mN/m, $0.61 \pm 5.81e-2$ mN/m. and $0.69 \pm 2.43e-2$ mN/m, respectively.

Image processing was systematically carried out by removing artifacts and noise filtrations. Beam hardening corrections followed by non-local means filters (Buades et al., 2005) were applied to stacked images to obtain transformed images suitable for segmentation of different phases (i.e., aqueous, oil and grains). The intensity-based threshold segmentation method was applied initially which gave the saturation distribution of two fluid phases in the pore space. Following this, watershed segmentation (Schluter et al., 2014) method was used, and the volumetric quantification of phases is within 1 % error. For instance, for initial saturation phase for LSS, the volume of oil phase is calculated to be 0.96 % more when the watershed segmentation method was applied than when threshold segmentation was applied.

5.3 RESULTS AND DISCUSSION

5.3.1 Initial saturation and condition

Image segmentation results show these initial oil wetting conditions of Doddington sandstone (refer to Table 5.3 and Figure 5.3). The adsorbed alkane molecules to the silica surface can interact directly with it, and adjacent adsorbed molecules (Chapter 4). The interface

formed between hydrophilic silica interfaces and nonpolar alkane solvents is polar (Brindza and Walker, 2009; Brindza et al., 2010). According to reported values of standard adsorption free energy $\Delta G^{\circ}_{\text{ads}}$ of alkanes on silica surface, $\Delta G^{\circ}_{\text{ads}}$ decrease in the range of -10 to -25 kJ/mol for hexane to nonane (Chapter 4). However, wherever there are the rock surface and brine interface, it is expected that at the concentration of and above 0.5 M, the thickness of the electrical double layer is comparable to the thickness of the radius of a hydrated Na^+ ion (Vinogradov et al., 2010; Jackson et al., 2016). Therefore, any reduction in the ionic strength can contribute towards the double layer expansion as expected from the low salinity effect (Vinogradov et al., 2010).

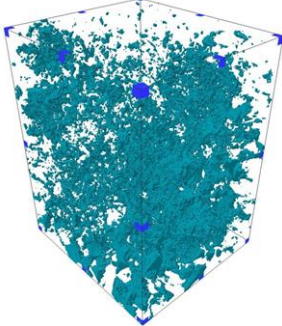
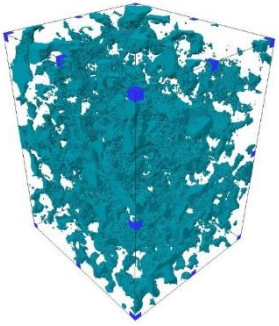
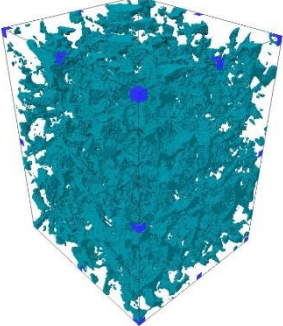
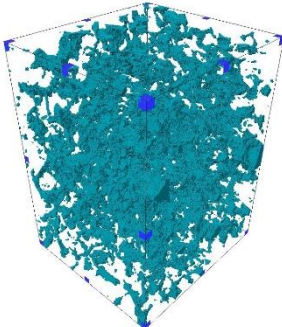
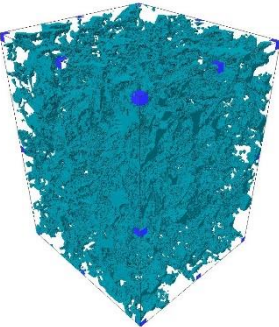
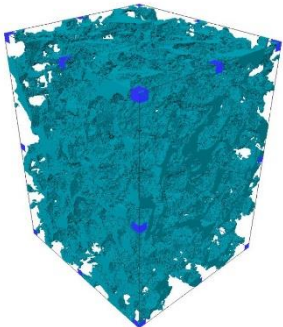
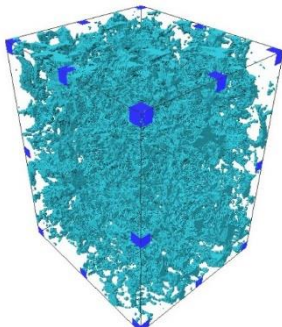
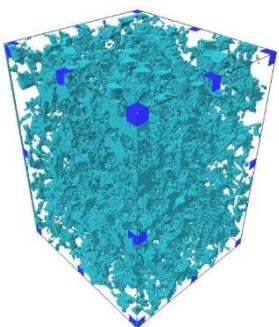
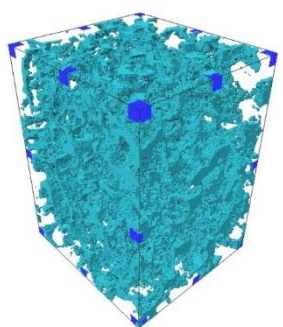
5.3.2 Coreflooding results

Table 5.3 presents the saturation profile and oil recovery for each sample at different stages of flooding. These results were calculated from the material statistics after the segmentation of images. It shows that overall recovery percent is highest in case of LSS + 0.01% ZNP of 77.9% at the end of 30 PV injection.

Table 5.3 Saturation Profile and oil Recovery

| Injection fluid | Initial water saturation | Water saturation at 10 PV | Oil recovery at 10 PV | Water saturation at 30 PV | Oil recovery at 30 PV |
|-----------------|--------------------------|---------------------------|-----------------------|---------------------------|-----------------------|
| | (%) | (%) | (%) | (%) | (%) |
| | LSS | 20.4 | 39.7 | 24.2 | 53.8 |
| LSS + 0.01%ZNP | 26.4 | 50.5 | 32.8 | 83.7 | 77.9 |
| LSS + 0.1%ZNP | 30.4 | 34.9 | 6.4 | 50.2 | 28.4 |

Table 5.4 Aqueous Phase Saturation Segmented 3D Images

| Solutions | Initial Saturation | Saturation after 10 PV injection | Saturation after 30 PV injection |
|------------------|---|--|---|
| LSS |  |  |  |
| LSS+0.01% ZNP |  |  |  |
| LSS+0.1% ZNP |  |  |  |

At 10 PV, oil recovery from injection of LSS + 0.01% ZNP is 8.6% higher than LSS alone. This difference becomes even higher (36%) when the rate of injection is doubled for an additional 20 PV. Contrary to this, injection of LSS + 0.1% ZNP shows poor recovery at 10 PV injection as well as at 30 PV. The segmented 3D images of the aqueous phase saturation have been presented in Table 5.4.

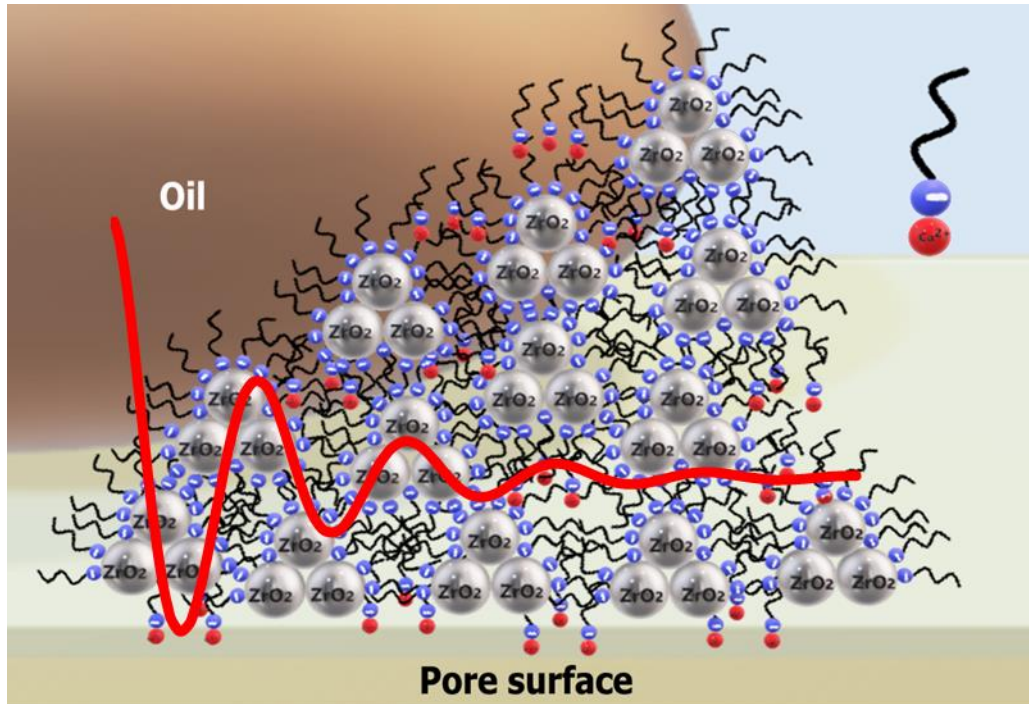


Figure 5.2 Schematic of wedge film formed at three-phase contact regions. The red curve represents the oscillatory decay of the structural disjoining pressure with the thickness of the wedge film.

5.3.3 Mechanism of oil recovery

The spreading of nanofluids on the silica surface and altering its wettability towards the detachment and displacement of oil were demonstrated earlier (Wasan and Nikolov, 2003; Kralchevsky et al., 2005) and, most recently, by Wu et al. (2018). Improvement in the spreading and frictional coefficients in the three-phase contact region are the main reasons attributed to the detachment/displacement of oil (Kralchevsky et al., 2005; Wu et al., 2018). The layering and structuring of nanoparticles in the confined wedge film induce the structural disjoining pressure, Figure 5.2 (Wasan and Nikolov, 2003; Kralchevsky et al., 2005; Zhang et al., 2016; Wu et al., 2018). This structural disjoining pressure has an oscillatory decay with the thickness of the wedge film, Figure 5.2 (Wasan and Nikolov, 2003; Kralchevsky et al., 2005; Zhang et al., 2016; Wu et al., 2018).

The magnitude of structural disjoining pressure was investigated to be dependent on effective nanoparticle volume fraction in the aqueous phase, particle size, dispersity, and particle charge (Liu et al., 2012; Kondiparty et al., 2011; Kondiparty et al., 2012). Spreading coefficient (S) is generally given by

$$S = \gamma_{sg} - \gamma_{sl} - \gamma_{lg} \quad (5.2)$$

Where, γ_{sg} , γ_{sl} and γ_{lg} are the respective solid-gas, solid-liquid, and liquid-gas interfacial tensions (Wasan and Nikolov, 2003). The de Gennes theory (de Gennes et al., 2004) relates the value of S to the disjoining pressure $\Pi(h)$ of a wetting film of film thickness h by the relation

$$S = P_c h_{eq} + \int_{h_{eq}}^{\infty} \Pi(h) dh \quad (5.3)$$

where, P_c is the capillary pressure of the bulk meniscus, h_{eq} is the equilibrium film thickness.

The capillary-pressure-driven liquid-liquid displacement can be represented by the relation (Wu et al., 2018)

$$2R \left(\gamma \cos \theta_e - \beta \frac{dh}{dt} \right) - R^2 \Delta \rho g h - 8\mu_a h \frac{dh}{dt} - 8\mu_o (L - h) \frac{dh}{dt} = 0 \quad (5.4)$$

where R is the capillary's inner radius, γ is the liquid-liquid interfacial tension, θ_e is the equilibrium liquid-liquid-solid contact angle, β is the frictional co-efficient with the same unit as viscosity, h is the displacement height at time t , $\Delta \rho$ is the density difference between two liquids, g is the gravitational acceleration constant, μ_a and μ_o are the bulk viscosities of the aqueous and oil phase, respectively, and L is the total length of the capillary.

To elucidate the displacement dynamics by the nanofluids, it was proposed that the understanding of the effect of nanoparticles on frictional co-efficient (β) needs focus, as the other parameters can be easily measured (Wu et al., 2018). The three-phase contact line moves during the displacement and oil detachment processes (Kralchevsky et al., 2005; Wu et al., 2018). This movement of contact line includes line viscous friction and thus the line friction

force (Kralchevsky et al., 2005; Wu et al., 2018). The rate dh/dt of the movement of the contact line is controlled by direct (due to capillary pressure, imbalance of interfacial tensions) and indirect forces (due to disjoining pressure, molecular level interaction) (Kralchevsky et al., 2005; Wu et al., 2018). The friction term $\beta \frac{dh}{dt}$ greatly depends on the value of frictional coefficient (β) which in its own turn quantifies the energy dissipation at the three-phase contact line in the dynamic process of oil molecules replaced by the aqueous phase [16,35]. The frictional co-efficient (β) are shown to be affected exponentially by the contribution from fluid-fluid interfacial tension (γ), nanoparticle structuring at the wedge film and the layering and structuring of oil molecules at the oil-solid interface (due to solvation forces, density at the vicinity of rock surface is higher than that of the bulk) (Kralchevsky et al., 2005; Wu et al., 2018). An increase in interfacial tension exponentially increases the frictional co-efficient (Wu et al., 2018) due to which detachment of oil droplets from the rock surface may become difficult. The rate of the movement of the contact line is majorly controlled by the imbalance of interfacial tensions (the difference between water-surface and oil phase-surface interfacial tensions) (Kralchevsky et al., 2005). If the frictional co-efficient (β) is high enough, this imbalance will not quickly relax, the rate of the movement of the contact line will be slow, and the oil detachment process will be hindered by viscous friction (Kralchevsky et al., 2005). Thus, it can be briefly concluded that β must be low due to very low measured fluid-fluid interfacial tensions; the imbalance of the other two interfacial tensions relax relatively quickly, and the viscous friction does not much hinder the detachment process.

During the flooding process and immediately after contact with the aqueous solution, the part of oil attached to the surface can detach due to necking instability (Kralchevsky et al., 2005). During the soaking period, due to disjoining pressure buildup in the wedge film, oil detachment process begins (Kralchevsky et al., 2005). Further injection of fluid can facilitate the detachment of oil due to shearing forces. The oil droplets, thus formed in the aqueous

medium, can also undergo emulsification process (Chevalier and Bolzinger, 2013) as visible from the images, Figure 5.3. This oil in water emulsion stabilized by surfactant bearing nanoparticles, Figure 5.4, prevents them to coalesce and form bigger drops (Chevalier and Bolzinger, 2013). Figure 5.5 shows that the oil phase has mostly been removed by the injection of aqueous phase. From the confining pore space, their movement to the mainstream or interconnected porous space is facilitated by the counter-current flow mechanism (Aziz et al., 2019), and later, their recovery is due to co-current flow.

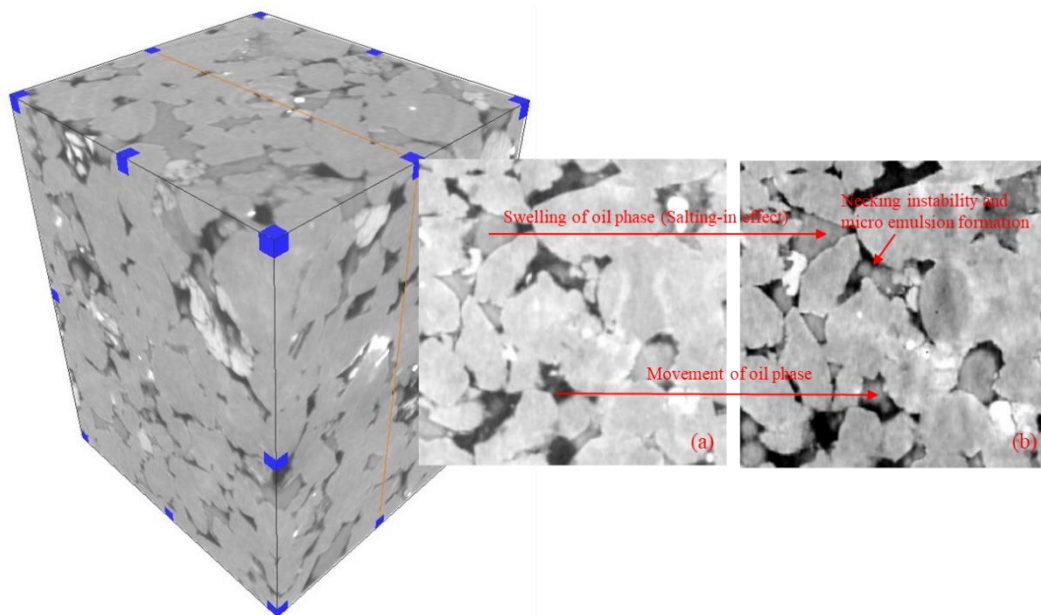


Figure 5.3 LSS + 0.01% ZNP – XZ plane (orange line) (a) Initial saturation (b) 10PV injection

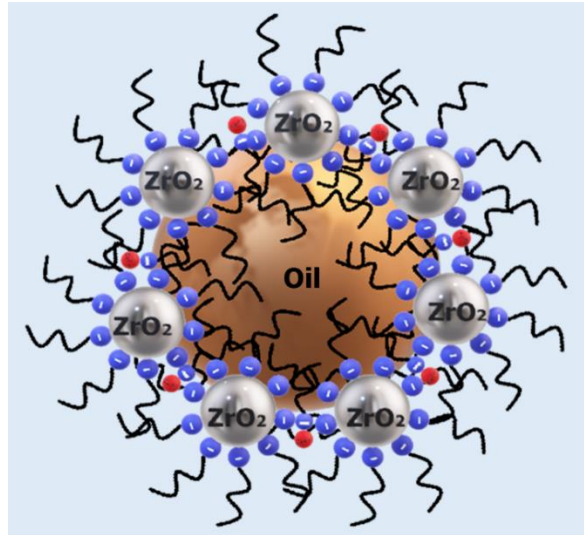


Figure 5.4 Schematic of the oil in water Pickering emulsion.

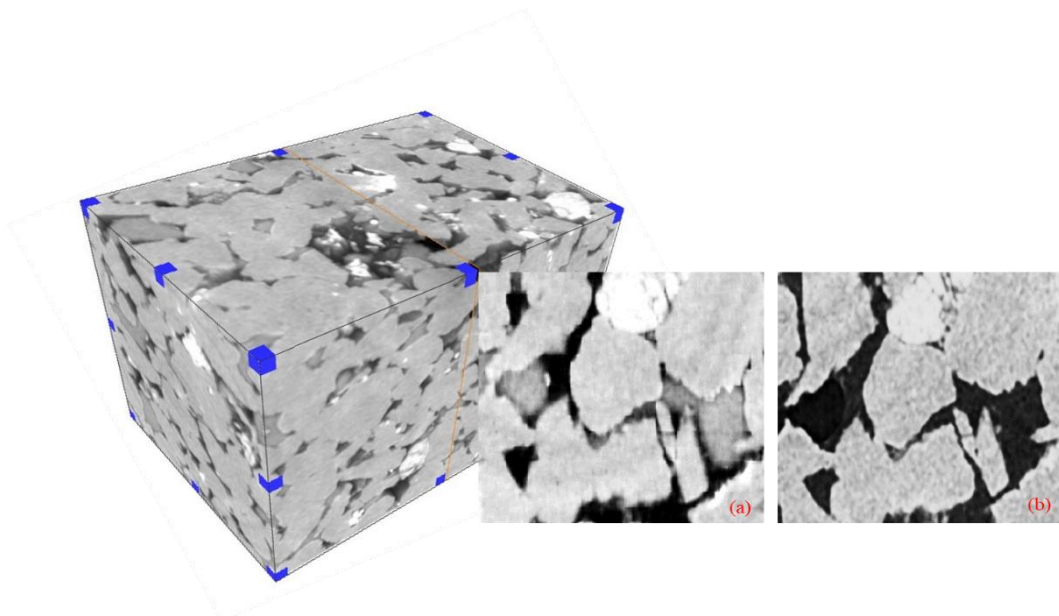


Figure 5.5 LSS + 0.01% ZNP – XY plane (orange line) (a) Initial saturation (b) 30PV

Injection

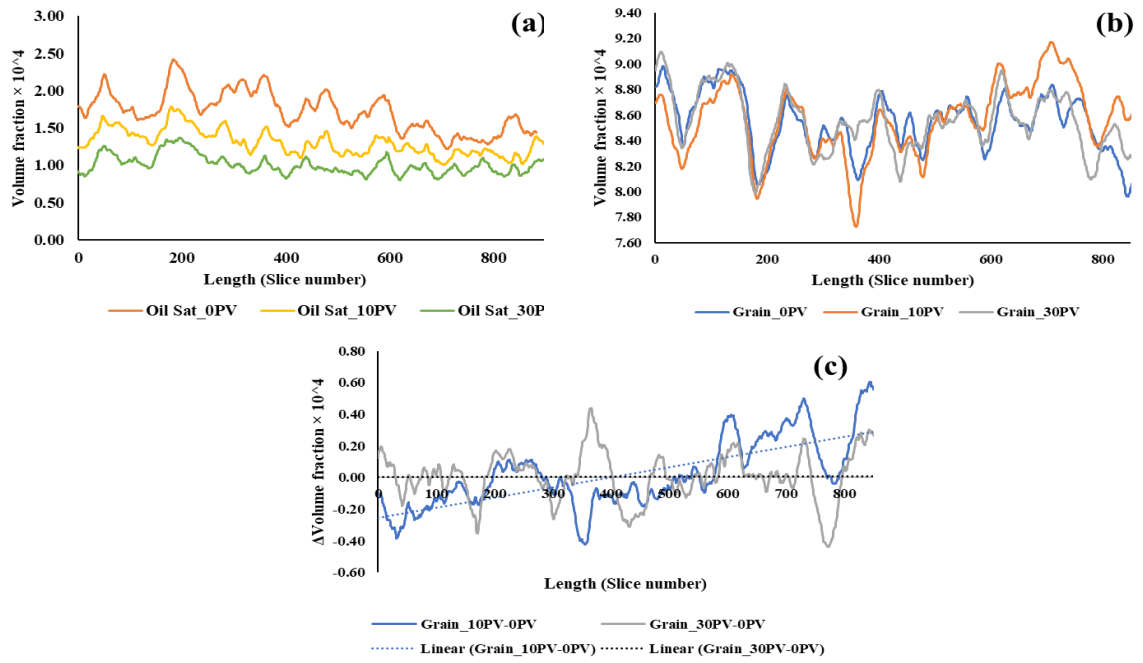


Figure 5.6 LSS injection. (a) oil saturation profile (b) grain distribution profile (c) grain fraction difference profile

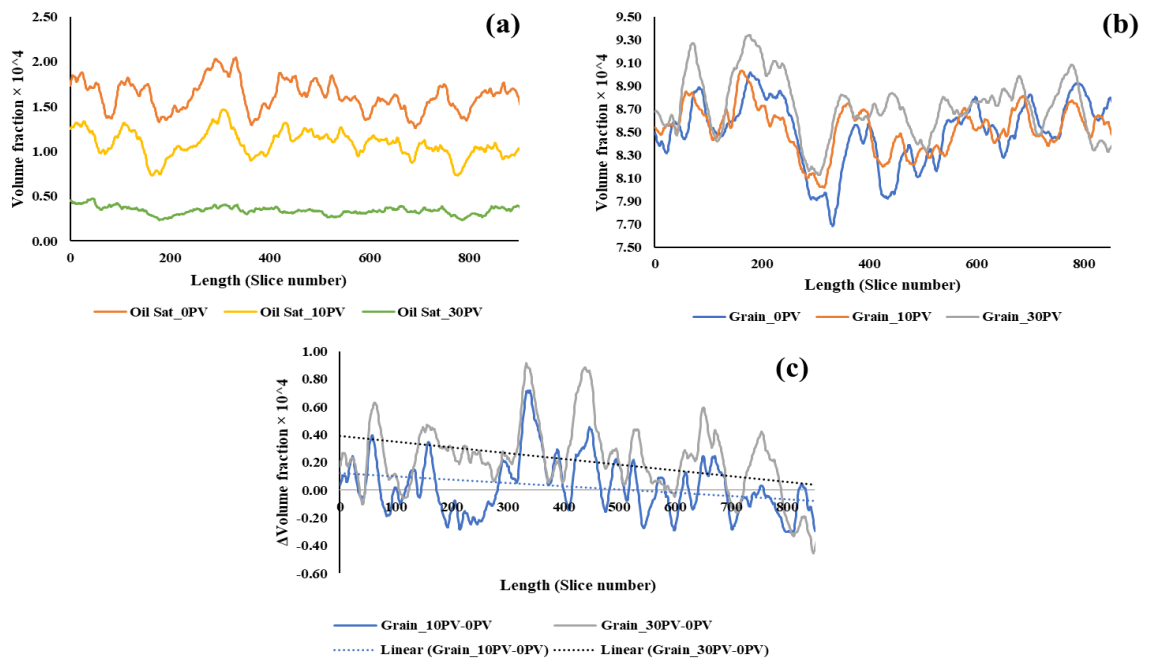


Figure 5.7 LSS + 0.01%NP (a) oil saturation profile (b) grain distribution profile (c) grain fraction difference profile.

It was argued that due to lowering of ionic strength after injection of low salinity brine, the electrical double layer expands (diffuse part of the electrical double layer expands), which causes the electrostatic repulsion between the charged mineral surfaces and adsorbed polar oil components (Anderson, 1987; Buckley et al., 1998; Durán et al., 2000; Hilner et al., 2015). When this repulsion is more than binding force, the polar oil components desorb rendering the surface more water wet. Further reduction of ionic strength below a threshold value can also cause detachment of clay particles, thus, leading to fines migration (Morrow and Buckley, 2011).

Fines migration could be clearly observed when LSS was injected up to 10 PV. From Figure 5.6 (c) extracted from Figure 5.6 (b), the grain difference plot before and after injection, the trendline shows that fines have been migrated along the lines of fluid flow. All negative values in this plot are a reduction in volume fraction whereas positive values are deposition of fines. Further injection of LSS up to 30 PV compensates this reduction from the earlier section of the rock volume, also, takes away the deposited fines, Figure 5.6(c). On the contrary, with the use of nanoparticles, it is evident that nanoparticles deposit throughout the pore walls, Figure 5.7(b and c). The trendline, Figure 5.7(b and c) clearly shows a gradient, which implies that the adsorption of nanoaggregate complexes on the rock surface has taken place, which decreases along the length of the plug. Thus, the use of higher concentration of nanoparticles, 0.1%, block pores near the inlet, and shows lesser recovery due to restriction in the flow preventing the movement of nanoaggregate complexes to farther pores, Figure 5.8(b and c). However, the mechanism of double-layer expansion needs further investigation in case the interface formed between hydrophilic silica interfaces and nonpolar alkane solvents is polar (Chapter 4; Brindza et al., 2010), i.e., where the electrostatic interaction is driven by induced polarity. This investigation may explain the situation where low salinity effect is not observed with reduced ionic strength (Sharma and Filoco, 2000; Skrettingland et al., 2011; Nasralla and

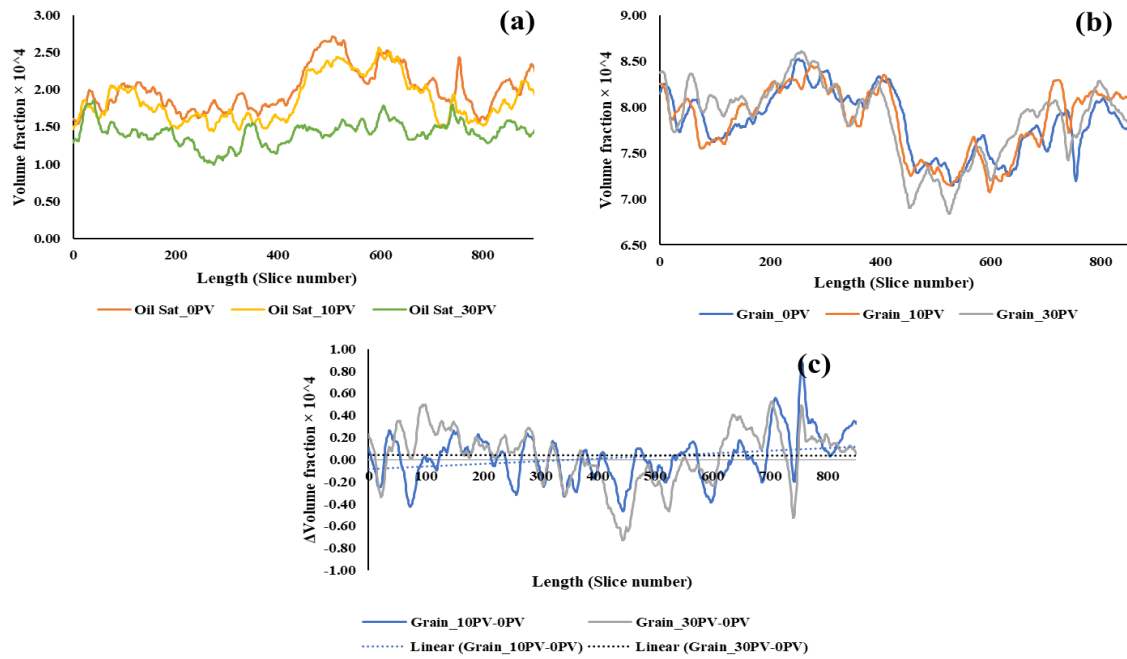


Figure 5.8 LSS + 0.1%NP (a) oil saturation profile (b) grain distribution profile (c) grain fraction difference profile.

Nasr-El-Din, 2014). Moreover, it is also broadly known that with decreasing salinity, the solubility of organic compounds in brine increases (salting-in/out effect) (RezaeiDoust et al., 2009). The mechanism of this effect has largely been ignored and needs to remain in investigation (RezaeiDoust et al., 2009; Doust et al., 2011; Jackson et al., 2016). The evidence in this work also suggests low salinity effect as oil phase swells and moves in pore throats (due to capillary effect) after LSS injection. Due to confined space, the swelling of the oil phase gives an impression (visual) that it is wetting the pore walls and throats, Figure 5.3.

5.3.4 Oil phase cluster statistics

Oil phase cluster size distributions correlate to remobilization and mass transfer effects (Iglauer et al., 2019). Thus, they were analyzed subsequently and systematically from the segmented oil phase saturation distribution. Larger clusters are prone to break into smaller clusters, however, can also be easily remobilized (Herring et al., 2016), but can slow down

mass transfer due to smaller surface area to volume ratio (Iglauer and Wulling, 2016; Jiang et al., 2016). The extraction of equivalent diameter for the segmented 3D volume of oil phase clusters use the following equation:

$$\text{Equivalent Diameter} = \sqrt[3]{6 \frac{\text{Volume}_{3d}}{\pi}} \quad (5.5)$$

The number of oil clusters are counted, and a frequency histogram are used for analysis. Thus, Figure 5.9 (a-c) shows the oil phase clusters frequency histograms for LSS+0%NP, LSS+0.01%NP, and LSS+0.1%NP, respectively.

Thus, from the analysis, it is evident from the Figure 5.9 (a), the frequency distribution histogram of LSS, frequency decreases rapidly in initial saturation and 10 PV injection conditions with the increase in cluster size, however, there is a slight increase in frequency initially (for 30 PV) and then rapid decrease with increase in cluster size. This implies that both with increased rate (between 10-30 PV) and large pore volumes (10 PV and 30 PV) of injection in case of LSS breaks larger clusters into smaller clusters. A similar observation was made in terms of frequency distribution histogram of LSS+0.01% ZNP and LSS+0.1% ZNP. Surprisingly there is a dramatic increase in small size clusters for LSS+0.01% ZNP (at 30PV, Figure 5.9 b) at residual saturation (Figure 5.7 a). This dramatic increase in smaller clusters can be attributed to breaking of relatively bigger clusters and the formation of microemulsions.

To further delineate this attribution, a sphericity analysis of the oil phase clusters has been carried out. Sphericity (ψ) can be calculated using the segmented cluster volume (volume_{3d}) and surface area (A) of the oil phase by the equation,

$$\psi = \frac{\pi^{1/3} (6 * \text{Volume}_{3d})^{2/3}}{A} \quad (5.6)$$

$\psi < 1$ means the cluster is non-spherical in shape. From all data, it has been analyzed that approximately 92 % of the clusters are less than 90 μm size. Thus, $\leq 90 \mu\text{m}$ size clusters were chosen for sphericity analysis. The conservative estimate for ψ in the range of ≥ 0.95 and strict estimate in the range of ≥ 0.98 were calculated (Table 5.5). A large fraction of oil phase clusters $\psi \geq 0.95$ and ≥ 0.98 were calculated for LSS1+0.01% ZNP in which the clusters fraction of high sphericity (i.e. $\psi \geq 0.98$) outnumbered fractions from other injection fluids significantly at 10PV and 30PV injection. This high fraction of high sphericity implies that nanoparticle interaction is much higher and significantly contributed to the formation of microemulsions.

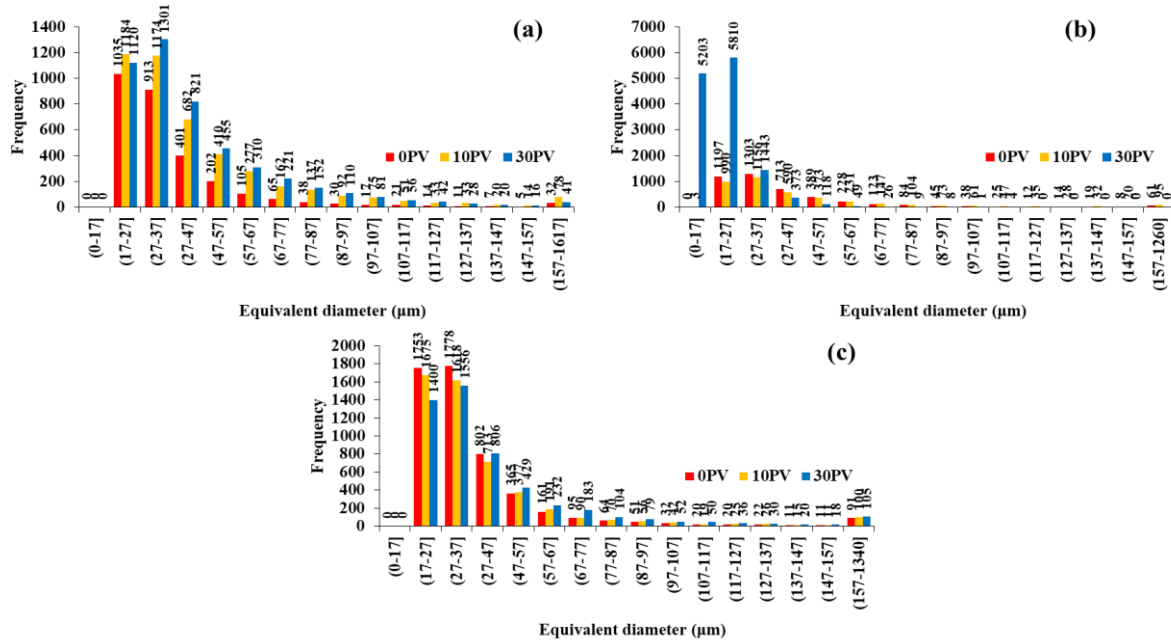


Figure 5.9 Oil phase cluster size distribution for (a) LSS (b) LSS + 0.01 % ZNP (c) LSS + 0.1 % ZNP.

5.3.5 Implications

This work evidence that the use of nanoparticles in optimal concentration (0.01%) with low salinity surfactant aqueous solutions increase the oil phase recovery mainly by means of wettability alteration towards water-wet state due to adsorption of nanoaggregates complexes and interfacial tension reduction between oil and aqueous phase. Fines migration caused by the low salinity effect, as seen in oil recovery by the low salinity surfactant injection only, could also be significantly controlled using nanoparticles. Moreover, the formation of microemulsions due to nanofluids injection at this optimal concentration is evident from the analysis. This study has implications in the performance enhancement of low salinity water injection projects.

5.4 CONCLUSIONS

Pore level understanding of a new class of low salinity fluids with surfactant and nanoparticles as additives to enhance the oil recovery performance by low salinity water injection has not been conceived yet. Their effect on the recovery performance, using ZrO_2 nanoparticles (0, 0.01% and 0.1% by weight) in low salinity surfactant solutions has been investigated, by injecting them into oil phase saturated real sandstone (Doddington) porous media at ambient conditions. Utilizing a very high resolution (voxel size $\sim 2 \mu m$) micro-visualization technique, interestingly, it was seen by analysis that fines migration by low salinity effect is prominent even with the surfactant present which can be suppressed significantly when we use ZrO_2 nanoparticles in the same solution. In combination with interfacial tension reduction and low salinity effect, moderate oil recovery is observed in the case when no nanoparticles were used. The use of optimal concentration of nanoparticles (0.01% by weight) shows a high recovery of 32.8% (at 10 PV injection) and 77.9% (at 30 PV injection). The reason for this high recovery is attributed to the wettability alteration to water-

wet condition due to adsorption of nanoaggregate complexes along with the interfacial tension reduction. Nanoaggregate complexes adsorption facilitates structural disjoining pressure and helps in the detachment of oil phase. After a rest or soaking period, further injection of injection fluids at higher rate helps in increasing the recovery. However, induction of structural disjoining pressure in the wedge film and subsequent wettability alteration by migration of fines of nanometre size (where no nanoparticles were used) towards the oil recovery cannot be ruled out. In this process of recovery using nanoparticles, microemulsion formation (high fraction of oil phase clusters of high sphericities, $\psi \geq 0.98$) is also evident, which might additionally contribute to the interfacial tension reduction and needs further investigation. An increase in the concentration of ZrO_2 nanoparticles has adverse effects in the oil recovery possibly mainly due to blockage of rock pores preventing the mobility of nanoaggregate complexes.

CHAPTER 6

CONCLUSION AND FUTURE RECOMMENDATIONS

Additives such as surfactant and nanoparticles in combination with low salinity water appeared to be promising formulations for oil/aqueous phase interfacial tension reduction, rock wettability modification, surfactant adsorption control, and enhanced oil recovery. Depending on the reservoir conditions (such as high temperature and pressure, acidic and basic conditions, sandstone with associated clays), low salinity water and additive compositions (such as divalent ions to sulphate ratio, types, and concentrations of surfactants and nanoparticles) can be optimized to effectively control the interfacial tension, surfactant adsorption and wettability.

Surfactants by spontaneous self-aggregation at the interface causes the interfacial tension reduction. The results of this investigation show that addition of salts into the aqueous solution further helps in reducing the oil and aqueous phase interfacial tension. Depending on the electric charge density, binding of counterion with the surfactant molecules helps in tight surfactant packing due to electrostatic repulsion between the head groups of the surfactant molecules.

Further, investigation showed that the effect of the divalent cation-sulphate ion ratio on anionic surfactant adsorption on clay in presence of nanoparticles at high alkaline and low salinity condition was pronounced for low ratios (M^{2+}/SO_4^{2-} values < 2.575). The effect of silica nanoparticles concentration on anionic surfactant adsorption was pronounced when used in higher concentrations (>1000 mg/L). The 1000 mg/L silica nanoparticles with high pH low salinity surfactant solution turned out to be a strong wettability modifier when USBM wettability index measurements were carried out for initial oil-wet Berea sandstone core plugs. Further increasing SNP concentration had no or minimal effect on the sandstone wettability. This wettability effect can be attributed to the co-adsorption of nanoaggregates surfactant complexes and surfactant molecules on the sandstone surface which can be prominent at an

optimal SNP concentration. Besides, our hypothesis is that there is an interplay of availability of divalent cations for bridging between clay/sandstone surface and SNP, SNP and anionic surfactant or between clay surface and anionic surfactant. Facilitated by cation bridging, co-adsorption of nanoaggregates and surfactants takes place over the clay containing sandstone surface and can alter its wettability, possibly, favorably towards oil recovery by low salinity surfactant nanofluids injection.

Under supercritical CO₂ loading at the high pressure and temperature, thus acidic condition, it has been found that the wettability alteration of quartz surface to towards water-wet is more pronounced when zirconium dioxide concentration ranges from 100 - 1000 mg/L for M²⁺/SO₄²⁻ values in the range of 2.575-4.427.

Pore level investigation using X-ray micro-CT coreflood shows that the optimal concentration of nanoparticles used in combination with low salinity surfactant aqueous phase is very effective in oil phase recovery by means of interfacial tension reduction, wettability alteration and micro-emulsion (Pickering emulsions) formation in large quantity. For the detachment of oil from the sandstone rock surface, the reason is attributed to the disjoining pressure induced by wedge film effect of nanoaggregates in three-phase (oil/aqueous/solid phase) contact regions followed by stabilized micro-emulsion formation in a large quantity. A larger concentration of nanoparticles adversely affects oil production by blocking the rock pores. Furthermore, the use of nanoparticles also suppresses the fines migration caused due to the low salinity effect. The use of surfactant alone as an additive is insufficient to mitigate this problem as the evidence from this study shows that fines migration still occurs and may block the rock pores.

This study has implications in the enhanced oil recovery by low salinity water injection, whereas, the implication on CO₂ EOR or CO₂ geosequestration is rather trivial.

RECOMMENDATIONS FOR THE FUTURE WORK

Recommendation for the future work are as follows:

- The above study can be replicated for oil bearing carbonate reservoir case too. The use of additives with low salinity surfactant nanofluids has never been tried and could be of major implications for carbonate reservoirs. Carbonate reservoir are even more challenging due to their high heterogeneities.
- Study can be carried out to see the effect of salt type on the interfacial tension between oil and aqueous phase containing cationic surfactants at low salinity conditions at high pressure and temperature conditions.
- It will be also interesting to study the synergistic effect of different types and mixture of surfactants and nanoparticles at low concentration in combination of low salinity aqueous phase.
- Study of the effect of low salinity surfactant nanofluids on carbonate at alkaline and acidic conditions can be carried out.
- X-ray micro-tomography core flood investigation can be carried out for carbonate case using aqueous solutions containing surface modified nanoparticles at low salinity conditions.
- The above study could be extended in different crude oil types (such as heavy crude, paraffinic, naphthenic, aromatic and low/high acidic) scenario both for sandstone and carbonates.

REFERENCES

- Ahmadall, T., Gonzalez, M. V., Harwell, J. H., and Scamehorn, J. F.** (1993) Reducing Surfactant Adsorption in Carbonate Reservoirs. *SPE Reservoir Engineering*, **8**, 117–122.
- Ahmadi, M. A. and Shadizadeh, S. R.** (2012) Adsorption of novel nonionic surfactant and particles mixture in carbonates: Enhanced oil recovery implication. *Energy and Fuels*, **26**, 4655–4663.
- Al-Anssari, S., Barifcani, A., Wang, S., Maxim, L., and Iglauer, S.** (2016) Wettability alteration of oil-wet carbonate by silica nanofluid. *Journal of Colloid and Interface Science*, **461**, 435–442.
- Al-Anssari, S., Wang, S., Barifcani, A., and Iglauer, S.** (2017) Oil-water interfacial tensions of silica nanoparticle-surfactant formulations. *Tenside, Surfactants, Detergents*, **54**, 334–341.
- Al-Anssari, S., Arif, M., Wang, S., Barifcani, A., Lebedev, M., and Iglauer, S.** (2017) Wettability of nano-treated calcite/CO₂/brine systems: Implication for enhanced CO₂ storage potential. *International Journal of Greenhouse Gas Control*, **66**, 97–105.
- Al-Anssari, S., Barifcani, A., Keshavarz, A., and Iglauer, S.** (2018) Impact of nanoparticles on the CO₂-brine interfacial tension at high pressure and temperature, *Journal of Colloid and Interface Science*, **532**, 136–142.
- Al-Anssari, S., Arif, M., Wang, S., Barifcani, A., Lebedev, M., and Iglauer, S.** (2018) Wettability of nanofluid-modified oil-wet calcite at reservoir conditions. *Fuel*, **211**, 405–414.
- Al-Bayati, D., Saeedi, A., Xie, Q., Myers, M. B., and White, C.** (2018) Influence of Permeability Heterogeneity on Miscible CO₂ Flooding Efficiency in Sandstone Reservoirs: An Experimental Investigation. *Transport in Porous Media*, **125**, 341–356.
- Al-Bayati, D., Saeedi, A., Myers, M., White, C., Xie, Q., and Clennell, B.** (2018) Insight

- investigation of miscible scCO₂ Water Alternating Gas (WAG) injection performance in heterogeneous sandstone reservoirs. *Journal of CO₂ Utilization*, **28**, 255–263.
- Al-Khdheawi, E. A., Vialle, S., Barifcani, A., Sarmadivaleh, M. and Iglauer, S.** (2018) Enhancement of CO₂ trapping efficiency in heterogeneous reservoirs by water-alternating gas injection. *Greenhouse Gases: Science and Technology*, **8**, 920–931.
- Al-Khdheawi, E. A., Vialle, S., Barifcani, A., Sarmadivaleh, M., Zhang, Y., and Iglauer, S.** (2018) Impact of salinity on CO₂ containment security in highly heterogeneous reservoirs. *Greenhouse Gases: Science and Technology*, **8**, 93–105.
- Al-Shalabi, E. W. and Sepehrnoori, K.** (2016) A comprehensive review of low salinity/engineered water injections and their applications in sandstone and carbonate rocks. *Journal of Petroleum Science and Engineering*, **139**, 137–161.
- Alagic, E. and Skauge, A.** (2010) Combined low salinity brine injection and surfactant flooding in mixed-wet sandstone cores. *Energy and Fuels*, **24**, 3551–3559.
- Alargova, R., Petkov, J., and Petsev, D.** (2003) Micellization and interfacial properties of alkyloxyethylene sulfate surfactants in the presence of multivalent counterions. *Journal of Colloid and Interface Science*, **26**, 1–11.
- Ali, M., Al-Anssari, S., Arif, M., Barifcani, A., Sarmadivaleh, M., Stalker, L., Lebedev, M., and Iglauer, S.** (2019) Organic acid concentration thresholds for ageing of carbonate minerals: Implications for CO₂ trapping/storage. *Journal of Colloid and Interface Science*. Academic Press, 534, 88–94.
- Ali, M., Sahito, M. F., Jha, N. K., Arain, Z. U. A., Memon, S., Keshavarz, A., Iglauer, S., Saeedi, A., and Sarmadivaleh, M.** (2020) Effect of nanofluid on CO₂-wettability reversal of sandstone formation, implications for CO₂ geo-storage. *Journal of Colloid and Interface Science*, **559**, 304–312.
- Allen, F. J., Griffin, L. R., Alloway, R. M., Gutfreund, P., Lee, S. Y., Truscott, C. L.,**

- Welbourn, R. J. L., Wood, M. H., and Clarke, S. M.** (2017) An Anionic surfactant on an anionic substrate: monovalent cation binding. *Langmuir*, **33**, 7881–7888.
- De Almeida, J. M. and Miranda, C. R.** (2016) Improved oil recovery in nanopores: NanoIOR. *Scientific Reports*, **6**, 28128.
- Anderson, W. G.** (1986) Wettability literature survey - Part 2: wettability measurement. *Journal of Petroleum Technology*, **38**, 1246–1262.
- Anderson, W. G.** (1987) Wettability literature survey - Part 6: The effects of wettability on waterflooding. *Journal of Petroleum Technology*, **39**, 1605–1622.
- Arif, M., Barifcani, A., Lebedev, M., and Iglauer, S.** (2016) Structural trapping capacity of oil-wet caprock as a function of pressure, temperature and salinity. *International Journal of Greenhouse Gas Control*, **50**, 112–120.
- Arif, M. Lebedev, M., Barifcani, A., and Iglauer, S.** (2017) CO₂ storage in carbonates: Wettability of calcite. *International Journal of Greenhouse Gas Control*, **62**, 113–121.
- Asakawa, T., Kitano, H., Ohta, A., and Miyagishi, S.** (2001) Convenient estimation for counterion dissociation of cationic micelles using chloride-sensitive fluorescence probe. *Journal of Colloid and Interface Science*, **242**, 284–287.
- Aziz, R., Joekar-Niasar, V., Martínez-Ferrer, P. J., Godinez-Brizuela, O. E., Theodoropoulos, C. and Mahani H.** (2019) Novel insights into pore-scale dynamics of wettability alteration during low salinity waterflooding. *Scientific Reports*, **9**, 9257.
- Babadagli, T.** (2007) Development of mature oil fields - A review. *Journal of Petroleum Science and Engineering*, **57**, 221–246.
- Baird, J. C. and Walz, J. Y.** (2006) The effects of added nanoparticles on aqueous kaolinite suspensions: I. Structural effects. *Journal of Colloid and Interface Science*, **297**, 161–169.
- Bartels, W. B., Rücker, M., Berg, S., Mahani, H., Georgiadis, A., Fadili, A., Brussee, N.,**

- Coorn, A., van L. Er, H., Hinz, C., Jacob, A., Wagner, C., Henkel, S., Enzmann, F., Bonnin, A., Stampanoni, M., Ott, H., Blunt, M., and Hassanizadeh, S. M.** (2017) Fast X-ray micro-CT study of the impact of brine salinity on the pore-scale fluid distribution during waterflooding. *Petrophysics*, **55**, 36–47.
- Berg, S., Cense, A. W., Jansen, E., and Bakker, K.** (2010) Direct experimental evidence of wettability modification by low salinity. *Petrophysics*, **51**, 314–322.
- Binks, B. P.** (2002) Particles as surfactants - Similarities and differences. *Current Opinion in Colloid and Interface Science*, **7**, 21–41.
- Boul, P. J. and Ajayan, P. M.** (2020) Nanotechnology research and development in upstream oil and gas. *Energy Technology*, **8**, 1-18.
- Brindza, M. R., Ding, F., Fourkas, J. T., and Walker, R. A.** (2010) N-alkane adsorption to polar silica surfaces. *Journal of Chemical Physics*, **132**, 114701.
- Brindza, M. R. and Walker, R. A.** (2009) Differentiating solvation mechanisms at polar solid/liquid interfaces. *Journal of the American Chemical Society*, **131**, 6207–6214.
- Buades, A., Coll, B., and Morel, J. M.** (2005) A non-local algorithm for image denoising. *Proceedings - 2005 IEEE Computer Society Conference on Computer Vision and Pattern Recognition, CVPR 2005*. IEEE, 60–65.
- Buckley, J. S., Liu, Y. and Monsterleet, S.** (1998) Mechanisms of wetting alteration by crude oils. *SPE Journal*, **3**, 54–61.
- Chavez-Miyauchi, T. E., Firoozabadi, A., and Fuller, G. G.** (2016) Nonmonotonic elasticity of the crude oil-brine interface in relation to improved oil recovery. *Langmuir*, **32**, 2192–2198.
- Chen, Y., Sari, A., Xie, Q., and Saeedi, A.** (2019) Excess H⁺ Increases hydrophilicity during CO₂-assisted enhanced oil recovery in sandstone reservoirs. *Energy & Fuels*, **33**, 814–821

- Chevalier, Y. and Bolzinger, M. A.** (2013) Emulsions stabilized with solid nanoparticles: Pickering emulsions. *Colloids and Surfaces A: Physicochemical and Engineering Aspects*, **439**, 23–34.
- Christian, S. D. and Scamehorn, J. F.** (1995) Solubilization in surfactant aggregates. CRC Press, 568.
- Connor, P. and Ottewill, R. H.** (1971) The adsorption of cationic surface active agents on polystyrene surfaces. *Journal of Colloid And Interface Science*, **37**, 642–651.
- Dey, J. Bhattacharjee, J., Hassan, P. A., Aswal, V. K., Das, S., and Ismail, K.** (2010) Micellar shape driven counterion binding. Small-angle neutron scattering study of AOT micelle, *Langmuir*, **26**, 15802–15806.
- Dey, J., Thapa, U. and Ismail, K.** (2012) Aggregation and adsorption of sodium dioctylsulfosuccinate in aqueous ammonium chloride solution: Role of mixed counterions. *Journal of Colloid and Interface Science*, **367**, 305–310.
- Dole, M.** (1938) A theory of surface tension of aqueous solutions. *Journal of the American Chemical Society*, **60**, 904–911.
- Donaldson, E. C., Thomas, R. D., and Lorenz, P. B.** (1969) Wettability determination and its effect on recovery efficiency. *SPE Journal*, **9**, 13–20.
- Doust, A. R., Puntervold, T., and Austad, T.** (2011) Chemical verification of the EOR mechanism by using low saline/smart water in sandstone. *Energy and Fuels*, **25**, 2151–2162.
- Dugyala, V. R. Muthukuru, J. S., Mani, E., and Basavaraj, M. G.** (2016) Role of electrostatic interactions in the adsorption kinetics of nanoparticles at fluid-fluid interfaces. *Physical Chemistry Chemical Physics*, **18**, 5499–5508.
- Durán, J. D. G., Ramos-Tejada, M. M., Arroyo, F. J., and González-Caballero, F.** (2000) Rheological and electrokinetic properties of sodium montmorillonite suspensions.

- Journal of Colloid and Interface Science*, **229**, 107–117.
- Fauziah, C. A., Al-Yaseri, A. Z., Beloborodov, R., Siddiqui, M. A. Q., Lebedev, M., Parsons, D., Roshan, H., Barifcani, A., and Iglauer, S.** (2019) Carbon dioxide/brine, nitrogen/brine, and oil/brine wettability of montmorillonite, illite, and kaolinite at elevated pressure and temperature. *Energy and Fuels*, **33**, 441–448.
- Fu, L., Wang, Z., Li, X., and Zhang, L.** (2017) Surface properties, micellar molecular interaction, and physical properties for binary systems of sodium oleate with three anionic surfactants. *Journal of Dispersion Science and Technology*, **38**, 712–720.
- Gee, M. L., Healy, T. W. and White, L. R.** (1989) Ellipsometric studies of alkane adsorption on quartz. *Journal of Colloid and Interface Science*, **131**, 18–23.
- de Gennes, P. G., Brochard-Wyart, F. and Quéré, D.** (2004) *Capillarity and Wetting Phenomena*.
- Giraldo, J., Benjumea, P., Lopera, S., Cortes, F. B., and Ruiz, M. A.** (2013) Wettability alteration of sandstone cores by alumina-based nanofluids. *Energy and Fuels*, **27**, 3659–3665.
- Griffin, L. R., Browning, K. L., Truscott, C. L., Clifton, L. A., Webster, J., and Clarke, S. M.** (2016) A comparison of didodecyldimethylammonium bromide adsorbed at mica/water and silica/water interfaces using neutron reflection. *Journal of Colloid and Interface Science*, **478**, 365–373.
- Guo, H., Li, Y., Wang, F., and Gu, Y.** (2017) Comparison of strong-alkali and weak-alkali ASP-flooding field tests in Daqing oilfield. *SPE Production & Operations*, **33**, 353-362.
- Gurkov, T. D., Dimitrova, D. T., Marinova, K. G., Bilke-Crause, C., Gerber, C., and Ivanov, I. B.** (2005) Ionic surfactants on fluid interfaces: Determination of the adsorption; Role of the salt and the type of the hydrophobic phase. *Colloids and Surfaces A: Physicochemical and Engineering Aspects*, **261**, 29–38.

- Hadia, N. J., Hansen, T., Tweheyo, M. T., and Torsæter, O.** (2012) Influence of crude oil components on recovery by high and low salinity waterflooding. *Energy and Fuels*, **26**, 4328–4335.
- Hadia, N. J., Ashraf, A., Tweheyo, M. T., and Torsæter, O.** (2013) Laboratory investigation on effects of initial wettabilities on performance of low salinity waterflooding. *Journal of Petroleum Science and Engineering*, **105**, 18–25.
- Hammond, P. S. and Unsal, E.** (2012) A dynamic pore network model for oil displacement by wettability-altering surfactant solution. *Transport in Porous Media*, **92**, 789–817.
- Hamon, G.** (2016) Low salinity waterflooding: facts, inconsistencies and the way forward. *Petrophysics*, **57**, 41–50.
- Hamouda, A. A. and Karoussi, O.** (2008) Effect of temperature, wettability and relative permeability on oil recovery from oil-wet chalk. *Energies*, **1**, 19–34.
- Hanna, H. S. and Somasundaran, P.** (1979) Equilibration of kaolinite in aqueous inorganic and surfactant solutions. *Journal of Colloid And Interface Science*, **70**, 181–191.
- Hendraningrat, L., Li, S. and Torsæter, O.** (2013) A coreflood investigation of nanofluid enhanced oil recovery. *Journal of Petroleum Science and Engineering*, **111**, 128–138.
- Herring, A. L., Andersson, L. and Wildenschild, D.** (2016) Enhancing residual trapping of supercritical CO₂ via cyclic injections. *Geophysical Research Letters*, **43**, 9677–9685.
- Hilner, E., Andersson, M. P., Hassenkam, T., Matthiesen, J., Salino, P. A., and Stipp, S. L. S.** (2015) The effect of ionic strength on oil adhesion in sandstone - The search for the low salinity mechanism. *Scientific Reports*, **5**, 9933.
- Holzwarth, A., Leporatti, S. and Riegler, H.** (2000) Molecular ordering and domain morphology of molecularly thin triacontane films at SiO₂/air interfaces. *Europhysics Letters*. **52**, 653–659.
- Hosseinzade Khanamiri, H., Nourani, M., Tichelkamp, T., Stensen, J. Å., Øye, G., and**

- Torsæter, O.** (2016a) Low-salinity-surfactant enhanced oil recovery (EOR) with a new surfactant blend: Effect of calcium cations, *Energy and Fuels*, **30**, 984–991.
- Hosseinzade Khanamiri, H., Baltzersen Enge, I., Nourani, M., Stensen, J. Å., Torsæter, O., and Hadia, N.** (2016b) EOR by low salinity water and surfactant at low concentration: impact of injection and in situ brine composition. *Energy and Fuels*, **30**, 2705–2713.
- Hosseinzade Khanamiri, H., Torsæter, O. and Stensen, J. A.** (2016c) Effect of calcium in pore scale oil trapping by low-salinity water and surfactant enhanced oil recovery at strongly water-wet conditions: In situ imaging by X-ray microtomography. *Energy and Fuels*, **30**, 8114–8124.
- Hunter, T. N., Pugh, R. J., Franks, G. V., and Jameson, G. J.** (2008) The role of particles in stabilising foams and emulsions. *Advances in Colloid and Interface Science*, **137**, 57–81.
- Iglauer, S., Wu, Y., Shuler, P., Tang, Y., and Goddard, W. A.** (2009) Alkyl polyglycoside surfactant-alcohol cosolvent formulations for improved oil recovery. *Colloids and Surfaces A: Physicochemical and Engineering Aspects*, **339**, 48–59.
- Iglauer, S., Wu, Y., Shuler, P., Tang, Y., and Goddard, W. A.** (2010) New surfactant classes for enhanced oil recovery and their tertiary oil recovery potential, *Journal of Petroleum Science and Engineering*, **71**, 23–29.
- Iglauer, S., Favretto, S., Spinelli, G., Schena, G., and Blunt, M. J.** (2010) X-ray tomography measurements of power-law cluster size distributions for the nonwetting phase in sandstones. *Physical Review E - Statistical, Nonlinear, and Soft Matter Physics*, **82**, 1–3.
- Iglauer, S., Wu, Y., Shuler, P., Tang, Y., and Goddard, W. A.** (2011) Alkyl polyglycoside/1-naphthol formulations: A case study of surfactant enhanced oil recovery, *Tenside Surfactants Detergents*, **48**, 121–126.

- Iglauer, S.** (2017) CO₂-water-rock wettability: variability, influencing factors, and implications for CO₂ geostorage. *Accounts of Chemical Research*, **50**, 1134–1142.
- Iglauer, S.** (2018) Optimum storage depths for structural CO₂ trapping. *International Journal of Greenhouse Gas Control*, **77**, 82–87.
- Iglauer, S., Paluszny, A., Rahman, T., Zhang, Y., Wüilling, W., and Lebdev, M.** (2019) Residual trapping of CO₂ in an oil-filled, oil-wet sandstone core: results of three-phase pore scale imaging. *Geophysical Research Letters*, **46**, 11,146-11,154 GL083401.
- Iglauer, S., Pentland, C. H. and Busch, A.** (2014) CO₂ wettability of seal and reservoir rocks and the implications for carbon geo-sequestration. *Water Resources Research*, 729-774.
- Iglauer, S. and Wüilling, W.** (2016) The scaling exponent of residual nonwetting phase cluster size distributions in porous media. *Geophysical Research Letters*, **43**, 11,253-11,260.
- Ivanova, A., Mitiurev, N., Cheremisin, A., Orekhov, A., Kamyshinsky, R., and Vasiliev, A.** (2019a) Characterization of organic layer in oil carbonate reservoir rocks and its effect on microscale wetting properties. *Scientific Reports*, **9**, 1-10.
- Ivanova, A. A., Phan, C., A. Barifcani, S. Iglauer, and Cheremisin, A. N.** (2019c) Effect of nanoparticles on viscosity and interfacial tension of aqueous surfactant solutions at high salinity and high temperature. *Journal of Surfactants and Detergents*.
- Ivanova, A. A., Cheremisin, A. N., Barifcani, A., Iglauer, S., and Phan, C.** (2019b) Molecular insights in the temperature effect on adsorption of cationic surfactants at liquid/liquid interfaces. *Journal of Molecular Liquids*, **299**, 1-9.
- Jackson, M. D., Vinogradov, J., Hamon, G., and Chamerois, M.** (2016) Evidence, mechanisms and improved understanding of controlled salinity waterflooding part 1: Sandstones. *Fuel*, **185**, 772–793.
- Jackson, M. D., Al-Mahrouqi, D. and Vinogradov, J.** (2016) Zeta potential in oil-water-carbonate systems and its impact on oil recovery during controlled salinity water-

- flooding. *Scientific Reports*, **6**, 1-13.
- Jha, N. K., Ojha, U., Kumar, A., and Mathur, A.** (2015) Analysis of CO₂ swelling and modeling of PVT properties of reservoir fluid of an onland field of Gujarat, India. *Carbon Management Technology Conference 2015: Sustainable and Economical CCUS Options, CMTC 2015*, 949–958.
- Jha, N. K., Ali, M., Sarmadivaleh, M., Iglauer, S., Barifcani, A., Lebedev, M., and Sangwai, J.** (2018) Low salinity surfactant nanofluids for enhanced CO₂ storage application at high pressure and temperature. *EAGE 5th CO₂ Geological Storage Workshop*.
- Jha, N. K., Iglauer, S., Barifcani, A., Sarmadivaleh, M., and Sangwai, J. S.** (2019) Low-salinity surfactant nanofluid formulations for wettability alteration of sandstone: Role of the SiO₂ nanoparticle concentration and divalent cation/SO₄²⁻ ratio. *Energy and Fuels*, **33**, 739–746.
- Jha, N. K., Ali, M., Iglauer, S., Lebedev, M., Roshan, H., Barifcani, A., Sangwai, J. S., and Sarmadivaleh, M.** (2019) Wettability alteration of quartz surface by low-salinity surfactant nanofluids at high-pressure and high-temperature conditions. *Energy and Fuels*, **33**, 7062–7068.
- Jha, N. K., Iglauer, S. and Sangwai, J. S.** (2018) Effect of monovalent and divalent salts on the interfacial tension of n -heptane against aqueous anionic surfactant solutions. *Journal of Chemical and Engineering Data*, **63**, 2341–2350.
- Jiang, L., Yu, M., Wu, B., Suekane, T., Li, W., and Song, Y.** (2016) Characterization of dissolution process during brine injection in Berea sandstones: an experiment study. *RSC Advances*, **6**, 114320–114328.
- Jones, G. and Ray, W. A.** (1935) The surface tension of solutions. *Journal of the American Chemical Society*, **57**, 957–958.

- Jones, G. and Ray, W. A.** (1937) The surface tension of solutions of electrolytes as a function of the concentration. I. A differential method for measuring relative surface tension. *Journal of the American Chemical Society*, **59**, 187–198.
- Jones, G. and Ray, W. A.** (1941a) The surface tension of solutions of electrolytes as a function of the concentration. II*. *Journal of the American Chemical Society*, **63**, 288–294.
- Jones, G. and Ray, W. A.** (1941b) The surface tension of solutions of electrolytes as a function of the concentration. III. Sodium chloride, *Journal of the American Chemical Society*, **63**, 3262–3263.
- Jones, G. and Ray, W. A.** (1942) The surface tension of solutions of electrolytes as a function of the concentration. IV. Magnesium sulfate. *Journal of the American Chemical Society*, **64**, 2744–2745.
- Ju, B. and Fan, T.** (2009) Experimental study and mathematical model of nanoparticle transport in porous media. *Powder Technology*, **192**, 195–202.
- Jungwirth, P. and Tobias, D. J.** (2002) Ions at the air/water interface. *Journal of Physical Chemistry B*, **106**, 6361–6373.
- Kakati, A. and Sangwai, J. S.** (2017) Effect of monovalent and divalent salts on the interfacial tension of pure hydrocarbon-brine systems relevant for low salinity water flooding, *Journal of Petroleum Science and Engineering*, **157**, 1106–1114.
- Kakati, A. and Sangwai, J. S.** (2018) Wettability alteration of mineral surface during low-salinity water flooding: Role of salt type, pure alkanes, and model oils containing polar components, *Energy and Fuels*, **32**, 3127–3137.
- Kareem, R., Cubillas, P., Gluyas, J., Bowen, L., Hillier, S., and Greenwell, H. C.** (2017) Multi-technique approach to the petrophysical characterization of Berea sandstone core plugs (Cleveland Quarries, USA). *Journal of Petroleum Science and Engineering*, **149**, 436–455.

- Karimaie, H. and Lindeberg, E.** (2017) Experimental verification of CO₂ dissolution rate due to diffusion induced convection. *Energy Procedia*, **114**, 4917–4925.
- Kobayashi, K., Liang, Y., Murata, S., Matsuoka, T., Takahashi, S., Amano, K. I., Nishi, N., and Sakka, T.** (2017) Stability evaluation of cation bridging on muscovite surface for improved description of ion-specific wettability alteration, *Journal of Physical Chemistry C*, **121**, 9273–9281.
- Kondiparty, K., Nikolov, A., Wu, S., and Wasan, D.** (2011) Wetting and spreading of nanofluids on solid surfaces driven by the structural disjoining pressure: Statics analysis and experiments. *Langmuir*, **27**, 3324–3335.
- Kondiparty, K., Nikolov, A. D., Wasan, D., and Liu, K. L.** (2012) Dynamic spreading of nanofluids on solids. part I: Experimental. *Langmuir*, **28**, 14618–14623.
- Kralchevsky, P. A., Danov, K. D., Kolev, V. L., Gurkov, T. D., Temelska, M. I., and Brenn, G.** (2005) Detachment of oil drops from solid surfaces in surfactant solutions: Molecular mechanisms at a moving contact line. *Industrial and Engineering Chemistry Research*, **44**, 1309–1321.
- Kuang, W., Saraji, S. and Piri, M.** (2018) A systematic experimental investigation on the synergistic effects of aqueous nanofluids on interfacial properties and their implications for enhanced oil recovery. *Fuel*, **220**, 849–870.
- Li, Y., Zhang, W., Kong, B., Puerto, M., Bao, X., Sha, O., Shen, Z., Yang, Y., Liu, Y., and Gu, S.** (2016) Mixtures of anionic-cationic surfactants: A new approach for enhanced oil recovery in low-salinity, high-temperature sandstone reservoir. *SPE Journal*, **21**, 1164–1177.
- Liu, K. L., Kondiparty, K., Nikolov, A. D., and Wasan, D.** (2012) Dynamic spreading of nanofluids on solids part II: Modeling. *Langmuir*, **28**, 16274–16284.
- Liu, X. and Bai, M.** (2017) Effect of chemical composition on the surface charge property and

- flotation behavior of pyrophyllite particles. *Advanced Powder Technology*, **28**, 836–841.
- Liu, Y.** (2009) Is the free energy change of adsorption correctly calculated? *Journal of Chemical and Engineering Data*, **54**, 1981–1985.
- Liu, Y., Chase, H. M. and Geiger, F. M.** (2019) Partially (resp . fully) reversible adsorption of monoterpenes (resp . alkanes and cycloalkanes) to fused silica. *The Journal of Chemical Physics*, **150**, 1-8.
- Mahani, H., Keya, A. L., Berg, S., Bartels, W. B., Nasralla, R., and Rossen, W. R.** (2015) Insights into the mechanism of wettability alteration by low-salinity flooding (LSF) in carbonates. *Energy and Fuels*, **29**, 1352–1367.
- Mahani, H., Berg, S., Ilic, D., Bartels, W. B., and Joekar-Niasar, V.** (2015) Kinetics of low-salinity-flooding effect, *SPE Journal*, **20**, 008–020.
- Maneedaeng, A., Flood, A. E., Haller, K. J., and Grady, B. P.** (2012) Modeling of precipitation phase boundaries in mixed surfactant systems using an improved counterion binding model. *Journal of Surfactants and Detergents*, **15**, 523–531.
- Maneedaeng, A. and Flood, A. E.** (2016) Synergisms in binary mixtures of anionic and pH-insensitive zwitterionic surfactants and their precipitation behavior with calcium ions. *Journal of Surfactants and Detergents*, **20**, 263–275.
- Marion, C., Jordens, A., McCarthy, S., Grammatikopoulos, T., and Waters, K. E.** (2015) An investigation into the flotation of muscovite with an amine collector and calcium lignin sulfonate depressant. *Separation and Purification Technology*, **149**, 216–227.
- McGuire, P. L., Chantham, J. R., Paskvan, F. K., Sommer, D. M., and Carini, F. H.** (2005) Low salinity oil recovery: an exciting new EOR opportunity for Alaska’s north slope. *Paper SPE 93903 presented at the 2005 SPE Western Regional Meeting*, Irvine, California, USA, 30 March-1 April.
- Michalkova, A., Gorb, L., Hill, F., and Leszczynski, J.** (2011) Can the gibbs free energy of

- adsorption be predicted efficiently and accurately: An M05-2X DFT study. *Journal of Physical Chemistry A*, **115**, 2423–2430.
- Miller, C. A. and Raney, K. H.** (1993) Solubilization-emulsification mechanisms of detergency. *Colloids and Surfaces A: Physicochemical and Engineering Aspects*, **74**, 169–215.
- Mohajeri, M., Hemmati, M. and Shekarabi, A. S.** (2015) An experimental study on using a nanosurfactant in an EOR process of heavy oil in a fractured micromodel. *Journal of Petroleum Science and Engineering*, **126**, 162–173. .
- Morrow, N. and Buckley, J.** (2011) Improved oil recovery by low-salinity waterflooding, *Journal of Petroleum Technology*, **63**, 106–112.
- Morrow, N. R.** (1990) Wettability and its effect on oil recovery. *Journal of Petroleum Technology*, **42**, 1476–1484.
- Namani, M., Souraki, Y., Kleppe, J., Høier, L., and Karimaie, H.** (2017) Scaled experimental and simulation study of segregation in water-above-gas injection. *SPE Reservoir Evaluation & Engineering*, **20**, 0809–0819.
- Nasralla, R. A. and Nasr-El-Din, H. A.** (2011) Impact of electrical surface charges and cation exchange on oil recovery by low salinity water. *SPE Asia Pacific Oil and Gas Conference and Exhibition, Jakarta, Indonesia*, 20-22 September.
- Nasralla, R. A. and Nasr-El-Din, H. A.** (2014) Double-layer expansion: Is it a primary mechanism of improved oil recovery by low-salinity waterflooding? *SPE Reservoir Evaluation and Engineering*, **17**, 49–59.
- Nwidee, L. N., Theophilus, S., Barifcani, A., Sarmadivaleh, M., and Iglauer, S.** (2016) EOR processes, opportunities and technological advancements. *Chemical Enhanced Oil Recovery (cEOR) - a Practical Overview*. InTech.
- Nwidee, L. N., Al-Anssari, S., Barifcani, A., Sarmadivaleh, M., Lebedev, M., and Iglauer,**

- S. (2017a) Nanoparticles influence on wetting behaviour of fractured limestone formation. *Journal of Petroleum Science and Engineering*, **149**, 782–788.
- Nwidee, L. N., Lebedev, M., Lebedev, M., Barifcani, A., Sarmadivaleh, M., and Iglauer, S.** (2017b) Wettability alteration of oil-wet limestone using surfactant-nanoparticle formulation. *Journal of Colloid and Interface Science*, **504**, 334–345.
- Nwidee, L. N., Barifcani, A., Sarmadivaleh, M., and Iglauer, S.** (2018) Nanofluids as novel alternative smart fluids for reservoir wettability alteration. *Novel Nanomaterials - Synthesis and Applications*, 327-357.
- Olajire, A. A.** (2014) Review of ASP EOR (alkaline surfactant polymer enhanced oil recovery) technology in the petroleum industry: Prospects and challenges. *Energy*, 963–982.
- Onsager, L. and Samaras, N. N. T.** (1934) The surface tension of Debye-Hückel electrolytes. *The Journal of Chemical Physics*, **2**, 528–536.
- Onyekonwu, M. O. and Ogolo, N. A.** (2010) Investigating the use of nanoparticles in enhancing oil recovery. *Society of Petroleum Engineers - Nigeria Annual International Conference and Exhibition 2010*, 974–987.
- Ostrowski, N., Sharma, V., Roy, A., and Kumta, P. N.** (2015) Systematic assessment of synthesized tri-magnesium phosphate powders (amorphous, semi-crystalline and crystalline) and cements for ceramic bone cement applications. *Journal of Materials Science and Technology*, **31**, 437–444.
- Pang, J., Zhao, T., Xin, X., Chen, Y., Tan, Y., and Xu, G.** (2016) Effect of inorganic salts on the aggregation behavior of AOT at the air/water interface. *Journal of Surfactants and Detergents*, **19**, 1015–1024.
- Papirer, E.** (2018) *Adsorption on Silica Surfaces*.
- Petersen, P. B. and Saykally, R. J.** (2005) Adsorption of ions to the surface of dilute electrolyte solutions: The Jones-Ray effect revisited. *Journal of the American Chemical*

- Society*, **127**, 15446–15452.
- Petkov, J. T., Tucker, I. M., Penfold, J., Thomas, R. K., Petsev, D. N., Dong, C. C., Golding, S., and Grillo, I.** (2010) The impact of multivalent counterions, Al^{3+} , on the surface adsorption and self-assembly of the anionic surfactant alkyloxyethylene sulfate and anionic/nonionic surfactant mixtures. *Langmuir*, **26**, 16699–16709.
- Pouryousefy, E., Xie, Q. and Saeedi, A.** (2016) Effect of multi-component ions exchange on low salinity EOR: Coupled geochemical simulation study. *Petroleum*, **2**, 215–224.
- Prosser, A. J. and Franses, E. I.** (2001) Adsorption and surface tension of ionic surfactants at the air–water interface: review and evaluation of equilibrium models. *Colloids and Surfaces A: Physicochemical and Engineering Aspects*, **178**, 1–40.
- Puntervold, T., Strand, S. and Austad, T.** (2007) Water flooding of carbonate reservoirs: Effects of a model base and natural crude oil bases on chalk wettability. *Energy and Fuels*, **21**, 1606–1616.
- Putnam, F. W. and Neurath, H.** (1944) Stoichiometric complexes of serum albumin and sodium dodecyl sulfate. *Journal of the American Chemical Society*, **66**, 1992.
- RezaeiDoust, A. Puntervold, T., Strand, S., and Austad, T.** (2009) Smart water as wettability modifier in carbonate and sandstone: A discussion of similarities/differences in the chemical mechanisms. *Energy and Fuels*, **23**, 4479–4485.
- Robb, I. D. and Smith, R.** (1974) Nuclear spin-lattice relaxation times of alkali metal counterions at micellar interfaces. *J.Chem.Soc., Faraday Trans.1*, **70**, 287–292.
- Rodriguez, C. H., Lowery, L. H., Scamehorn, J. F., and Harwell, J. H.** (2001) Kinetics of precipitation of surfactants. I. Anionic surfactants with calcium and with cationic surfactants. *Journal of Surfactants and Detergents*, **4**, 1–14.
- Rosen, M. J.** (1976) The relationship of structure to properties in surfactants. IV. Effectiveness in surface or interfacial tension reduction. *Journal of Colloid And Interface Science*, **56**,

320–327.

- Rosen, M. J. and Kunjappu, J. T.** (2012) *Surfactants and Phenomena, Fourth Edition*.
- Roshan, H., Al-Yaseri, A. Z., Sarmadivaleh, M., and Iglauer, S.** (2016) On wettability of shale rocks. *Journal of Colloid and Interface Science*, **475**, 104–111.
- Roustaeei, A. and Bagherzadeh, H.** (2015) Experimental investigation of SiO₂ nanoparticles on enhanced oil recovery of carbonate reservoirs. *Journal of Petroleum Exploration and Production Technology*, **5**, 27–33.
- Sakthivel, S. Velusamy, S., Gardas, R. L., and Sangwai, J. S.** (2015a) Adsorption of aliphatic ionic liquids at low waxy crude oil-water interfaces and the effect of brine. *Colloids and Surfaces A: Physicochemical and Engineering Aspects*, **468**, 62–75.
- Sakthivel, S. Velusamy, S., Gardas, R. L., and Sangwai, J. S.** (2015b) Use of aromatic ionic liquids in the reduction of surface phenomena of crude oil-water system and their synergism with brine. *Industrial and Engineering Chemistry Research*, **54**, 968–978.
- Sandoval, T. E., Gárate, M. P. and Olea, A. F.** (2014) Aggregation of alcohols ethoxylates (CiEOj) in dibutoxymethane and surface activity at the water/dibutoxymethane interface. *Colloids and Surfaces A: Physicochemical and Engineering Aspects*, **441**, 211–216.
- Schlagen, L. J. M., Koopal, L. K., Stuart, M. A. C., and Lyklema, J.** (1995) Thin hydrocarbon and water films on bare and methylated silica: Vapor adsorption, wettability, adhesion, and surface forces. *Langmuir*, **11**, 1701–1710.
- Schlagen, L. J. M. and Koopal, L. K.** (1996) Self-consistent field theory for the adsorption of alkanes on solid surfaces. *Langmuir*, **12**, 1863–1869.
- Schlüter, S., Sheppard, A., Brown, K., and Wildenschild, D.** (2014) Image processing of multiphase images obtained via X-ray microtomography: A review. *Water Resources Research*, **50**, 3615–3639.
- ShamsiJazeyi, H., Miller, C. A., Wong, M. S., Tour, J. M., and Verduzco, R.** (2014)

- Polymer-coated nanoparticles for enhanced oil recovery, *Journal of Applied Polymer Science*, **131**, 221–246.
- Shamsijazeyi, H., Hirasaki, G. J. and Verduzco, R.** (2013) Sacrificial agent for reducing adsorption of anionic surfactants. *Paper SPE-164061-MS presented at the SPE International Symposium on Oilfield Chemistry*, The Woodlands, Texas, USA, 8-10 April., 1–16.
- Sharma, H., Dufour, S., Arachchilage, G. W. P. P., Weerasooriya, U., Pope, G. A., and Mohanty, K.** (2015) Alternative alkalis for ASP flooding in anhydrite containing oil reservoirs. *Fuel*, Elsevier, **140**, 407–420.
- Sharma, M. M. and Filoco, P. R.** (2000) Effect of brine salinity and crude-oil properties on oil recovery and residual saturations, *SPE Journal*, **5**, 293–300.
- Sharma, T., Iglauer, S. and Sangwai, J. S.** (2016) Silica nanofluids in an oilfield polymer polyacrylamide: Interfacial properties, wettability alteration, and applications for chemical enhanced oil recovery. *Industrial and Engineering Chemistry Research*, **55**, 12387–12397.
- Sharma, T., Kumar, G. S. and Sangwai, J. S.** (2015) Comparative effectiveness of production performance of Pickering emulsion stabilized by nanoparticle-surfactant-polymer over surfactant-polymer (SP) flooding for enhanced oil recovery for Brownfield reservoir. *Journal of Petroleum Science and Engineering*, **129**, 221–232.
- Sheng, J.** (2010) *Modern Chemical Enhanced Oil Recovery: Theory and Practice*. Gulf Professional Publishing.
- Siddiqui, M. A. Q., Ali, S., Fei, H., and Roshan, H.** (2018) Current understanding of shale wettability: A review on contact angle measurements. *Earth-Science Reviews*, **181**, 1–11.
- Skrettingland, K., Holt, T., Tveheyo, M. T., and Skjevrak, I.** (2011) Snorre low-salinity-water injection-coreflooding experiments and single-well field pilot. *SPE Reservoir*

Evaluation and Engineering, **14**, 182–192.

Stosur, G. J. (2003) EOR: Past, present and what the next 25 years may bring. *Paper 84864 presented at the SPE IOR Conference in Asia Pacific*, Kuala Lumpur, Malaysia, October 20-21.

Stosur, G. J., Hite, J. R., and Carnahan, N. F. (2003) The alphabet soup of IOR, EOR and AOR: Effective communication requires a definition of terms. *Paper 84908 presented at the SPE International IOR Conference in Asia Pacific*, Kuala Lumpur, Malaysia, October 20-21.

Strand, S., Høgnesen, E. J. and Austad, T. (2006) Wettability alteration of carbonates - Effects of potential determining ions (Ca^{2+} and SO_4^{2-}) and temperature. *Colloids and Surfaces A: Physicochemical and Engineering Aspects*, **275**, 1–10.

Suzzoni, A., Barre, L., Kohler, E., Levitz, P., Michot, L. J., and MHamdi, J. (2018) Interactions between kaolinite clay and AOT. *Colloids and Surfaces A: Physicochemical and Engineering Aspects*, **556**, 309–315.

Tang, G. Q. and Morrow, N. R. (1999) Influence of brine composition and fines migration on crude oil/brine/rock interactions and oil recovery. *Journal of Petroleum Science and Engineering*, **24**, 99–111.

Tavassoli, S., Kazemi Nia Korrani, A., Pope, G. A., and Sepehrnoori, K. (2016) Low-salinity surfactant flooding - A multimechanistic enhanced-oil-recovery method. *SPE Journal*, **21**, 0744–0760.

Tiab, D. and Donaldson, E. C. (2012) Wettability. *Petrophysics 4th Edition*, 371–418.

Tichelkamp, T., Vu, Y., Nourani, M., and Øye, G. (2014) Interfacial tension between low salinity solutions of sulfonate surfactants and crude and model oils. *Energy and Fuels*, **28**, 2408–2414.

Tichelkamp, T., Teigen, E., Nourani, M., and Øye, G. (2015) Systematic study of the effect

- of electrolyte composition on interfacial tensions between surfactant solutions and crude oils. *Chemical Engineering Science*, **132**, 244–249.
- Tola, S., Sasaki, K. and Sugai, Y.** (2017) Wettability alteration of sandstone with zinc oxide nano-particles. *Society of Petrophysicists and Well-Log Analysts*, 1–4.
- Tong, W., Zheng, Q., Shao, S., Lei, Q., and Fang, W.** (2010) Critical micellar concentrations of quaternary ammonium surfactants with hydroxyethyl substituents on headgroups determined by isothermal titration calorimetry, *Journal of Chemical and Engineering Data*, **55**, 3766–3771.
- Umlong, I. M. and Ismail, K.** (2005) Micellization of AOT in aqueous sodium chloride, sodium acetate, sodium propionate, and sodium butyrate media: A case of two different concentration regions of counterion binding, *Journal of Colloid and Interface Science*, **291**, 529–536.
- Unsal, E., Rücker, M., Berg, S., Bartels, W. B., and Bonnin, A.** (2019) Imaging of compositional gradients during in situ emulsification using X-ray micro-tomography, *Journal of Colloid and Interface Science*, **550**, 159–169.
- Vinogradov, J., Jaafar, M. Z. and Jackson, M. D.** (2010) Measurement of streaming potential coupling coefficient in sandstones saturated with natural and artificial brines at high salinity. *Journal of Geophysical Research: Solid Earth*, **115**, 1-18.
- Wamkam, C. T., Opoku, M. K., Hong, H., and Smith, P.** (2011) Effects of pH on heat transfer nanofluids containing ZrO₂ and TiO₂ nanoparticles. *Journal of Applied Physics*, **109**, 1-5.
- Wang, Z.** (2010) Interactions between an anionic fluorosurfactant and a PEO-PPO-PEO triblock copolymer in aqueous solutions. *Journal of Surfactants and Detergents*, **13**, 97–102.
- Ward, A. F. H. and Tordai, L.** (1946) Time-dependence of boundary tensions of solutions I.

- The role of diffusion in time-effects, *The Journal of Chemical Physics*, **14**, 453–461.
- Wasan, D. T. and Nikolov, A. D.** (2003) Spreading of nanofluids on solids, *Nature*, **423**, 156–159.
- Wei, B., Wu, R., Lu, L., Ning, X., Xu, X., Wood, C., and Yang, Y.** (2017) Influence of individual ions on oil/brine/rock interfacial interactions and oil-water flow behaviors in porous media. *Energy and Fuels*, **31**, 12035–12045.
- Wilhelmy, L.** (1863) Ueber die abhängigkeit der capillaritäts-constanten des alkohols von substanz und gestalt des benetzten festen körpers. *Annalen der Physik und Chemie*, **195**, 177–217.
- Wu, P., Nikolov, A. D. and Wasan, D. T.** (2018) Two-phase displacement dynamics in capillaries-nanofluid reduces the frictional coefficient. *Journal of Colloid and Interface Science*, **532**, 153–160.
- Wu, S., Nikolov, A. and Wasan, D.** (2013) Cleansing dynamics of oily soil using nanofluids, *Journal of Colloid and Interface Science*, **396**, 293–306.
- Wu, Y., Iglauer, S., Shuler, P., Tang, Y., and Goddard, W. A.** (2010) Alkyl polyglycoside-sorbitan ester formulations for improved oil recovery, *Tenside Surfactants Detergents*, **47**, 280–287.
- Wu, Y., Iglauer, S., Shuler, P., Tang, Y., and Goddard, W. A.** (2011) Experimental study of surfactant retention on Kaolinite clay. *Tenside, Surfactants, Detergents*, **48**, 346–358.
- Wu, Y., Chen, W., Dai, C., Huang, Y., Li, H., Zhao, M., He, L., and Jiao, B.** (2017) Reducing surfactant adsorption on rock by silica nanoparticles for enhanced oil recovery, *Journal of Petroleum Science and Engineering*, **153**, 283–287.
- Xie, Q., Saeedi, A., Pooryousefy, E., and Liu, Y.** (2016) Extended DLVO-based estimates of surface force in low salinity water flooding. *Journal of Molecular Liquids*, **221**, 658–665.

- Yang, Y., Li, Y., Yao, J., Zhang, K., Iglauer, S., Luquot, L., and Wang, Z.** (2019) Formation damage evaluation of a sandstone reservoir via pore-scale X-ray computed tomography analysis. *Journal of Petroleum Science and Engineering*, **183**, 1-11.
- Yang, Y., Yang, H., Tao, L., Yao, J., Wang, W., Zhang, K., and Luquot, L.** (2019) Microscopic determination of remaining oil distribution in sandstones with different permeability scales using computed tomography scanning. *Journal of Energy Resources Technology, Transactions of the ASME*, **141**, 1-11.
- Yarranton, H. W. and Masliyah, J. H.** (1996) Gibbs-Langmuir model for interfacial tension of nonideal organic mixtures over water. *The Journal of Physical Chemistry*, **100**, 1786–1792.
- Yu, H., Zhang, Y., Lebedev, M., Han, T., Verrall, M., Wang, Z., Al-Khdheawi, E., Al-Yaseri, A., and Iglauer, S.** (2018) Nanoscale geomechanical properties of Western Australian coal. *Journal of Petroleum Science and Engineering*, **162**, 736–746.
- Zachara, J. M., Cowan, C. E., Schmidt, R. L., and Ainsworth, C. C.** (1988) Chromate Adsorption by Kaolinite. *Clays and Clay Minerals*, **36**, 317–326.
- Zhang, C., Valsaraj, K. T., Constant, W. D., and Roy, D.** (1999) Aerobic biodegradation kinetics of four anionic and nonionic surfactants at sub- and supra-critical micelle concentrations (CMCs). *Water Research*, **33**, 115–124.
- Zhang, H. T., Ramakrishnan, S., Nikolov, A., and Wasan, D.** (2016) Enhanced oil recovery driven by nanofilm structural disjoining pressure: Flooding experiments and microvisualization. *Energy and Fuels*, **30**, 2771–2779.
- Zhang, L., Zhang, J., Wang, Y., Yang, R., Zhang, Y., Gu, J., Zhang, M., and Ren, S.** (2018) Experimental investigation of low-salinity water flooding in a low-permeability oil reservoir. *Energy and Fuels*, **32**, 3108–3118.
- Zhang, P., Tweheyo, M. T. and Austad, T.** (2006) Wettability alteration and improved oil

recovery in chalk: The effect of calcium in the presence of sulfate. *Energy and Fuels*, **20**, 2056–2062.

Zhang, S., Lu, X. Wu, J., Tong W., Lei, Q., and Fang, W. (2014) Interfacial tensions for system of n-heptane + water with quaternary ammonium surfactants and additives of NaCl or C₂-C₄ alcohols. *Journal of Chemical and Engineering Data*, **59**, 860–868.

Zhang, Y., Xu, X., Lebedev, M., Sarmadivaleh, M., Barifcani, A., and Iglauer, S. (2016) Multi-scale x-ray computed tomography analysis of coal microstructure and permeability changes as a function of effective stress. *International Journal of Coal Geology*, **165**, 149–156.

Zhang, Y. and Morrow, N. R. (2006) Comparison of Secondary and Tertiary Recovery with Change in Injection Brine Composition for Crude Oil/ Sandstone Combinations. *Paper SPE 99757-MS presented at the 2006 SPE/DOE Symposium on Improved Oil Recovery*, Tulsa, Oklahoma, USA 22-26 April.

APPENDIX

Table S1. γ Values for n-Heptane – (NaCl-SDS) Aqueous System

| Salt | Salt conc. (mM) | Surfactant | Surfactant conc. (mM) | γ (mN/m) | $u(\gamma)$ (mN/m) |
|-------|--------------------|------------|--------------------------|--------------------|-----------------------|
| NaCl | 17.110 | SDS | 0.217 | 20.507 | 0.004 |
| | | | 0.433 | 15.275 | 0.003 |
| | | | 0.867 | 9.490 | 0.002 |
| | | | 1.300 | 6.154 | 0.004 |
| | | | 1.730 | 4.840 | 0.008 |
| | | | 2.167 | 4.867 | 0.003 |
| | | | 0.217 | 11.898 | 0.009 |
| | 0.433 | | 5.146 | 0.017 | |
| | 0.867 | | 3.562 | 0.003 | |
| | 1.300 | | 4.162 | 0.002 | |
| | 1.730 | | 4.345 | 0.003 | |
| | 2.167 | | 4.620 | 0.007 | |
| | 0.217 | | 6.493 | 0.004 | |
| | 0.433 | | 3.180 | 0.003 | |
| 0.867 | 3.789 | 0.004 | | | |
| 1.300 | 4.045 | 0.001 | | | |
| 1.730 | 4.226 | 0.002 | | | |
| 2.167 | 4.415 | 0.002 | | | |

Table S2. γ Values for n-Heptane – (CaCl₂-SDS) Aqueous System

| Salt | Salt conc. (mM) | Surfactant | Surfactant conc. (mM) | γ (mN/m) | $u(\gamma)$ (mN/m) |
|-------------------|--------------------|------------|--------------------------|--------------------|-----------------------|
| | | | 0.217 | 4.949 | 0.004 |
| | | | 0.433 | 3.421 | 0.004 |
| | 9.010 | | 0.867 | 1.944 | 0.002 |
| | | | 1.300 | 1.944 | 0.003 |
| | | | 1.730 | 1.975 | 0.012 |
| | | | 0.217 | 2.797 | 0.002 |
| | | | 0.433 | 2.265 | 0.003 |
| CaCl ₂ | 31.530 | SDS | 0.867 | 1.949 | 0.014 |
| | | | 1.300 | 1.517 | 0.022 |
| | | | 1.730 | 1.481 | 0.014 |
| | | | 0.217 | 3.418 | 0.004 |
| | | | 0.433 | 2.370 | 0.014 |
| | 63.070 | | 0.867 | 1.132 | 0.025 |
| | | | 1.300 | 0.713 | 0.016 |
| | | | 1.730 | 0.722 | 0.028 |
| | | | 0.217 | 2.911 | 0.003 |
| | 126.150 | | 0.867 | 2.045 | 0.004 |
| | | | 1.730 | 2.045 | 0.001 |

Table S3. γ Values for n-Heptane – (NaCl-AOT) Aqueous System

| Salt | Salt conc. (mM) | Surfactant | Surfactant conc. (mM) | γ (mN/m) | $u(\gamma)$ (mN/m) |
|------|--------------------|------------|--------------------------|--------------------|-----------------------|
| | | | 0.141 | 10.718 | 0.006 |
| | | | 0.562 | 4.156 | 0 |
| | 17.110 | | 0.844 | 1.820 | 0.006 |
| | | | 1.125 | 0.730 | 0.003 |
| | | | 1.406 | 0.631 | 0.003 |
| | | | 0.141 | 5.572 | 0.001 |
| | | | 0.281 | 2.058 | 0.015 |
| NaCl | 59.890 | AOT | 0.844 | 0.377 | 0.004 |
| | | | 1.125 | 0.308 | 0.002 |
| | | | 1.406 | 0.161 | 0.007 |
| | | | 0.141 | 3.159 | 0.006 |
| | | | 0.281 | 0.300 | 0.002 |
| | 119.780 | | 0.562 | 0.359 | 0.002 |
| | | | 0.844 | 0.400 | 0.003 |
| | | | 1.406 | 0.441 | 0.001 |

Table S4. Capillary Pressure Data

| LSS1 | | | | | | LSS2 | | | | | | LSS3 | | | | | |
|------------------|-------|------------|-------|--------------------|-------|------------------|-------|------------|-------|--------------------|-------|------------------|-------|------------|-------|--------------------|-------|
| Primary Drainage | | Imbibition | | Secondary Drainage | | Primary Drainage | | Imbibition | | Secondary Drainage | | Primary Drainage | | Imbibition | | Secondary Drainage | |
| Sw | Pc | Sw | -Pc | Sw | Pc | Sw | Pc | Sw | -Pc | Sw | Pc | Sw | Pc | Sw | -Pc | Sw | Pc |
| 92.45 | 1.12 | 40.26* | 3.96 | 47.50* | 1.05 | 94.34 | 1.12 | 45.77* | 3.96 | 50.67* | 1.05 | 97.27 | 1.12 | 43.58* | 3.96 | 54.12* | 1.05 |
| 80.07 | 2.51 | 41.96 | 8.90 | 40.03 | 2.37 | 80.57 | 2.51 | 46.90 | 8.90 | 47.19 | 2.37 | 83.24 | 2.51 | 47.23 | 8.90 | 44.88 | 2.37 |
| 62.13 | 4.47 | 43.08 | 15.83 | 35.39 | 4.21 | 61.87 | 4.47 | 47.28 | 15.83 | 40.30 | 4.21 | 65.23 | 4.47 | 48.66 | 15.83 | 38.58 | 4.21 |
| 50.25 | 6.98 | 43.63 | 24.73 | 30.74 | 6.57 | 50.23 | 6.98 | 47.82 | 24.73 | 36.13 | 6.57 | 53.87 | 6.98 | 50.76 | 24.73 | 35.10 | 6.57 |
| 42.53 | 10.05 | 44.24 | 35.60 | 27.70 | 9.46 | 42.90 | 10.05 | 48.58 | 35.60 | 31.97 | 9.46 | 46.46 | 10.05 | 52.33 | 35.60 | 31.54 | 9.46 |
| 34.07 | 17.86 | 46.18 | 63.28 | 25.80 | 16.82 | 35.53 | 17.86 | 50.63 | 63.29 | 29.06 | 16.82 | 38.98 | 17.86 | 53.73 | 49.41 | 29.19 | 16.82 |
| 29.43 | 27.90 | 47.95* | 98.84 | 24.37 | 26.28 | 30.94 | 27.90 | 51.19* | 98.88 | 27.22 | 26.28 | 34.30 | 27.90 | 54.48* | 63.29 | 27.54 | 26.29 |
| 26.67 | 40.18 | | | 23.26 | 37.83 | 28.23 | 40.18 | | | 25.93 | 37.85 | 31.37 | 40.18 | | | 26.29 | 37.85 |
| 24.94 | 54.68 | | | 22.42 | 51.49 | 26.51 | 54.68 | | | 25.03 | 51.52 | 29.53 | 54.68 | | | 25.27 | 51.52 |
| 23.67 | 71.42 | | | 21.74* | 67.24 | 25.31 | 71.42 | | | 24.24 | 67.29 | 28.23 | 71.42 | | | 24.43 | 67.28 |
| 22.67 | 90.39 | | | | | 24.42 | 90.39 | | | 23.73* | 85.16 | 27.28 | 90.39 | | | 23.74* | 85.16 |

*Limits used for area under curve calculation

Capillary pressure (Pc) calculation

$$Pc = 7.94 * 10^{-8}(\rho_1 - \rho_2)RPM^2 r^2$$

Where, ρ_1 and ρ_2 are the densities of the two liquids in g/ml, RPM is rotation per minute and r (8.6 cm) is the radial distance from the axis of rotation to the core sample.

Density of high salinity water (HSW) = 1.02 g/ml

Density of light paraffin oil = 0.83 g/ml

Density of Nanofluids = 1.009 g/ml

Copyrights

All the chapters contain either a portion or full of any of these copyrighted materials.

Chapter 2

Effect of Monovalent and Divalent Salts on the Interfacial Tension of n-Heptane against Aqueous Anionic Surfactant Solutions



Author: Nilesh Kumar Jha, Stefan Iglauer, Jitendra S. Sangwai

Publication: Journal of Chemical and Engineering Data

Publisher: American Chemical Society

Date: Jul 1, 2018

Copyright © 2018, American Chemical Society

PERMISSION/LICENSE IS GRANTED FOR YOUR ORDER AT NO CHARGE

This type of permission/license, instead of the standard Terms & Conditions, is sent to you because no fee is being charged for your order. Please note the following:

- Permission is granted for your request in both print and electronic formats, and translations.
- If figures and/or tables were requested, they may be adapted or used in part.
- Please print this page for your records and send a copy of it to your publisher/graduate school.
- Appropriate credit for the requested material should be given as follows: "Reprinted (adapted) with permission from (COMPLETE REFERENCE CITATION). Copyright (YEAR) American Chemical Society." Insert appropriate information in place of the capitalized words.
- One-time permission is granted only for the use specified in your request. No additional uses are granted (such as derivative works or other editions). For any other uses, please submit a new request.

[BACK](#)

[CLOSE WINDOW](#)

Chapter 3

Low-Salinity Surfactant Nanofluid Formulations for Wettability Alteration of Sandstone: Role of the SiO₂ Nanoparticle Concentration and Divalent Cation/SO₄²⁻ Ratio



Author: Nilesh Kumar Jha, Stefan Iglauer, Ahmed Barifcani, et al

Publication: Energy & Fuels

Publisher: American Chemical Society

Date: Feb 1, 2019

Copyright © 2019, American Chemical Society

PERMISSION/LICENSE IS GRANTED FOR YOUR ORDER AT NO CHARGE

This type of permission/license, instead of the standard Terms & Conditions, is sent to you because no fee is being charged for your order. Please note the following:

- Permission is granted for your request in both print and electronic formats, and translations.
- If figures and/or tables were requested, they may be adapted or used in part.
- Please print this page for your records and send a copy of it to your publisher/graduate school.
- Appropriate credit for the requested material should be given as follows: "Reprinted (adapted) with permission from (COMPLETE REFERENCE CITATION). Copyright (YEAR) American Chemical Society." Insert appropriate information in place of the capitalized words.
- One-time permission is granted only for the use specified in your request. No additional uses are granted (such as derivative works or other editions). For any other uses, please submit a new request.

[BACK](#)

[CLOSE WINDOW](#)

Chapter 4



RightsLink®



Home



Help



Email Support



Sign in



Create Account

Wettability Alteration of Quartz Surface by Low-Salinity Surfactant Nanofluids at High-Pressure and High-Temperature Conditions



Author: Nilesh Kumar Jha, Muhammad Ali, Stefan Iglauer, et al

Publication: Energy & Fuels

Publisher: American Chemical Society

Date: Aug 1, 2019

Copyright © 2019, American Chemical Society

PERMISSION/LICENSE IS GRANTED FOR YOUR ORDER AT NO CHARGE

This type of permission/license, instead of the standard Terms & Conditions, is sent to you because no fee is being charged for your order. Please note the following:

- Permission is granted for your request in both print and electronic formats, and translations.
- If figures and/or tables were requested, they may be adapted or used in part.
- Please print this page for your records and send a copy of it to your publisher/graduate school.
- Appropriate credit for the requested material should be given as follows: "Reprinted (adapted) with permission from (COMPLETE REFERENCE CITATION). Copyright (YEAR) American Chemical Society." Insert appropriate information in place of the capitalized words.
- One-time permission is granted only for the use specified in your request. No additional uses are granted (such as derivative works or other editions). For any other uses, please submit a new request.

BACK

CLOSE WINDOW

Chapter 5



RightsLink®



Home



Help



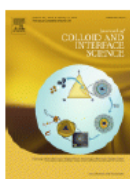
Email Support



Sign in



Create Account



Pore scale investigation of low salinity surfactant nanofluid injection into oil saturated sandstone via X-ray micro-tomography

Author:

Nilesh Kumar Jha, Maxim Lebedev, Stefan Iglauer, Muhammad Ali, Hamid Roshan, Ahmed Barifcani, Jitendra S. Sangwai, Mohammad Sarmadivaleh

Publication: Journal of Colloid and Interface Science

Publisher: Elsevier

Date: 7 March 2020

© 2019 Elsevier Inc. All rights reserved.

Please note that, as the author of this Elsevier article, you retain the right to include it in a thesis or dissertation, provided it is not published commercially. Permission is not required, but please ensure that you reference the journal as the original source. For more information on this and on your other retained rights, please visit: <https://www.elsevier.com/about/our-business/policies/copyright#Author-rights>

BACK

CLOSE WINDOW

PUBLICATIONS

International peer-reviewed journals

1. **Jha, N. K.**, Lebedev, M., Iglauer, S., Ali, M., Roshan, H., Barifcani, A., Sangwai, J. S., Sarmadivaleh, M. Pore Scale Investigation of Low Salinity Surfactant Nanofluid Injection in to Oil Saturated Sandstone via X-ray Micro-tomography. *Journal of Colloids and Interface Science*, 2020, 572, 370-380. (Elsevier, IF: **6.36**).
2. **Jha, N. K.**, Ali, M., Iglauer, S., Lebedev, M., Roshan, H., Barifcani, A., Sangwai, J. S., Sarmadivaleh, M. Wettability Alteration of Quartz Surface by Low Salinity Surfactant Nano fluids at High Pressure and High Temperature Conditions. *Energy & Fuels*, 2019, 33(8), 7062-7068. (ACS Publications, IF: **3.02**)
3. **Jha, N. K.**, Iglauer, S., Barifcani, A., Sarmadivaleh, M., Sangwai, J. S. Low Salinity Surfactant Nanofluid Formulations for Wettability Alteration of Sandstone: Role of SiO₂ Nano particles Concentration and Divalent Cation to SO₄²⁻Ratio. *Energy & Fuels*, 2019,33(2), 739-746. (ACS Publications, IF: **3.02**)
4. **Jha, N. K.**, Iglauer, S., Sangwai, J. S. Effect of Monovalent and Divalent Salts on the Interfacial Tension of n-Heptane against Aqueous Anionic Surfactant solutions. *Journal of Chemical & Engineering Data*, 2017, 63 (7), 2341-2350. (Emerging Investigators Special Issue, ACS Publications, IF: **2.32**)

Conferences/Conference proceedings

1. **Jha, N. K.**, Ali, M., Sarmadivaleh, M., Iglauer, S., Barifcani, A., Lebedev, M., Sangwai, J. S. Low Salinity Surfactant Nanofluids For Enhanced CO₂ Storage Application at High Pressure and Temperature. *The EAGE Fifth CO₂ Geological Storage Workshop*, 2018, 21-23 November, Utrecht, The Netherlands.

2. **Jha, N. K.**, Iglauer, S., Sangwai, J. S. Reducing Interfacial Tension and Surfactant Adsorption for Low Salinity Surfactant Enhanced Oil Recovery. *2017 One Curtin Postgraduate Conference*. 2017, 10-12 December, Curtin University, Miri, Sarawak, Malaysia.